UNIVERSIDADE FEDERAL DE PERNAMBUCO
CENTRO DE CIÊNCIAS EXATAS E DA NATUREZA
PROGRAMA DE PÓS-GRADUAÇÃO EM FÍSICA

RICARDO DE LIMA SILVEIRA

Confinement induced variation of the power-law decay of the order parameter in the low-temperature proximity effect

Recife

2022

RICARDO DE LIMA SILVEIRA

Confinement induced variation of the power-law decay of the order parameter in the low-temperature proximity effect

Thesis presented to the Physics Graduate Program at the Federal University of Pernambuco as a partial requirement to obtain the degree of Master in Physics.

Concentration area: Condensed Matter Physics and Materials

Advisor: Mihail Croitoru

Recife

2022

Catalogação na fonte
Bibliotecária Nataly Soares Leite Moro, CRB4-1722

S587c Silveira, Ricardo de Lima
Confinement induced variation of the power-law decay of the order parameter in the low-temperature proximity effect / Ricardo de Lima Silveira. – 2022.
84 f.: il., fig., tab.

Orientador: Mihail Croitoru.
Dissertação (Mestrado) – Universidade Federal de Pernambuco. CCEN, Física, Recife, 2022.
Inclui referências.

1. Física da matéria condensada e de materiais. 2. Efeito de proximidade. 3. Confinamento quântico. 4. Equações de Bogoliubov-de Gennes. I. Croitoru, Mihail (orientador). II. Título.

530.41 CDD (23. ed.) UFPE- CCEN 2023 - 45

RICARDO DE LIMA SILVEIRA

CONFINEMENT INDUCED VARIATION OF THE POWER-LAW DECAY OF THE ORDER PARAMETER IN THE LOW-TEMPERATURE PROXIMITY EFFECT

Dissertação apresentada ao Programa de Pós-Graduação em Física da Universidade Federal de Pernambuco, como requisito parcial para a obtenção do título de Mestre em Física.

Aprovada em: 21/03/2022.

BANCA EXAMINADORA

_____

Prof. Mihail Croitoru
Orientador
Universidade Federal de Pernambuco

_____

Prof. José Albino Oliveira de Aguiar
Examinador Interno
Universidade Federal de Pernambuco

_____

Prof. Antonio Rodrigues de Castro Romaguera
Examinador Externo
Universidade Federal Rural de Pernambuco

_____

Profª. Natalia Pugach
Examinadora Externa
HSE University

ABSTRACT

This thesis aims to investigate how the proximity effect is affected by the quantum confinement of charge carriers. This phenomenon, which consists essentially in the diffusion of superconducting correlations into a non-superconducting metal, has been widely studied over several decades, but not so much in the quasi-low dimensionality regime, taking into account the effect of the quantum confinement of electrons on the properties of the system. We aim, more specifically, to determine the functional form for the decay of the pair amplitude in cylindrical nanowires of normal metals in the clean limit and at zero temperature. It is known that quantum confinement leads to fluctuations in the values of superconducting quantities, such as the energy gap and transition temperature. This can be expected to affect how strongly the wave function of an electron pair decays in the normal metal. To investigate this problem, we solve the Bogoliubov-de Gennes equations self-consistently in nanowires with different diameters. Based on the literature on the proximity effect at low temperatures in clean metals, we model the behavior of the superconducting correlations in the normal metal by an inverse power law decay, with exponent α. The value of this parameter is extracted from the data obtained numerically for each diameter. We found that this parameter follows an oscillatory pattern whose peaks and valleys correspond to those observed in the energy gap.

Keywords: proximity effect; quantum confinement; Bogoliubov-de Gennes equations.

RESUMO

Essa dissertação tem por obejtivo investigar como o efeito de proximidade é afetado pelo confinamento quântico de portadores de carga. Esse fenômeno, que consiste essencialmente na difusão de correlações supercondutoras para um metal não supercondutor, tem sido amplamente estudado ao longo de várias décadas, mas nem tanto no regime de dimensionalidade quase baixa, levando em consideração o efeito do confinamento quântico de elétrons sobre as propriedades do sistema. Almejamos, mais especificamete, determinar a forma funcional para o decaimento da amplitude de pares em nanocilindrindos de metal normal no limite balístico e à temperatura nula. Sabe-se que o confinameno quântico leva a oscilações nos valores de grandezas supercondutoras, como o gap de energia e a temperatura de transição. Pode-se esperar que isso afete o quão forte é o decaimento da função de onda de um par no metal normal. Para investigar esse problema, resolvemos as equações de Bogoliubov-de Gennes de forma autoconsistente em nanofios com diferentes valores de diâmetro. Baseados na literatura sobre o efeito de proximidade em baixas temperaturas em metais balísticos, modelamos o comportamento das correlações supercondutoras no metal normal por um decaimento em lei de potência inversa, com expoente α. O valor desse parâmetro é extraído dos dados obtidos numericamente para cada diâmetro. Obtivemos que esse parâmetro segue um padrão oscilatório cujos picos e vales correspondem àqueles observados no gap de energia.

Palavras-chaves: efeito de proximidade; confinamento quântico; equações de Bogoliubov-de Gennes.

LIST OF FIGURES

LIST OF TABLES

CONTENTS

1 INTRODUCTION

Since its discovery in 1911 (ONNES, 1911), superconductivity has developed into a wide and rich field of research. A typical superconductor possesses some quite remarkable characteristics. Perhaps the most celebrated one is the absence of electrical resistivity: below a critical temperature, a superconductor is capable of sustaining an electrical current for an astonishing long time without any apparent dissipation. But a superconductor is not merely a perfect conductor, it is also a perfect diamagnet, that is, any external magnetic field that is not too strong diminishes rapidly over a characteristic length away from the surface of a superconductor and vanishes in its interior. This is the so-called Meissner effect (MEISSNER; OCHSENFELD, 1933).

Moreover, a typical superconductor possesses a gapped spectrum (although gapless superconductivity is also possible). This means that for such materials there exists an interval in the energy spectrum in which single electron levels are not allowed. The existence of an energy gap manifests itself in observable properties of the superconducting material, like in an exponential decay of the specific heat as temperature decreases.

The drive to accurately explain superconductivity and its related phenomena led, over the course of several decades, to the development of many fruitful ideas and theoretical frameworks. Some highlights are London's early phenomenological theory, which was able to account for the Meissner effect (LONDON; LONDON, 1935a; LONDON; LONDON, 1935b). Ginzburg and Landau's theory approached superconductivity from the perspective of phase transitions and described superconductors close to the critical temperature with the aid of a complex macroscopic wave function as an order parameter. A successful microscopic description for homogeneous *s*-wave superconductors with constant energy gap Δ is BCS theory, brought forth in 1957, which is based on the concept of Cooper pairs, bound states formed by two electrons with opposite momenta and spins that attract each other through an interaction mediated by virtual phonons (BARDEEN; COOPER; SCHRIEFFER, 1957a; BARDEEN; COOPER; SCHRIEFFER, 1957b). For inhomogeneous systems, like nanowires and nanofilms, where the gap $\Delta(\mathbf{r})$ cannot be considered constant throughout the material, a more appropriate description is provided by the Bogoliubov-de Gennes (BdG) equations (GENNES, 1966). Superconductivity can also be described by means of Green's functions. It is necessary to introduce anomalous Green's functions related to the pairing of electrons. Gor'kov developed a set of coupled differential

equations for the normal and anomalous Green's functions of a superconductor.

If a superconductor is appropriately connected to a non-superconducting metal (which may be a nonmagnetic metal or a ferromagnet), one observes that some superconducting properties, otherwise absent, are induced in the normal metal. Electronic interactions in the system are characterized by the potential $V(\mathbf{r}-\mathbf{r}') = g(z)\delta(\mathbf{r}-\mathbf{r}')$. Most noticeably, the pair amplitude $F(z) = \left\langle \Psi_\uparrow^\dagger(z)\Psi_\downarrow^\dagger(z)\right\rangle = \Delta(z)/g(z)$, which is related to the probability amplitude of finding a pair at z, does not vanish completely in the normal metal but instead decays over appreciable length scales. This is the so-called proximity effect. Additionally, this leakage of superconducting correlations into the normal metal is accompanied by a weakening of superconductivity on the superconductor itself: the value of the pair potential $\Delta(z)$ (and of $F(z)$) is reduced near the interface. The proximity effect was first observed by Holm and Meissner (1932). More experiments were only carried out much later, in the 1950s (BEDARD; MEISSNER, 1956) and flourished from the 1960s (CLARKE, 1968) onwards. Theoretical investigations began gaining traction in the 1960s, initially in the framework of Ginzburg-Landau theory and Gor'kov equations (GENNES, 1964; DEUTSCHER; GENNES, 1969). The development of the quasiclassical theory of superconductivity (EILENBERGER, 1968; USADEL, 1970) also played an important role in the unravelling of proximity-related problems. It has been useful, for example, in the treatment of a type of proximity effect that has received much attention since the 1990s: the induction of superconductivity in ferromagnets (BERGERET; VOLKOV; EFETOV, 2005; BUZDIN, 2005). Additionally, the increase in computational power has allowed researches to approach these problems numerically using more precise formalism such as the Bogoliubov-de Gennes equations without needing to resort to potentially harmful approximations (HALTERMAN; VALLS, 2001).

Another subfield with notably rich physics is superconductivity at nanoscales, when the thickness of a superconducting sample is reduced. This confinement of electronic motion along some directions may cause the values of key properties of the system to significantly deviate from those observed in bulk samples. Several of the characteristic quantities of superconductor develop a remarkable oscillatory behavior as functions of sample thickness: the energy gap, critical temperature, density of states at the Fermi level, coherence length, for example. The initial steps in uncovering these phenomena were taken sixty years ago, by Blatt and Thompson (1963), who studied energy gap oscillations in nanofilms based on the then recently developed BCS theory. For several decades, experimental advances in this area stalled due to the lack of nanostructures with satisfactory quality. The situation changed as technological improvements

allowed for the creation of high-quality samples. Additionally, a more appropriate treatment of such inhomogeneous nanostructures was achieved with the introduction of the Bogoliubov-de Gennes equations.

The proximity effect and the oscillations in superconducting properties due to quantum confinement are two classes of important superconductivity-related phenomena. What remains to be extensively investigated with a proper microscopic self-consistent treatment, however, is the interplay of these two effects, i.e, how the proximity effect is altered in the presence of quantum confinement. Some work has been carried out in that direction (REEG; LOSS; KLINOVAJA, 2017; REEG; LOSS; KLINOVAJA, 2018).

With these points in mind, the goal of this thesis is to explore some aspects of the proximity effect in clean cylindrical nanowires at zero temperature. The nanowires are half superconducting, half normal metal, and these two parts are separated by a plane boundaries perpendicular to the wire axis. More specifically, we aim to investigate how the functional form for the decay of the pair amplitude $F(z)$ in the normal metal is modified as wire thickness is changed, in the regime where oscillations in $F(z)$ induced by quantum confinement are present.

2 OVERVIEW OF SUPERCONDUCTIVITY

Superconductivity was discovered in 1911 by the Dutch physicist Heike Kamerlingh Onnes (ONNES, 1911). He had previously successfully liquefied helium for the first time, allowing him to reach record low temperatures in his lab. Onnes realized that the resistivity of mercury (Hg) suddenly dropped from a finite value to virtually zero at a critical temperature of $4.2\ \mathrm{K}$.

2.1 LONDON PHENOMENOLOGICAL THEORY

An early attempt at explaining both perfect conductivity and perfect diamagnetism was made in 1935 by Heinz and Fritz London (LONDON; LONDON, 1935a; LONDON; LONDON, 1935b). To understand their reasoning, we may initially investigate a metal that exhibits perfect conductivity with the aide of Maxwell's equations. In the presence of an electric field E, the free charges in the system will be accelerated according to

$$m\frac{d^2\mathbf{r}}{dt^2} = -e\mathbf{E} \tag{2.1}$$

where m and e are the mass and charge of the electron, respectively. In general, a current density can be written as the product of the volume charge density, ρ, and the velocity field, $\mathbf{v}$:

$$\mathbf{J} = \rho\mathbf{v} \tag{2.2}$$

If n is the density of electrons which are able to move without resistance, the current density can be written as

$$\mathbf{J} = -en\frac{d\mathbf{r}}{dt} \tag{2.3}$$

By taking the derivative of this expression with respect to time, we obtain a new expression for $\frac{d^2\mathbf{r}}{dt^2}$ which can be substituted in (2.1), resulting in

$$\mathbf{E} = \frac{m}{e^2 n}\frac{d\mathbf{J}}{dt} \tag{2.4}$$

Faraday's law, which is given by

$$\boldsymbol{\nabla} \times \mathbf{E} = -\frac{\partial \mathbf{B}}{\partial t}, \tag{2.5}$$

takes the form

$$\boldsymbol{\nabla} \times \frac{\partial \mathbf{J}}{\partial t} = -\frac{e^2 n}{m}\frac{\partial \mathbf{B}}{\partial t}. \tag{2.6}$$

The magnetic field and the current density are related through Ampère's law:

$$\boldsymbol{\nabla} \times \mathbf{B} = \mu_0 \mathbf{J}. \tag{2.7}$$

Using (2.7), Eq.(2.6) becomes

$$\boldsymbol{\nabla} \times \boldsymbol{\nabla} \times \frac{\partial \mathbf{B}}{\partial t} = -\frac{ne^2\mu_0}{m}\frac{\partial \mathbf{B}}{\partial t} \tag{2.8}$$

The repeated curl can be simplified with the help of the vector identity

$$\boldsymbol{\nabla} \times \boldsymbol{\nabla} \times \mathbf{A} = \boldsymbol{\nabla}(\boldsymbol{\nabla} \cdot \mathbf{A}) - \nabla^2 \mathbf{A} \tag{2.9}$$

and Gauss's law for magnetism

$$\boldsymbol{\nabla} \cdot \mathbf{B} = 0 \tag{2.10}$$

Finally, we obtain

$$\nabla^2\left(\frac{\partial \mathbf{B}}{\partial t}\right) = \lambda_L^{-2}\left(\frac{\partial \mathbf{B}}{\partial t}\right), \tag{2.11}$$

where

$$\lambda_L = \sqrt{\frac{m}{e^2 n \mu_0}} = \sqrt{\frac{m\epsilon_0 c^2}{e^2 n}} \tag{2.12}$$

To illustrate the significance of this equation, we can examine a one dimensional perfect conductor, with a magnetic field $\mathbf{B}$ applied along the transverse direction. In this particular setting, Eq. (2.11) becomes

$$\frac{\partial \mathbf{B}}{\partial t} = \left(\frac{\partial \mathbf{B}}{\partial t}\right)_{z=0} \exp\left(-\frac{z}{\lambda_L}\right) \tag{2.13}$$

So inside this perfect conductor, away from the $z = 0$ surface, we have that $\frac{\partial \mathbf{B}}{\partial t} = 0$. In other words, the magnetic field in the interior of the sample would be constant. However, this is in clear disagreement from what is known from the Meissner effect, which establishes that the magnetic field inside a superconductor is not only constant, but exactly zero. This line of reasoning therefore shows that a superconductor is more than just a perfect conductor. The London brothers observed that this issue can be resolved if the partial derivatives in time are remove from Eq.(2.11):

$$\nabla^2 \mathbf{B} = \lambda_L^{-2}\mathbf{B}. \tag{2.14}$$

The implication now is that an external magnetic field decays exponentially to zero over a distance λ_L, which is called the London penetration depth.

2.2 BCS THEORY

A satisfactory microscopic description of the superconducting state was presented in 1957 by John Bardeen, Leon Cooper and John Robert Schrieffer, and became known as the BCS theory (BARDEEN; COOPER; SCHRIEFFER, 1957a; BARDEEN; COOPER; SCHRIEFFER, 1957b). At the core of the BCS description of superconductivity is the idea that an effective attractive interaction may arise between two electrons, leading to the formation of a bound state called a Cooper pair. We may picture a metal as a see of electrons and a lattice of positively charged ions that oscillate around fixed positions. The electrostatic interaction between the electrons is, of course, repulsive, but when ionic movement is taken into account, the resultant effective interaction is attractive. We may speak, then, of an electron-electron interaction mediated by phonons (FRöHLICH, 1950). For a simple description of this phenomenon, we can imagine a propagating electron that locally disturbs the lattice, creating a region of net positive charge. The speed of the electron is considerably higher than the speed with which the lattice relaxes, so the original electron goes away but the positive disturbance remains for a while and can attract a second electron without much eletrostatic repulsion from the first one. The net result is then an effective attraction between the two electrons. From this simplified description, it is also clear that the interaction is not instantaneous, but time-retarded, and this is crucial to circumvent the Coulomb repulsion.

Electrons are fermions, but out of two of them a new entity of bosonic character arises. Being bosons, the Cooper pairs can all occupy the lowest energy state, as in a Bose-Einstein condensate. This Cooper pair condensate is the superconducting ground state.

2.2.1 Single pair of electrons

Initially, Cooper considered how two electrons, taken in isolation, can form a bound state. The particles interact via an attractive potential $V(\mathbf{r}_1 - \mathbf{r}_2)$, where $\mathbf{r}_1$ and $\mathbf{r}_2$ are their position vectors. This two-particle system is described by the wave function $\Psi(\mathbf{r}_1, \mathbf{r}_2)$, for which the Schrödinger equation can be written as

$$\left[-\frac{\hbar^2}{2m}\nabla^2_{\mathbf{r}_1} - \frac{\hbar^2}{2m}\nabla^2_{\mathbf{r}_2} + V(\mathbf{r}_1 - \mathbf{r}_2)\right]\Psi(\mathbf{r}_1, \mathbf{r}_2) = E\Psi(\mathbf{r}_1, \mathbf{r}_2) \tag{2.15}$$

Here, it is convenient to change coordinates and work instead with the separation vector and the position of the center of mass

$$\mathbf{r} = \mathbf{r}_2 - \mathbf{r}_1, \quad \mathbf{R} = \frac{\mathbf{r}_1 + \mathbf{r}_2}{2}. \tag{2.16}$$

The new Schrödinger equation is given by

$$\left[-\frac{\hbar^2}{2M}\nabla^2_{\mathbf{R}} - \frac{\hbar^2}{2\mu}\nabla^2_{\mathbf{r}} + V(\mathbf{r})\right]\Psi(\mathbf{r},\mathbf{R}) = E\Psi(\mathbf{r},\mathbf{R}), \tag{2.17}$$

where $M = 2m$ and $\mu = m/2$. It is now possible to approach solving this equation by separation of variables. We may write

$$\Psi(\mathbf{r},\mathbf{R}) = \psi(\mathbf{r})\Phi(\mathbf{R}). \tag{2.18}$$

Substituting this expression in Eq.(2.17) results in separate differential equations for $\psi(\mathbf{r})$ and $\Phi(\mathbf{R})$. A general solution for $\Phi(\mathbf{R})$ is of the form

$$\Phi(\mathbf{R}) = e^{i\mathbf{K}\cdot\mathbf{R}}, \tag{2.19}$$

whilst $\psi(\mathbf{r})$ can be determined from a new Schrödinger equation:

$$\left[-\frac{\hbar^2}{2\mu}\nabla^2_{\mathbf{r}} + V(\mathbf{r})\right]\psi(\mathbf{r}) = \bar{E}\psi(\mathbf{r}), \tag{2.20}$$

where

$$\bar{E} = E - \frac{\hbar^2 K^2}{2M}. \tag{2.21}$$

As one can clearly see, $\bar{E}$ will be minimum when the center of mass momentum $\mathbf{K}$ vanishes or, in other words, when the two electrons have opposite momenta. This is the situation traditionally considered in BCS theory. To solve eq. (2.20), we use the method of Fourier transforms. Here, we introduce

$$\psi(\mathbf{k}) = \int \psi(\mathbf{r})e^{-i\mathbf{k}\cdot\mathbf{r}}\, d^3r \tag{2.22}$$

and note that

$$\begin{gathered}\int d^3r V(\mathbf{r})\psi(\mathbf{r})e^{-i\mathbf{k}\cdot\mathbf{r}}\, d^3r = \int \frac{d^3q}{(2\pi)^3}V(\mathbf{q})\int d^3r\psi(\mathbf{r})e^{-i(\mathbf{k}-\mathbf{q})\cdot\mathbf{r}} = \\ \int \frac{d^3k'}{(2\pi)^3}V(\mathbf{k}-\mathbf{k}')\psi(\mathbf{k}')\end{gathered} \tag{2.23}$$

By multiplying Eq.(2.20) by $e^{-i\mathbf{k}\cdot\mathbf{r}}$ and integrating in $\mathbf{r}$, we obtain

$$\int \frac{d^3k'}{(2\pi)^3}V(\mathbf{k}-\mathbf{k}')\psi(\mathbf{k}') = (E - 2\epsilon_k)\psi(\mathbf{k}), \tag{2.24}$$

with $\epsilon_k = \hbar^2 k^2/2m$. Because we take $K = 0$ in Eq.(2.21), we can write E instead of $\bar{E}$ in Eq.(2.24). It is convenient to write everything in terms of a new wave function $\Delta(\mathbf{k}) = \psi(\mathbf{k})(E - 2\epsilon_k)$. This leads to

$$\Delta(\mathbf{k}) = \int \frac{d^3k'}{(2\pi)^3} \frac{V(\mathbf{k}-\mathbf{k}')}{(E-2\epsilon_k)} \Delta(\mathbf{k}'), \tag{2.25}$$

This expression becomes more tractable if we integrate over energy instead of momentum:

$$\int \frac{d^3k'}{(2\pi)^3} = \int d\epsilon \rho(\epsilon), \tag{2.26}$$

with the density of states per spin given by

$$\rho(\epsilon) = \frac{1}{2\pi^2}\left(\frac{2m}{\hbar^2}\right)^{3/2} \epsilon^{1/2} \tag{2.27}$$

To proceed, we must know the form of the potential $V(\mathbf{k}-\mathbf{k}')$. It is reasonable to take the simple attractive potential $V(\mathbf{k}-\mathbf{k}') = -V_0$. The energy scales for phonons in a lattice is set by $\hbar\omega_D$, where ω_D is the Debye frequency. Since we assume that the net attractive interaction between the electrons arises due to interaction with phonons, it is appropriate to take as an upper bound for the energies in the problem. For a homogeneous three dimensional system, we can look for solutions with uniform $\Delta(\mathbf{k}) = \Delta$. Then,

$$\Delta = V_0 \Delta \int_0^{\hbar\omega_D} \frac{d\epsilon \rho(\epsilon)}{2\epsilon - E} \tag{2.28}$$

and ultimately

$$\sqrt{\frac{-E}{2}} \arctan\left(\frac{2\hbar\omega_D}{-E}\right) = -\frac{2\pi^2}{V_0}\left(\frac{\hbar^2}{2m}\right)^{3/2} + \sqrt{\hbar\omega_D}. \tag{2.29}$$

This is the expression for the energy E of the pair. Note that we are considering a bound pair of two electrons, so $E < 0$. From this, we can infer the minimal value of V_0 that allows for the formation of bound pairs. Taking the limit $E \to 0$ of Eq.(2.29) from negative energies, we arrive at

$$V_{0,min} = \frac{2\pi^2}{\sqrt{\hbar\omega_D}}\left(\frac{\hbar^2}{2m}\right)^{3/2} \tag{2.30}$$

In more physical terms, this means that the attraction must be stronger than a minimum value if bound pairs are to be formed. This simplified model, however, failed to take into account an important feature of the system: the Fermi surface. In an actual many-body system with a well-defined Fermi surface, only the electrons in the vicinity of the Fermi level ϵ_F can interact to form pairs. We look at Eq.(2.28) once again, but now the lower and upper limits in the integarl must be changed to ϵ_F and $\epsilon_F + \hbar\omega_D$, respectively. Additionally, $\hbar\omega_D \ll \epsilon_F$, so

we can approximate the density of states by its value at the Fermi level: $\rho(\epsilon) \approx \rho(\epsilon_F)$. Thus, we obtain

$$\frac{1}{V_0\rho(\epsilon_F)} = \int_{\epsilon_F}^{\epsilon_F+\omega_D} \frac{d\epsilon}{2\epsilon_F - E} = \frac{1}{2}\ln\left(\frac{2\epsilon_F + 2\hbar\omega_D - E}{2\epsilon_F - E}\right) \tag{2.31}$$

We can now introduce binding energy, that which is need in order to break a pair into isolated electrons:

$$E_b = 2\epsilon_F - E \tag{2.32}$$

In the limit of $V_0\rho(\epsilon_F) \ll 1$, Eq.(2.31) yields

$$E_b = 2\hbar\omega_D \exp\left\{-\frac{2}{V_0\rho(\epsilon_F)}\right\} \tag{2.33}$$

.

We see that two electrons in a many-body system with a well-defined Fermi surface can form bound states for an arbitrarily weak attractive interaction. These states are called Cooper pairs and the binding energy E_b is the energy required to break one. Here, the condition $\hbar\omega_D \ll \epsilon_F$ is crucial, since it effectively reduces the problem from 3D to 2D. We would not reach the same conclusions in a strictly 3D system (ZAGOSKIN, 2014).

2.2.2 Multiple Cooper pairs and canonical transformations

As we recall from the preceding discussions, a naive model in which two electrons interact in isolation will only result in a bound system if such an attractive interaction is strong enough. However, when this pair of electrons is considered as part of a many-body system, the physical picture is considerably altered. We see that no interaction threshold needs to be overcome, and any value of the interaction potential, however small, will lead to the formation of a bound state (Cooper pair). Going further, we can now investigate the more realistic situation in which many pairs of electrons interact close to the Fermi surface, instead of just one.

An appropriate description of a many-electron system in which particles interact pairwise is provided by the following Hamiltonian in k-representation:

$$H = \sum_{\mathbf{k}\sigma} \xi_{\mathbf{k}} c^\dagger_{\mathbf{k}\sigma} c_{\mathbf{k}\sigma} + \frac{1}{N}\sum_{\mathbf{k}\mathbf{k}'} V_{\mathbf{k}\mathbf{k}'} c^\dagger_{\mathbf{k}\uparrow} c^\dagger_{-\mathbf{k}\downarrow} c_{-\mathbf{k}'\downarrow} c_{\mathbf{k}'\uparrow} \tag{2.34}$$

In this expression, $c^\dagger_{\mathbf{k}\sigma}$ is the creation operator for an electron with momentum $\mathbf{k}$ and spin σ. In the first part of the Hamiltonian, $\xi_{\mathbf{k}} = \epsilon_{\mathbf{k}} - \mu = \frac{\hbar^2\mathbf{k}^2}{2m} - \mu$ is the energy associated

with the single-particle state with momentum $\mathbf{k}$ measured from the Fermi energy. The second term, the interactive part of the Hamiltonian, describes how the destruction of a pair of electrons in the state $-\mathbf{k}'\downarrow, \mathbf{k}'\uparrow$ is followed by the creation of a pair in state $\mathbf{k}\uparrow, -\mathbf{k}\downarrow$. As it stands, the quartic term in the Hamiltonian renders the problem too complicated. One way around this is to introduce a mean field treatment. The appropriate mean field approach that allows for the formation of particle pairs is the Hartree-Fock-Bogoliubov mean field theory. In the standard Hartree-Fock theory, averages like $\left\langle c^\dagger_{\mathbf{k}\uparrow} c^\dagger_{-\mathbf{k}\downarrow} \right\rangle$ vanish, but in an investigation of superconductivity they must not simply disappear, since they represent the Cooper pairs.

The gap function is conveniently defined as

$$\Delta_{\mathbf{k}} \equiv \frac{1}{N} \sum_{\mathbf{k}'} V_{\mathbf{k}\mathbf{k}'} \left\langle c_{-\mathbf{k}'\downarrow} c_{\mathbf{k}'\downarrow} \right\rangle \tag{2.35}$$

With the previous modifications in mind, the Hamiltonian acquires a simplified form

$$H = \sum_{\mathbf{k}\sigma} \xi_{\mathbf{k}} c^\dagger_{\mathbf{k}\sigma} c_{\mathbf{k}\sigma} - \sum_{\mathbf{k}\mathbf{k}'} \left(\Delta_{\mathbf{k}} c^\dagger_{\mathbf{k}\uparrow} c^\dagger_{-\mathbf{k}\downarrow} + \Delta^*_{\mathbf{k}} c_{-\mathbf{k}'\downarrow} c_{\mathbf{k}'\downarrow} \right) + \sum_{\mathbf{k}} \Delta_{\mathbf{k}} \left\langle c^\dagger_{\mathbf{k}'\uparrow} c^\dagger_{-\mathbf{k}'\downarrow} \right\rangle \tag{2.36}$$

However, little information about the system can be obtained from direct inspection of this expression. Fortunately, it can be recast in a more instructive form by means of a canonical transfromation of the operators. The so-called Bogoliubov-Valatin transformation introduces new fermionic operators $\gamma^\dagger_{-\mathbf{k}\downarrow}, \gamma_{\mathbf{k}\uparrow}$ and coefficients $u_{\mathbf{k}}, v_{\mathbf{k}}$:

$$c_{\mathbf{k}\uparrow} = u^*_{\mathbf{k}} \gamma_{\mathbf{k}\uparrow} + v_{\mathbf{k}\downarrow} \gamma^\dagger_{-\mathbf{k}\downarrow} \tag{2.37a}$$

$$c^\dagger_{-\mathbf{k}\downarrow} = u_{\mathbf{k}} \gamma^\dagger_{-\mathbf{k}\downarrow} + v^*_{\mathbf{k}} \gamma_{\mathbf{k}\uparrow} \tag{2.37b}$$

We recall that the original creation and annihilation operators must satisfy certain anticommutation relations. This requirement is extended to the γ operators introduced in the transformation. Considering as an example the anticommutator of $c_{\mathbf{k}\uparrow}$ and $c^\dagger_{\mathbf{k}\uparrow}$, we obtain:

$$\left\{ c_{\mathbf{k}\uparrow}, c^\dagger_{\mathbf{k}\uparrow} \right\} = |u_k|^2 + |v_k|^2 \tag{2.38}$$

which indicates that the following normalization condition must hold:

$$|u_k|^2 + |v_k|^2 = 1. \tag{2.39}$$

Sometimes, bare fundamental particles are not the most convenient entities with which to describe a system. An electron in a many-body system, for example, is affected by the

interactions with its environment. It can be more instructive to approach this situation in a way that takes into account the many-body nature of the process from the onset. We speak then of a quasielectron: an electron *dressed* by the interactions which retains some characteristics of a fundamental electron, but can be associated with new properties (a different mass, for example). We can define other quasiparticles: collective excitations or non-trivial combinations of fundamental particles that can be treated as if they were particles (VENEMA L.; VERBERCK et al., 2016), (CHANDRAN A.; IADECOLA et al., 2023).

The role of $\gamma_{\mathbf{k}\uparrow}$ and $\gamma^{\dagger}_{-\mathbf{k}\downarrow}$ can be more easily comprehended if we solve for them in Eqs.(2.37):

$$\gamma_{\mathbf{k}\uparrow} = u_{\mathbf{k}} c_{\mathbf{k}\uparrow} - v_{\mathbf{k}} c^{\dagger}_{-\mathbf{k}\downarrow}, \tag{2.40a}$$

$$\gamma^{\dagger}_{-\mathbf{k}\downarrow} = u^{*}_{\mathbf{k}} c^{\dagger}_{-\mathbf{k}\downarrow} + v^{*}_{\mathbf{k}} c^{\dagger}_{\mathbf{k}\uparrow}. \tag{2.40b}$$

From this we see that $\gamma^{\dagger}_{-\mathbf{k}\downarrow}$ and $\gamma_{\mathbf{k}\uparrow}$ are creation and annihilation operators for quasiparticle excitations, the so-called Bogolons, which can be interpreted as a linear combination of electrons and holes (ZAGOSKIN, 2014), (KIVELSON; ROKHSAR, 1990).

Substituting Eqs.(2.37) into Eq.(2.36) yields a new effective Hamiltonian:

$$\begin{aligned} H = \sum_{\mathbf{k}} \xi_{\mathbf{k}} \Big[\Big(|u_{\mathbf{k}}|^2 - |v_{\mathbf{k}}|^2 \Big) \Big] \Big(\gamma^{\dagger}_{\mathbf{k}\uparrow} \gamma_{\mathbf{k}\uparrow} + \gamma^{\dagger}_{-\mathbf{k}\downarrow} \gamma_{-\mathbf{k}\downarrow} \Big) + 2|v_{\mathbf{k}}|^2 + 2u_{\mathbf{k}} v_{\mathbf{k}} \gamma^{\dagger}_{\mathbf{k}\uparrow} \gamma^{\dagger}_{-\mathbf{k}\downarrow} + 2u^{*}_{\mathbf{k}} v^{*}_{\mathbf{k}} \gamma_{-\mathbf{k}\downarrow} \gamma_{\mathbf{k}\uparrow} \\ + \sum_{\mathbf{k}} \Big[(\Delta_{\mathbf{k}} u_{\mathbf{k}} v^{*}_{\mathbf{k}} + \Delta^{*}_{\mathbf{k}} u^{*}_{\mathbf{k}} v_{\mathbf{k}}) \Big(\gamma^{\dagger}_{\mathbf{k}\uparrow} \gamma_{\mathbf{k}\uparrow} + \gamma^{\dagger}_{-\mathbf{k}\downarrow} \gamma_{-\mathbf{k}\downarrow} \Big) - (\Delta_{\mathbf{k}} u_{\mathbf{k}} v^{*}_{\mathbf{k}} + \Delta^{*}_{\mathbf{k}} u^{*}_{\mathbf{k}} v_{\mathbf{k}}) \Big] \\ - \sum_{\mathbf{k}} \Big[\Big(\Delta_{\mathbf{k}} u^{2}_{\mathbf{k}} + \Delta^{*}_{\mathbf{k}} v^{2}_{\mathbf{k}} \Big) \gamma^{\dagger}_{\mathbf{k}\uparrow} \gamma^{\dagger}_{-\mathbf{k}\downarrow} - (\Delta_{\mathbf{k}} u_{\mathbf{k}} v^{*}_{\mathbf{k}} + \Delta^{*}_{\mathbf{k}} u^{*}_{\mathbf{k}} v_{\mathbf{k}}) \gamma_{-\mathbf{k}\downarrow} \gamma_{\mathbf{k}\uparrow} \Big] \end{aligned} \tag{2.41}$$

This expression is reminiscent of the quantum harmonic oscillator Hamiltonian, $H_{H.O} = \hbar\omega_D \Big(\frac{1}{2} + a^{\dagger} a \Big)$, where $a^{\dagger}$ and a are the ladder operators of that system. A crucial difference lies in the terms containing the factors $\gamma^{\dagger}_{\mathbf{k}\uparrow} \gamma^{\dagger}_{-\mathbf{k}\downarrow}$ and $\gamma_{-\mathbf{k}\downarrow} \gamma_{\mathbf{k}\uparrow}$. These terms must be eliminated in order to diagonalize the Hamiltonian. This is accomplished by requiring that the $u_{\mathbf{k}}$ and $v_{\mathbf{k}}$ satisfy the following equation:

$$2\xi_{\mathbf{k}} u_{\mathbf{k}} v_{\mathbf{k}} - \Delta_{\mathbf{k}} u^{2}_{\mathbf{k}} + \Delta^{*}_{\mathbf{k}} v^{2}_{\mathbf{k}} = 0 \tag{2.42}$$

Dividing throughout by $u^{2}_{\mathbf{k}}$, we obtain a quadratic equation for the ratio $\frac{v_{\mathbf{k}}}{u_{\mathbf{k}}}$. The positive root of the solution is given by:

$$\frac{v_{\mathbf{k}}}{u_{\mathbf{k}}} = \frac{-\xi_{\mathbf{k}} + \sqrt{\xi^{2}_{\mathbf{k}} + |\Delta_{\mathbf{k}}|^{2}}}{\Delta^{*}_{\mathbf{k}}} \tag{2.43}$$

Here, it is convenient to introduce the notation $E_{\mathbf{k}} = \sqrt{\xi_{\mathbf{k}}^2 + |\Delta_{\mathbf{k}}|^2}$. An already known equation that relates $u_{\mathbf{k}}$ and $v_{\mathbf{k}}$ is the normalization condition:

$$1 = \frac{1}{|u_{\mathbf{k}}^2| + |v_{\mathbf{k}}^2|} \implies \left|u_{\mathbf{k}}^2\right| = \frac{1}{1 + \left|\frac{v_{\mathbf{k}}}{u_{\mathbf{k}}}\right|^2} \tag{2.44}$$

Substitution of Eq.(2.43) in Eq.(2.44) results is expressions for $|u_{\mathbf{k}}^2|$ and $|v_{\mathbf{k}}^2|$:

$$\left|u_{\mathbf{k}}^2\right| = \frac{1}{2}\left(1 + \frac{\xi_{\mathbf{k}}}{E_{\mathbf{k}}}\right), \tag{2.45a}$$

$$\left|v_{\mathbf{k}}^2\right| = \frac{1}{2}\left(1 - \frac{\xi_{\mathbf{k}}}{E_{\mathbf{k}}}\right), \tag{2.45b}$$

where the excitation energy is defined by

$$E_{\mathbf{k}} = \sqrt{\xi_{\mathbf{k}}^2 + |\Delta_{\mathbf{k}}|^2}. \tag{2.46}$$

In terms of the quantities calculated until now, the Hamiltonian in Eq.(2.41) can be written in a diagonalized form:

$$H = \sum_{\mathbf{k}\sigma} E_{\mathbf{k}} \gamma_{\mathbf{k}\sigma}^{\dagger} \gamma_{\mathbf{k}\sigma} + E_0 \tag{2.47}$$

with

$$E_0 = \sum_{\mathbf{k}} \left(\Delta_{\mathbf{k}} \left\langle c_{\mathbf{k}\uparrow}^{\dagger} c_{-\mathbf{k}\downarrow}^{\dagger} \right\rangle + \xi_{\mathbf{k}} - E_{\mathbf{k}}\right). \tag{2.48}$$

It is clear from Eq.(2.46) and Eq.(2.47) that a superconductor possesses a gapped excitation spectrum.

2.2.3 Gap function

We can now investigate the gap function in the light of the canonical transformations. Substituting $c_{-\mathbf{k}'\downarrow}$ and $c_{\mathbf{k}'\downarrow}$ in Eq.(2.35), we get

$$\Delta_{\mathbf{k}} = -\frac{1}{N} \sum_{\mathbf{k}'} V_{\mathbf{k}\mathbf{k}'} u_{\mathbf{k}'}^* v_{\mathbf{k}'} \left(\left\langle \gamma_{-\mathbf{k}'\downarrow}^{\dagger} \gamma_{-\mathbf{k}'\downarrow} \right\rangle - \left\langle \gamma_{\mathbf{k}'\uparrow}^{\dagger} \gamma_{\mathbf{k}'\uparrow} \right\rangle\right). \tag{2.49}$$

The Bogolons quasiparticles are of fermionic nature. Thus, they obey the Fermi-Dirac distribution:

$$\left\langle \gamma_{\mathbf{k}'\uparrow}^{\dagger} \gamma_{\mathbf{k}'\uparrow} \right\rangle = \left\langle \gamma_{-\mathbf{k}'\downarrow}^{\dagger} \gamma_{-\mathbf{k}'\downarrow} \right\rangle = \frac{1}{e^{\beta E_{k'}} + 1} \tag{2.50}$$

A quick manipulation is needed in the first expected value in Eq.(2.49):

$$\gamma_{-\mathbf{k}'\downarrow} \gamma_{-\mathbf{k}'\downarrow}^{\dagger} = \left\{\gamma_{-\mathbf{k}'\downarrow}, \gamma_{-\mathbf{k}'\downarrow}^{\dagger}\right\} - \gamma_{-\mathbf{k}'\downarrow}^{\dagger} \gamma_{-\mathbf{k}'\downarrow} = 1 - \gamma_{-\mathbf{k}'\downarrow}^{\dagger} \gamma_{-\mathbf{k}'\downarrow}. \tag{2.51}$$

Thus, combining Eqs.(2.50) and Eqs.(2.51) we get

$$\left\langle \gamma_{-\mathbf{k}'\downarrow}\gamma^{\dagger}_{-\mathbf{k}'\downarrow}\right\rangle - \left\langle \gamma^{\dagger}_{-\mathbf{k}'\downarrow}\gamma_{-\mathbf{k}'\downarrow}\right\rangle = \frac{e^{\frac{1}{2}\beta E_{k'}} - e^{-\frac{1}{2}\beta E_{k'}}}{e^{\frac{1}{2}\beta E_{k'}} + e^{-\frac{1}{2}\beta E_{k'}}} = \tanh\left(\frac{E_{\mathbf{k}'}}{2k_BT}\right) \tag{2.52}$$

We also note that $u^{*}_{\mathbf{k}'}v_{\mathbf{k}'} = |u^{2}_{\mathbf{k}'}|\frac{v_{\mathbf{k}'}}{u_{\mathbf{k}'}}$ and can be calculated from Eqs.(2.43) and Eqs.(2.45a). Ultimately, we arrive at a new expression for the gap function:

$$\Delta_{\mathbf{k}} = -\frac{1}{N}\sum_{\mathbf{k}'}\frac{V_{\mathbf{k}\mathbf{k}'}\Delta_{\mathbf{k}'}}{2E_k}\tanh\left(\frac{E_{\mathbf{k}'}}{2k_BT}\right). \tag{2.53}$$

In the traditional BCS approach, it is customary to the contact potential $V(\mathbf{r}-\mathbf{r}') = V_0\delta(\mathbf{r}-\mathbf{r}')$, which a constant in momentum space, $V_{\mathbf{k}\mathbf{k}'} = V_0$. Only the states with energy in a small interval around the Fermi level are taken into account. This is the so-called Debye window, and consists in the states that satisfy $|\xi_{\mathbf{k}}|, |\xi_{\mathbf{k}'}| < \hbar\omega_D$ ($\xi_{\mathbf{k}} = \epsilon_{\mathbf{k}} - \mu$ and ω_D is the Debye frequency). Furthermore, it is natural to look for a $\Delta_{\mathbf{k}} = \Delta$, since the potential does not depend on momentum here. With these points in mind, we arrive at

$$1 = -\frac{V_0}{N}\sum_{\mathbf{k}}\frac{1}{2E_k}\tanh\left(\frac{E_{\mathbf{k}'}}{2k_BT}\right), \tag{2.54}$$

where the sum is restricted to those states that lei inside the Debye window, otherwise it would diverge as consequence of the approximate contact potential we chose to consider (GENNES, 1966). It is convenient to make a substitution and instead integrate over energy. Because we work in the approximation that $\hbar\omega_D \ll \mu$, we can replace the density of states as a function of energy by its value at the Fermi level. Hence, we obtain

$$1 = V_0\rho_F\int_0^{\hbar\omega_D}\frac{d\epsilon}{\sqrt{\epsilon^2+\Delta^2}}\tanh\left(\frac{\sqrt{\epsilon^2+\Delta^2}}{2k_BT}\right) \tag{2.55}$$

In the particular case of $T = 0, \tanh(x\to\infty)\to 1$, Eq.(2.55) becomes

$$1 = V_0\rho_F\int_0^{\hbar\omega_D}\frac{d\epsilon}{\sqrt{\epsilon^2+\Delta^2}}. \tag{2.56}$$

If we keep only the leading term for $\Delta_0 \ll \hbar\omega_D$, we get

$$\frac{1}{V_0\rho_F} = \ln\left(\frac{2\hbar\omega_D}{\Delta_0}\right), \tag{2.57}$$

or equivalently

$$\Delta_0 = 2\hbar\omega_D e^{-\frac{1}{V_0\rho_F}}. \tag{2.58}$$

The quantity $2\Delta_0$ is the energy required to break a Cooper pair at $T = 0$. Now with a more general many-body discussion, we once again see that a gap can appear at $T = 0$ for arbitrary values of the attractive potential.

We could also investigate the case where $\Delta \to 0$ in order to determine the critical temperature T_c. The, Eq.(2.55) becomes

$$1 = V_0 \rho_F \int_0^{\hbar\omega_D} \frac{d\epsilon}{\epsilon} \tanh\Big(\frac{\epsilon}{2k_B T}\Big). \tag{2.59}$$

This integration can be carried out with the approximation $\hbar\omega_D \gg k_B T_c$ and ultimately yields

$$\frac{1}{V_0 \rho_F} = \ln\left(\frac{2\hbar\omega_D e^{\gamma_E}}{\pi k_B T_c}\right), \tag{2.60}$$

where $\gamma_E \approx 0.577$ is the Euler constant. From this, we get

$$k_B T_c = \frac{2\hbar\omega_D e^{\gamma_E}}{\pi} e^{-\frac{1}{V_0\rho_F}} \tag{2.61}$$

It is common to combine Eq.(2.58) and Eq.(2.61) in the form of a celebrated result of BCS theory, the universal ratio

$$\frac{\Delta_0}{k_B T_c} \approx 1.76. \tag{2.62}$$

2.3 SECOND QUANTIZATION

A convenient way of studying many-body systems is provided by the language of second quantization. In this formalism, we introduce the concept of field operators, represented by $\Psi_\sigma^\dagger(\mathbf{r})$ and $\Psi_\sigma(\mathbf{r})$. When acting on a state ket, $\Psi_\sigma^\dagger(\mathbf{r})$ creates a particle of spin σ at position $\mathbf{r}$ (creation operator) whereas $\Psi_\sigma(\mathbf{r})$ destroys a particle of spin σ at position $\mathbf{r}$ (annihilation operator).

These field operators obey quantization rules. In the case of bosons, the following commutation relations must be respected:

$$\Big[\Psi_\sigma(\mathbf{r}), \Psi_{\sigma'}^\dagger(\mathbf{r}')\Big] = \delta_{\sigma\sigma'}\delta(\mathbf{r}-\mathbf{r}'), \tag{2.63}$$

$$[\Psi_\sigma(\mathbf{r}), \Psi_{\sigma'}(\mathbf{r}')] = 0, \tag{2.64}$$

where the brackets represent a commutator $[A, B] = AB - BA$. For a fermionic system, similar relations hold, but now in terms of anticommutators, represented by curly brackets: $\{A, B\} = AB + BA$.

$$\Big\{\Psi_\sigma(\mathbf{r}), \Psi_{\sigma'}^\dagger(\mathbf{r}')\Big\} = \delta_{\sigma\sigma'}\delta(\mathbf{r}-\mathbf{r}') \tag{2.65}$$

$$\{\Psi_\sigma(\mathbf{r}), \Psi_{\sigma'}(\mathbf{r}')\} = 0 \tag{2.66}$$

The Hamiltonian of a general system characterized by a single-electron energy $T(\mathbf{r})$ and a potential energy function $V(\mathbf{r}, \mathbf{r}')$ can be written in the language of second quantization as:

$$H = \int d^3r \psi^\dagger(\mathbf{r}) T(\mathbf{r}) \psi(\mathbf{r}) + \frac{1}{2} \iint d^3r\, d^3r' \psi^\dagger(\mathbf{r}) \psi^\dagger(\mathbf{r}') V(\mathbf{r}, \mathbf{r}') \psi(\mathbf{r}') \psi(\mathbf{r}) \tag{2.67}$$

In the traditional conception of Cooper pairs in the BCS theory, the electrons have opposite momenta and spins: $\mathbf{k} = -\mathbf{k}'$, $\sigma' = -\sigma$. This considerably simplifies the problem.

Again, we ought to work with the mean field version of the Hamiltonian in Eq.(2.67). In the process, the pair potential is introduced

$$\Delta(\mathbf{r}) \equiv g \left\langle \psi_\uparrow(\mathbf{r}) \psi_\downarrow(\mathbf{r}) \right\rangle. \tag{2.68}$$

In terms of $\Delta(\mathbf{r})$, the interactive part of the Hamiltonian becomes

$$H_{int} = \int d\mathbf{r} \psi^\dagger_\uparrow(\mathbf{r}) \psi^\dagger_\downarrow(\mathbf{r}) \Delta(\mathbf{r}) + \Delta^*(\mathbf{r}) \psi_\downarrow(\mathbf{r}) \psi_\uparrow(\mathbf{r}) + \frac{|\Delta(\mathbf{r})|^2}{g} \tag{2.69}$$

While the single-electron part of the Hamiltonian is given by

$$H_{se} = \sum_\sigma \int d\mathbf{r} \psi^\dagger_\sigma(\mathbf{r}) \left[\frac{-\hbar^2}{2m} \left(\nabla - \frac{ie}{\hbar c} \mathbf{A} \right)^2 - \mu \right] \psi_\sigma(\mathbf{r}), \tag{2.70}$$

the chemical potential μ is included due to the gran-canonical nature of this formalism.

2.3.1 Bogoliubov-de Gennes equations

Having arrived at the mean-field Hamiltonian for superconductivity, we can now derive the Bogoliubov-de Gennes equations, that provide a general description of superconductor. This approach allows us to circumvent problems encountered when other methods are used, like the requirement for spatial homogeneity.

The total mean field Hamiltonian is, of course, $H_{BCS} = H_{se} + H_{int}$. As a first step in the derivation, we rewrite the fields in the Heisenberg picture

$$\psi_\sigma(\mathbf{r}, t) = e^{\frac{i}{\hbar} H_{BCS} t} \psi_\sigma(\mathbf{r}) e^{-\frac{i}{\hbar} H_{BCS} t}, \tag{2.71}$$

where σ represents the spin, which can be up or down. To proceed, we want to employ the equations of motion for Heisenberg fields:

$$i\hbar \frac{\partial \psi_\sigma(\mathbf{r}, t)}{\partial t} = [\psi_\sigma(\mathbf{r}, t), H_{BCS}] = e^{\frac{i}{\hbar} H_{BCS} t} [\psi_\sigma(\mathbf{r}), H_{BCS}] e^{-\frac{i}{\hbar} H_{BCS} t}. \tag{2.72}$$

With some work, we can show that

$$\left[\psi_{\uparrow}(\mathbf{r}), H_{BCS}\right] = T_x\psi_{\uparrow}(\mathbf{r}) + \Delta(\mathbf{r})\psi_{\downarrow}^{\dagger}(\mathbf{r}) \tag{2.73a}$$

$$\left[\psi_{\downarrow}(\mathbf{r}), H_{BCS}\right] = T_r\psi_{\downarrow}(\mathbf{r}) - \Delta(\mathbf{r})\psi_{\uparrow}^{\dagger}(\mathbf{r}) \tag{2.73b}$$

Taking the Hermitian conjugate of the last commutation relation, we obtain the relevant commutation relation for $\psi_{\downarrow}^{\dagger}(\mathbf{r})$:

$$\left[\psi_{\downarrow}^{\dagger}(\mathbf{r}), H_{BCS}\right] = \Delta^{*}(\mathbf{r})\psi_{\uparrow}(\mathbf{r}) - T_r^{*}\psi_{\downarrow}^{\dagger}(\mathbf{r}). \tag{2.74}$$

Therefore

$$i\hbar\frac{\partial\psi_{\uparrow}(\mathbf{r},t)}{\partial t} = T_r\psi_{\uparrow}(\mathbf{r},t) + \Delta(\mathbf{r})\psi_{\downarrow}^{\dagger}(\mathbf{r},t) \tag{2.75}$$

$$i\hbar\frac{\partial\psi_{\downarrow}^{\dagger}(\mathbf{r},t)}{\partial t} = \Delta^{*}(\mathbf{r})\psi_{\uparrow}(\mathbf{r},t) - T_r^{*}\psi_{\downarrow}^{\dagger}(\mathbf{r},t) \tag{2.76}$$

The two equations above can be rewritten as a matrix expression:

$$i\hbar\frac{\partial}{\partial t}\begin{pmatrix}\psi_{\uparrow}(\mathbf{r},t)\\ \psi_{\downarrow}^{\dagger}(\mathbf{r},t)\end{pmatrix} = \underbrace{\begin{pmatrix}T_r & \Delta(\mathbf{r})\\ \Delta^{*}(\mathbf{r}) & -T_r^{*}\end{pmatrix}}_{\mathbb{H}_{BdG}}\begin{pmatrix}\psi_{\uparrow}(\mathbf{r},t)\\ \psi_{\downarrow}^{\dagger}(\mathbf{r},t)\end{pmatrix} \tag{2.77}$$

The highlighted part in the previous equation is the Bogoliubov-de Gennes matrix differential operator. At this point, it is convenient to introduce to the coherent factors $u_{\lambda}(\mathbf{r})$ and $v_{\lambda}(\mathbf{r})$ in the eigenstates that diagonalize $\mathbb{H}_{BdG}$:

$$\begin{pmatrix}T_r & \Delta(\mathbf{r})\\ \Delta^{*}(\mathbf{r}) & -T_r^{*}\end{pmatrix}\begin{pmatrix}u_{\lambda}(\mathbf{r})\\ v_{\lambda}(\mathbf{r})\end{pmatrix} = E_{\lambda}\begin{pmatrix}u_{\lambda}(\mathbf{r})\\ v_{\lambda}(\mathbf{r})\end{pmatrix} \tag{2.78}$$

These are the Bogoliubov-de Gennes equations for $u_{\lambda}(\mathbf{r})$ and $v_{\lambda}(\mathbf{r})$. These equations provide a powerful framework for the study of superconductivity. They are particularly useful for describing inhomogeneous systems, such as the nanostructures and contacts of different materials. For a deeper understanding of the theory and applications of the Bogoliubov-de Gennes equations, see for example Zhu (2016), Gennes (1966), Altomare and Chang (2013).

2.3.2 Gor'kov equations

Another powerful set of tools in the study of superconductors are the Gor'kov equations. A well-organized discussion of this topic can be found in Fetter and Walecka (2003). The single-particle Green's function can be defined as

$$G(\mathbf{r}\tau, \mathbf{r}'\tau') = -\left\langle T_\tau[\psi_\uparrow(\mathbf{r},\tau)\psi_\uparrow^\dagger(\mathbf{r}',\tau')]\right\rangle, \tag{2.79}$$

where $\psi_\uparrow(\mathbf{r},\tau)$ is like in Eq.(2.72), but with the substitution $\tau = it$, and T_τ is the time ordering operator. We can take the partial derivative of $G(\mathbf{r}\tau, \mathbf{r}'\tau')$ with respect to τ and use the equations of motion of $\psi_\uparrow(\mathbf{r},\tau)$ and $\psi_\uparrow^\dagger(\mathbf{r}',\tau')$ in the calculations. This will yield

$$\begin{aligned} \hbar\frac{\partial}{\partial\tau}G(\mathbf{r}\tau,\mathbf{r}'\tau') &= -\hbar\delta(\mathbf{r}-\mathbf{r}')\delta(\tau-\tau') \\ -\left[-\frac{\hbar^2}{2m}\nabla^2-\mu\right]G(\mathbf{r}\tau,\mathbf{r}'\tau') &+ g\left\langle\psi_\uparrow(\mathbf{r})\psi_\downarrow(\mathbf{r})\right\rangle\left\langle T_\tau[\psi_\downarrow^\dagger(\mathbf{r},\tau)\psi_\uparrow^\dagger(\mathbf{r}',\tau')]\right\rangle. \end{aligned} \tag{2.80}$$

We are primarily interested in the cases where there is no magnetic field, $\mathbf{A} = 0$. Eq.(2.80) motivates the introduction of new quantities, the anomalous Green's functions

$$F(\mathbf{r}\tau, \mathbf{r}'\tau') = -\left\langle T_\tau[\psi_\uparrow(\mathbf{r},\tau)\psi_\downarrow(\mathbf{r}',\tau')]\right\rangle \tag{2.81}$$

and

$$F^\dagger(\mathbf{r}\tau, \mathbf{r}'\tau') = -\left\langle T_\tau[\psi_\downarrow^\dagger(\mathbf{r},\tau)\psi_\uparrow^\dagger(\mathbf{r}',\tau')]\right\rangle. \tag{2.82}$$

In the case of time-independent Hamiltonians, these Green's functions depend only on the difference $\tau - \tau'$, and the gap function can be defined as

$$\Delta(\mathbf{r}) = gF(\mathbf{r}\tau^+, \mathbf{r}\tau) = g\left\langle\psi_\uparrow(\mathbf{r})\psi_\downarrow(\mathbf{r})\right\rangle. \tag{2.83}$$

Thus, Eq.(2.80) can be written as

$$\left[-\hbar\frac{\partial}{\partial\tau}+\frac{\hbar^2}{2m}\nabla^2+\mu\right]G(\mathbf{r}\tau,\mathbf{r}'\tau')+\Delta(\mathbf{r})F^\dagger(\mathbf{r}\tau,\mathbf{r}'\tau') = \hbar\delta(\mathbf{r}-\mathbf{r}')\delta(\tau-\tau'). \tag{2.84}$$

Similar equations can be derived for $F(\mathbf{r}\tau, \mathbf{r}'\tau')$ and $F^\dagger(\mathbf{r}\tau, \mathbf{r}'\tau')$:

$$\left[-\hbar\frac{\partial}{\partial\tau}+\frac{\hbar^2}{2m}\nabla^2+\mu\right]F(\mathbf{r}\tau,\mathbf{r}'\tau') = \Delta(\mathbf{r})G(\mathbf{r}\tau,\mathbf{r}'\tau'), \tag{2.85}$$

$$\left[\hbar\frac{\partial}{\partial\tau}+\frac{\hbar^2}{2m}\nabla^2+\mu\right]F^\dagger(\mathbf{r}\tau,\mathbf{r}'\tau') = \Delta^*(\mathbf{r})G(\mathbf{r}\tau,\mathbf{r}'\tau'). \tag{2.86}$$

These are the Gor'kov equations for the normal (G) and anomalous ($F, F^\dagger$) Green's functions. If the Hamiltonian is time independent, these Green's functions depend only on $\tau - \tau'$ and can therefore be expanded in Fourier series:

$$G(\mathbf{r}\tau, \mathbf{r}'\tau') = \frac{kT}{\hbar} \sum_n e^{-i\omega_n(\tau-\tau')} G_{\omega_n}(\mathbf{r}, \mathbf{r}'), \tag{2.87}$$

$$F^\dagger(\mathbf{r}\tau, \mathbf{r}'\tau') = \frac{kT}{\hbar} \sum_n e^{-i\omega_n(\tau-\tau')} F^\dagger_{\omega_n}(\mathbf{r}, \mathbf{r}'), \tag{2.88}$$

where $\omega_n = (2n+1)\pi kT/\hbar$ for fermionic particles.

The relevant Gor'kov equations then become

$$\left[i\hbar\omega_n + \frac{\hbar^2}{2m}\nabla^2 + \mu \right] G_{\omega_n}(\mathbf{r}, \mathbf{r}') + \Delta(\mathbf{r}) F^\dagger_{\omega_n}(\mathbf{r}, \mathbf{r}') = \hbar\delta(\mathbf{r} - \mathbf{r}'), \tag{2.89}$$

$$\left[-i\hbar\omega_n + \frac{\hbar^2}{2m}\nabla^2 + \mu \right] F^\dagger_{\omega_n}(\mathbf{r}, \mathbf{r}') - \Delta^*(\mathbf{r}) G^\dagger_{\omega_n}(\mathbf{r}, \mathbf{r}') = 0, \tag{2.90}$$

together with the self-consistency condition

$$\Delta^*(\mathbf{r}) = \frac{gkT}{\hbar} \sum_n F^\dagger_{\omega_n}(\mathbf{r}, \mathbf{r}). \tag{2.91}$$

3 NANOSCALE SUPERCONDUCTIVITY

One might wonder how the properties of a superconductor would change if the shape of the sample deviated from the simpler homogeneous 3D configuration. What would happen if the size of a superconductor was drastically reduced in one or more directions, leading to geometries like nanofilms, nanowires or nanograins? Some early investigations in this field were carried out by Blatt and Thompson, who studied superconductivity in nanofilms with a multiband BCS model (BLATT; THOMPSON, 1963; THOMPSON; BLATT, 1963). Their work showed that confining particle motion along the transverse direction of the superconducting nanofilms to nanoscales indeed led to remarkable new physics. However, this field could not immediately be properly explored, since it was not possible to produce the required nanosamples with satisfactory quality. This picture has changed in more recent decades as advances in nanofabrication technology made it possible to create metallic structures in nanometric scales while maintaining reduced impurity concentration. Improvement has also been made on theoretical grounds, with the introduction of the Bogoliubov-de Gennes formalism to scene. The Bogoliubov-de Gennes equations are the adequate tools to study inhomogeneous systems such as nanofilms and nanowires and are more accurate than Blatt and Thompson's original model.

In a material containing impurities, the electron mean free path l is the typical distance an electron will travel between collisions with impurities or with the sample boundaries. Experimental investigations involving nanostructures synthesized with modern techniques show that l scales with the confined dimension of the sample, d (the thickness of a nanofilm, for instance), instead of l_{imp}, the electron mean free path due to scattering by nonmagnetic impurities. In one of these studies, for example, an approximation of the kind $\frac{1}{l} \approx \frac{1}{2d} + \frac{1}{l_{imp}}$ was found to be applicable to the system (ÖZER et al., 2007). In this case, the term $\frac{1}{2d}$ represents the contribution of the boundaries, and $\frac{1}{l_{imp}}$, the contribution due to nonmagnetic impurities. For such nanostructures, the scaling $l \propto d$ indicates that l is dominated by boundary scattering and, consequently, $l_{imp} \gg d$ and $k_F l_{imp} \gg 1$, where k_F is the three dimensional Fermi wave vector. Thus, the available technology is indeed capable of producing nanowires and nanofilms with minor impurity content, insufficient to smear the transverse electron spectrum.

A long established result is that a small amount of impurity will not result in an appreciable alteration in the equilibrium properties of a superconductor (ANDERSON, 1959), (CROITORU;

SHANENKO et al., 2009). Therefore, the high quality superconducting nanostructures considered here can be taken to be in the clean limit.

In summary, electron motion in such systems is confined to a very narrow region in the transverse direction, but is unimpeded in other directions. The consequence of this confinement is the splitting up of the conduction band into a series of subbands. The idea is conceptually similar to formation of discrete energy levels when a particle is confined to a quantum well. As pointed out above, sufficiently clean samples can be fabricated, such that this transverse spectrum will not be smeared by impurity. The energy of each subband decreases as the thickness of the system increases. Thus, by varying the thickness of the superconductor these subbands can be made to sequentially cross the Fermi surface. Every time this happens, the number of single-electron states near the Fermi level (inside the Debye window) increases dramatically. As the size of the system along the confining direction continues to be changed, the density of states inside the Debye window drops again, until the bottom of the next subband reachs the Fermi surface. Clearly, what arises from this is an oscillatory pattern of the density of states near the Fermi level. Each instance of rapid increase in this quantity is called a shape resonance.

An important result of BCS theory for a 3D homogeneous superconductor establishes the manner in which the energy gap Δ_0 and critical temperature T_c depend on the electronic density of states at the Fermi level, $N(0)$:

$$\Delta_0 = 1.76T_c = 1.14\hbar\omega_D e^{-1/N(0)g} \tag{3.1}$$

It is easy to see that due to the exponential dependence, even a slight variation in $N(0)$ would lead to substantial changes in Δ_0 and T_c. Although this expression cannot be expected to hold exactly for systems with reduced dimensions, the general trend indicates that oscillations in the density of states $N(0)$ have a dramatic effect on superconducting properties.

3.1 EARLY TREATMENT

The investigations of such oscillatory behavior of superconducting properties in nanostructures was pioneered by Blatt and Thompson in the early 1960s. They considered a superconducting clean slab described in the BCS multiband model (THOMPSON; BLATT, 1963). Their analyses revealed that the energy gap parameter exhibits a series of periodic spikes as a function of slab thickness.

If the system under investigation is a 2D film limited in the z direction by $z = 0$ and $z = a$ but unlimited in the x and y directions, translational symmetry in the plane of the film implies that the wavefunctions in the x and y directions are plane waves subject to periodic boundary conditions, with periodicity L. Thus, the fundamental one-electron wavefunction has the form

$$\phi_{n,\mathbf{k}_\perp}(\mathbf{r}) = \frac{1}{L} e^{i(k_x x + k_y y)} w_n(z) = \frac{1}{L} e^{i\mathbf{k}_\perp \cdot \mathbf{r}_\perp} w_n(z), \tag{3.2}$$

where $\mathbf{r}_\perp$ is a general vector in the plane perpendicular to the z-axis. In the transverse direction, the wavefunctions vanish at the boundaries:

$$w_n(0) = 0 = w_n(a). \tag{3.3}$$

The eigenenergy, measured from the Fermi level, is

$$\epsilon_{n,\mathbf{k}_\perp} = \eta_n + \frac{\hbar^2 \mathbf{k}_\perp^2}{2m}. \tag{3.4}$$

Ultimately, the relevant equation to be solved is

$$-\frac{\hbar^2}{2m} \frac{d^2 w_n}{dz^2} = (\eta_n + \mu) w_n. \tag{3.5}$$

Next, it is necessary to examine how wavefunctions of the form (3.2) combine in pairs in the superconducting state. Blatt and Thompson adopted the usual point contact attractive interaction, taking the necessary care to avoid the divergence that may arise from this. As suggested by Anderson (1959), the pairing takes place between the time reversed states $(n, \mathbf{k}_\perp, \uparrow)$ and $(n, -\mathbf{k}_\perp, \downarrow)$. The energy gaps Δ_n is calculated from the usual self-consistency equation in terms of w_n. This quantity is, of course, independent of k_x and k_y due to the translational invariance in the xy plane. Moreover, the chemical potential μ can be obtained from the electron density N/V (N is the total number of electrons in the volume aL^2). With these points in mind, Blatt and Thomson obtained and solved numerically a complete set of equations for Δ_n and μ. The dependence of the energy gap Δ_n on slab thickness is shown in Figure 1, for $N/V = 2 \times 10^{22} cm^{-3}$, $gN(0) = 0.3$ and $\hbar\omega_D/k_B = 100K$.

As each $\eta_n(z)$, energy level for motion in the transverse direction, passes through the Fermi surface, a new spike appears in the Δ_n plot. The horizontal line marks the bulk value of the gap energy, Δ_{bulk}. The figure shows the impressive increase in Δ_n above Δ_{bulk} at the resonant points. A new value of n starts to contribute at each new resonance. The plots of Δ_1 through Δ_4 are shown for small thicknesses, but above the second peak only the lowest and highest values of the energy gap are presented.

Figure 1 – Shape resonances in the superconducting energy gaps, Δ_n, as a function of film thickness. A new Δ_n starts to contribute at each resonant thickness. The horizontal line indicates the bulk value Δ_∞.

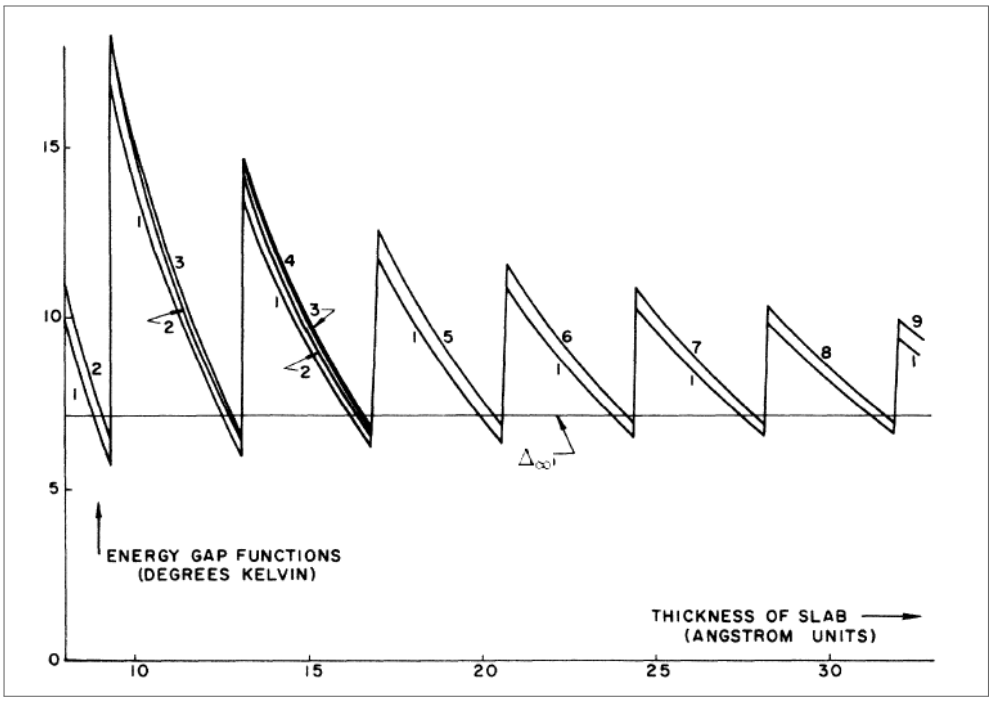

Source: Blatt and Thompson (1963)

The energy gap increases too steeply at resonances. The sharpness of this increase is determined by the size of the Debye window, as shown in Figure 2, where the emergence of the second peak of Figure 1 is shown in greater detail. The new energy gap contribution is given by Δ_4 and starts at $\eta_4 - \mu = 100\ \mathrm{K}$, that is, when a new energy level η_n enters the Debye window.

Figure 2 – A more detailed view of the second peak in Figure 1, showing the sharp transition into the resonant regime and the emergence of a new gap, Δ_4.

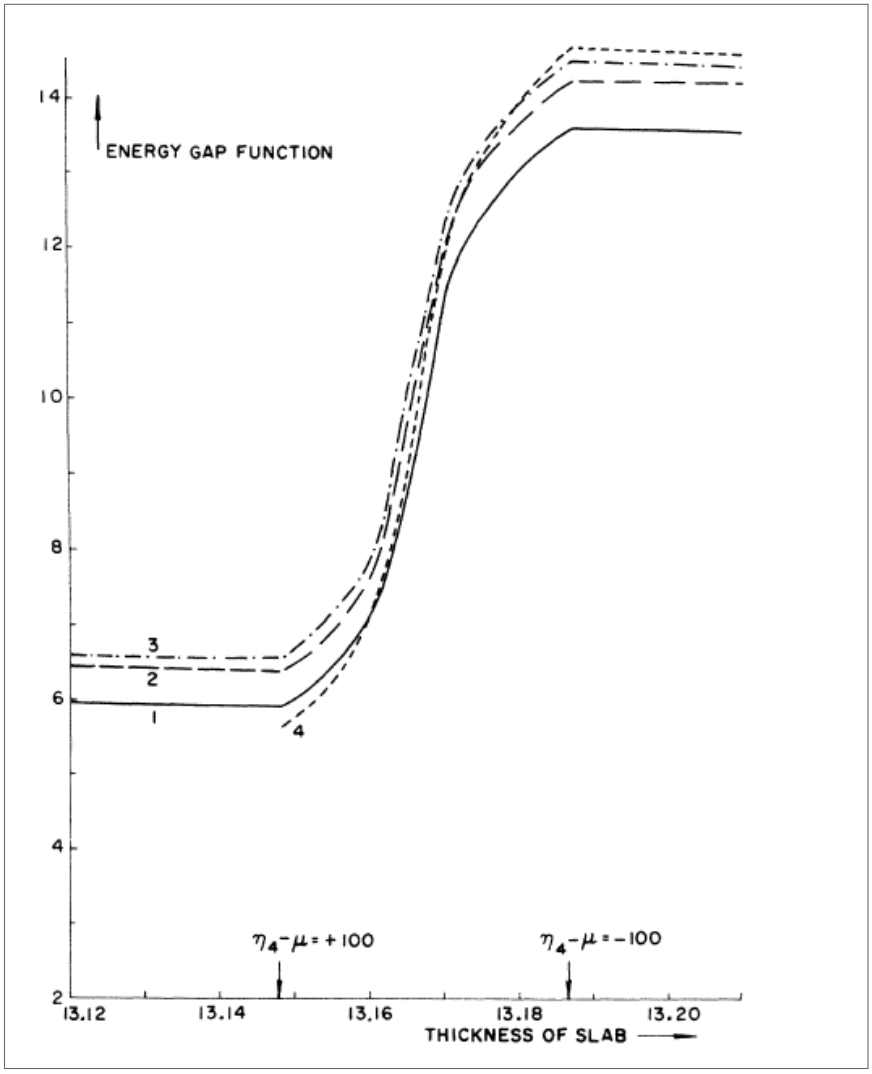

Source: Blatt and Thompson (1963)

3.2 TREATMENT IN THE BOGOLIUBOV-DE GENNES FORMALISM

Although the studies by Blatt and Thompson yielded interesting results, the simplified multiband BCS model they employed is not the most appropriate formalism for highly inhomogeneous systems as nanofilms. The need for a good microscopic description is fulfilled, as discussed previously, by the Bogoliubov-de Gennes (BdG) formalism. Shanenko, Croitoru and Peeters have investigated superconductivity in nanofilms and nanowires by self-consistently solving the BdG equations in such geometries. In this manner, they have been able to study the previously unexplored relationship of the critical temperature T_c with the governing parameters when the system is subjected to quantum confinement. They have also been able to make more direct comparisons of theory and experiment, among other advantages over older

approaches. A brief but systematic comparison of the Bogoliubov-de Gennes method and that employed but Blatt and Thompson can be found in Croitoru, Shanenko and Peeters (2007a). Expositions of the methods and results presented here can be found in Peeters, Shanenko and Croitoru (2009) and in Altomare and Chang (2013)

As a simplifying assumption, the detailed band structure of the materials is disregarded, and is instead approximated by a parabolic dependence on the momentum $\mathbf{k}$ of the form $\frac{\hbar^2 k^2}{2m^*}$, where m^* is the effective band mass, which is set to the free-electron mass in the calculations. This is the so-called parabolic band approximation. This approach, however, can lead to results that do not really match the experimental measurements. The way to avoid this problem is to work with an effective Fermi level instead of the real one (SHANENKO; CROITORU; PEETERS, 2007; WEI; Y., 2002).

We recall that the BdG equations for the eigenfunctions $u_i(\mathbf{r})$ and $v_i(\mathbf{r})$ have the form

$$\begin{aligned} E_i u_i(\mathbf{r}) &= \left(-\frac{\hbar^2}{2m}\nabla^2 + U(\mathbf{r}) - \mu\right) u_i(\mathbf{r}) + \Delta(\mathbf{r}) v_i(\mathbf{r}), \\ E_i v_i(\mathbf{r}) &= \Delta(\mathbf{r}) u_i(\mathbf{r}) - \left(-\frac{\hbar^2}{2m}\nabla^2 + U(\mathbf{r}) - \mu\right) v_i(\mathbf{r}), \end{aligned} \tag{3.6}$$

where $U(\mathbf{r})$ and $\Delta(\mathbf{r})$ are the normal and anomalous mean-field potentials, respectively, and are given by

$$U(\mathbf{r}) = -g \sum_i \left[|u_i(\mathbf{r})|^2 f_i + |v_i(\mathbf{r})|^2 (1 - f_i) \right], \tag{3.7}$$

$$\Delta(\mathbf{r}) = g \sum_{|\xi_i| < \hbar\omega_D} u_i(\mathbf{r}) v_i^*(\mathbf{r}) (1 - 2f_i), \tag{3.8}$$

where, as usual, $f_i = f_i(E_i)$ is the Fermi function and g is the coupling constant. For $U(\mathbf{r})$, the sum in Eq.(3.7) runs over all positive energy states. In Eq.(3.8), on the other hand, the sum must be restricted to single-electron energy states ξ_i inside the Debye window, $|\xi_i| < \hbar\omega_D$, otherwise this sum would be divergent (GENNES, 1966). The single-electron energy is given by

$$\xi_i = \int d^3r \left[u_i^*(\mathbf{r}) \left(-\frac{\hbar^2}{2m}\nabla^2 + U(\mathbf{r}) - \mu\right) u_i(\mathbf{r}) + v_i^*(\mathbf{r}) \left(-\frac{\hbar^2}{2m}\nabla^2 + U(\mathbf{r}) - \mu\right) v_i(\mathbf{r}) \right], \tag{3.9}$$

and the chemical potential is calculated from the mean electron density n_e:

$$n_e = \frac{2}{V} \sum_i \int d^3r \left[|u_i(\mathbf{r})|^2 f_i + |v_i(\mathbf{r})|^2 (1 - f_i) \right] \tag{3.10}$$

As explained in Chapter 13 of Fetter and Walecka (2003), in the spatially homogeneous case the Hartree-Fock contribution $U(\mathbf{r})$ may be ignored, under the assumption that it does

not change from the normal to the superconducting phase. Shanenko, Croitoru and Peeters (2007) argue that this is also valid in the case of nanofilms. Taking $U(\mathbf{r})$ into account amounts only to very small changes in $\Delta(\mathbf{r})$, which allows one to simply set $U = 0$. The role of the Hartree-Fock potential in nanowires is more systematically explored in Chen et al. (2009).

When solving differential equations numerically, a useful technique is the expansion of the sought-after solution in terms of a set of $\mathcal{N}$ basis functions. We might, for example, be interested in determining the wavefunction in some quantum mechanical problem, as is the case here. This wavefunction can be viewed as a state vector in a Hilbert space. A complete description of the wavefunction would generally require expansion in an infinite number of basis states. If, however, the basis functions are conveniently chosen, an accurate representation can be achieve with a finite and manageable number $\mathcal{N}$ of basis functions. The desired wavefunction can now be represented by a vector containing its expansion coefficients and the whole original differential equation is recast as an eigenvalue problem, which can be solved with the use of well-known numerical techniques.

3.2.1 Nanofilms

To illustrate how the techniques presented above are implemented, we first consider a nanofilm with dimensions $L_x,\ L_y \text{ and } L_z$, such that $L_z \ll L_x, L_y$. Periodic boundary conditions are imposed in the plane of the nanofilm, as was done by Blatt and Thompson, and the spatial dependence of the energy gap is limited to transverse direction: $\Delta(\mathbf{r}) = \Delta(z)$. The electron-like and hole-like wavefunctions can thus be written in the form:

$$u_{k_x k_y j}(\mathbf{r}) = \frac{e^{ik_x x}}{\sqrt{L_x}} \frac{e^{ik_y y}}{\sqrt{L_y}} \tilde{u}_{k_x k_y j}(z) \tag{3.11a}$$

$$v_{k_x k_y j}(\mathbf{r}) = \frac{e^{ik_x x}}{\sqrt{L_x}} \frac{e^{ik_y y}}{\sqrt{L_y}} \tilde{v}_{k_x k_y j}(z) \tag{3.11b}$$

The normalization for $u_j(\mathbf{r})$ and $v_j(\mathbf{r})$ leads to an equivalent expression for $\tilde{u}_i(z)$ and $\tilde{v}_i(z)$:

$$\int dz \left[|\tilde{u}_i(z)|^2 + |\tilde{v}_i(z)|^2 \right] = 1. \tag{3.12}$$

The confinement of electrons in the transverse direction can be expressed through the boundary conditions

$$\tilde{u}_i(0) = \tilde{u}_i\left(L_z\right) = 0, \quad \tilde{v}_i(0) = \tilde{v}_i\left(L_z\right) = 0, \tag{3.13}$$

which suggest as suitable basis functions for the expansion of $\tilde{u}_i(z)$ and $\tilde{v}_i(z)$ the quantum well states (QWS) given by

$$\varphi_l(z) = \sqrt{\frac{2}{L_z}} \sin\left[\frac{\pi(l+1)z}{L_z}\right] \tag{3.14}$$

Thus, the electron-like and hole-like wavefunctions can be written as

$$\tilde{u}_i(z) = \sum_l \tilde{u}_i^{(l)} \varphi_l(z), \quad \tilde{v}_i(z) = \sum_l \tilde{v}_i^{(l)} \varphi_l(z) \tag{3.15}$$

The coefficients of this expansion are given by

$$\tilde{u}_i^{(l)} = \int_0^{L_z} dz \varphi_l^*(z) \tilde{u}_i(z), \quad \tilde{v}_i^{(l)} = \int_0^{L_z} dz \varphi_l^*(z) \tilde{v}_i(z), \tag{3.16}$$

and the BdG equations get the form

$$\left[\frac{\hbar^2}{2m}\left(\frac{\pi^2(l+1)^2}{L_z^2} + k_x^2 + k_y^2\right) - \mu\right] \tilde{u}_i^{(l)} + \sum_{l'} \Delta_{ll'} \tilde{v}_i^{(l')} = E_i \tilde{u}_i^{(l)}, \tag{3.17a}$$

$$\left[\mu - \frac{\hbar^2}{2m}\left(\frac{\pi^2(l+1)^2}{L_z^2} + k_x^2 + k_y^2\right)\right] \tilde{v}_i^{(l)} + \sum_{l'} \Delta_{ll'} \tilde{u}_i^{(l')} = E_i \tilde{v}_i^{(l)}, \tag{3.17b}$$

with

$$\Delta_{ll'} = \int dz \varphi_l^*(z) \Delta(z) \varphi_{l'}(z) \tag{3.18}$$

These equations can now be approached numerically as an eigenvalue problem.

Only electrons in the vicinity of the Fermi level make relevant contributions to the superconducting state. The scale of such vicinity is set by the Debye energy $\hbar\omega_D$. Confinement of electron motion in the transverse direction leads to the splitting of the band of single-electron states into a series of subbands, the energy of which varies as thickness is changed. If the bottom of such subbands is made to cross the Fermi surface, the number of single-electron states near the Fermi level increases significantly. This effect is, of course, less pronounced as the dimensions of the system approach bulk values. Thus, the density of single-electron states per unit volume and spin projection develops into a series of damped oscillations as thickness increases. This tendency then extends to other characteristic quantities of the superconductor that have some relation to the density of states.

The behaviour of T_c/T_{bulk}, for example, is shown in Figure 3. In the numerical procedure, T_c is calculated as the first temperature value for which $\Delta(z) = 0$. At the resonant points, T_c is considerably higher than T_{bulk}, but steadily decreases at off-resonant points, at times even

Figure 3 – Critical temperature T_c, relative to the bulk value $T_{c,bulk}$, as a function of film thickness for superconducting nanofilms of several materials: cadmium (Cd), aluminum (Al), tin (Sn) and lead (Pb).

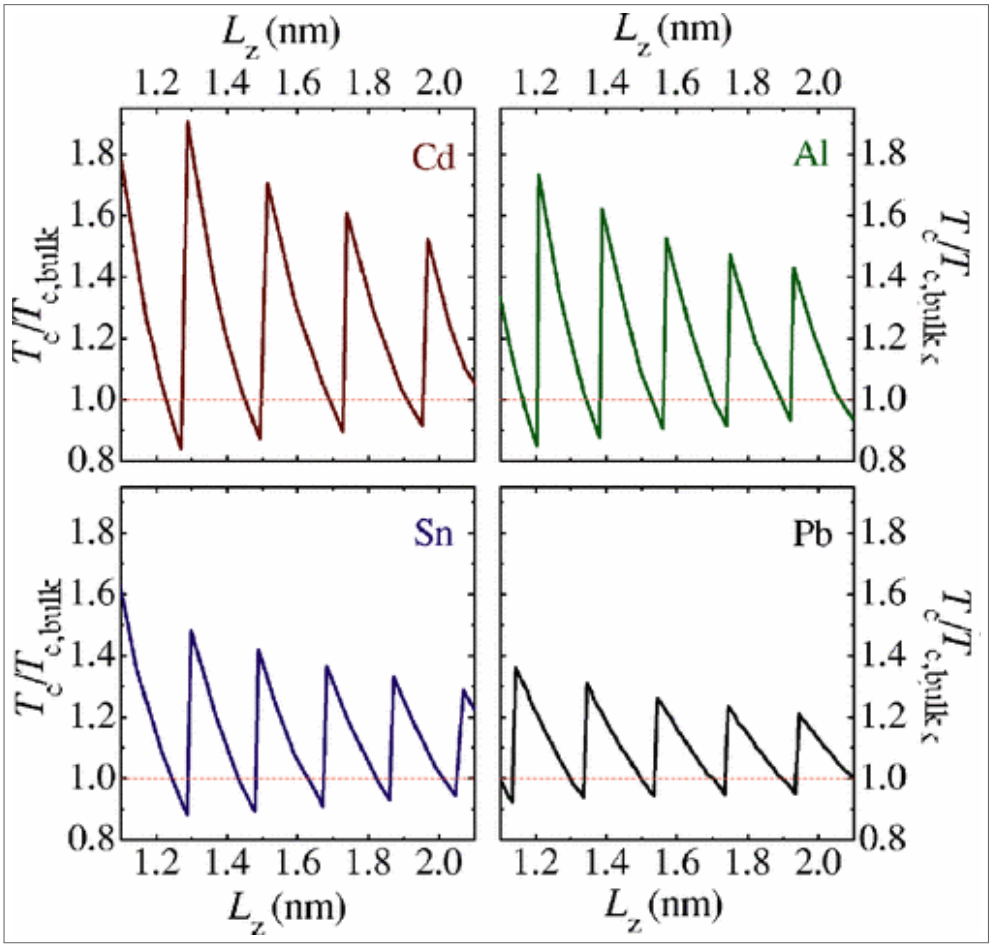

Source: Shanenko, Croitoru and Peeters (2007)

becoming smaller than T_{bulk}. The magnitude of the enhancements at resonances, however, is much larger than the drops bellow T_{bulk}.

The governing parameters behind the shape resonances in Figure 3 are ω_D, g and μ_{bulk}. The quantity $N_{bulk}(0)$, in Table 1, is ultimately determined by μ_{bulk}, as $N_{bulk}(0) = mk_F/2\pi\hbar^2$, and, for $T < T_c$, the chemical potential does not change appreciably with temperature, so that the $3\mathrm{D}$ Fermi wave number is given by $k_F = \sqrt{2m\mu_{bulk}}/\hbar$. Increasing any of these governing parameters leads to a reduction in the amplitudes of the oscillations, as can be seen by comparing the data in Table 1 with the plots in Figure 3: the oscillations are most pronounced in cadmium; in aluminum (Al), the reduction is due to a bigger Debye window, and in lead (Pb) and tin (Sn), it is a consequence of higher values of the coupling constant.

The dependence of the density of states at Fermi level, $\mathrm{N}(0)$, on film thickness in shown in Figure 4. The quantity $\mathrm{N}(0)$ is the number of single-electron states in the Debye window,

Table 1 – Governing nanofilm parameters

Metal	$\hbar\omega_D/k_B$	$gN_{bulk}(0)$	Femi level
Cd	164 K	0.18	7.47 eV
Al	375 K	0.18	11.7 eV
Sn	195 K	0.25	10.2 eV
Pb	96 K	0.39	9.47 eV

Source: The author (2022)

Figure 4 – Density of single-electron states at the Fermi level $N(0)$ relative to the bulk value $N_{bulk}(0)$ vs film thickness, for nanofilms of aluminum (Al) and tin (Sn).

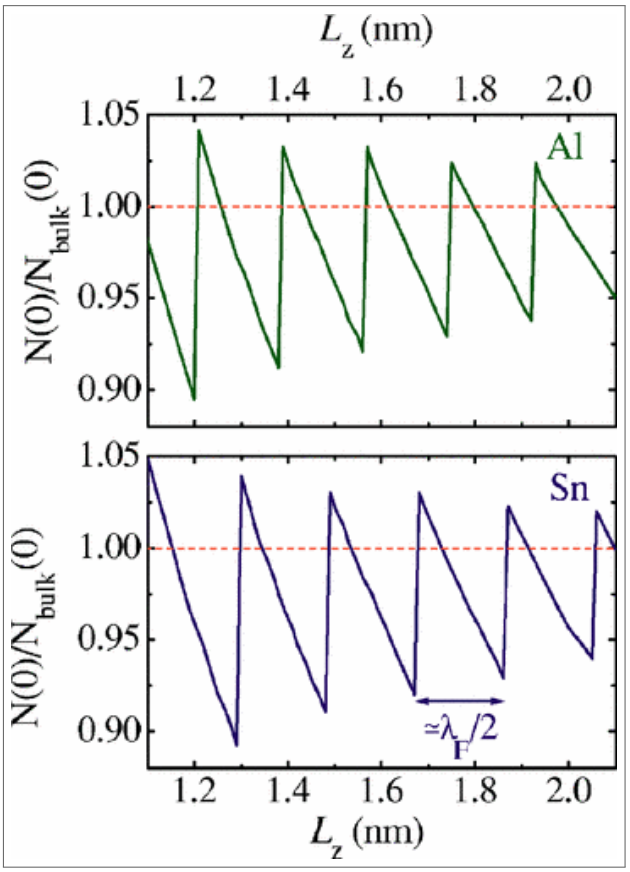

Source: Shanenko, Croitoru and Peeters (2007)

divided by $2\hbar\omega_D$ and V, volume of the slab. We note that, contrary to what is observed for T_c, the drops of $\mathrm{N}(0)$ bellow $\mathrm{N}_{\mathrm{bulk}}$ are much more pronounced that the enhancements at resonant points. The periodicity of such oscillations is numerically determined to be approximately $\lambda_F/2$, where λ_F is the $3\mathrm{D}$ Fermi wavelength, $\lambda_F = 2\pi/k_F$. This can be understood with the help of the quantum well states of Eq.(3.14). Although single-electron states in the absence

of interactions are not the same as the states in the presence of Cooper pairing, they are close enough to allow an analysis of oscillations of superconductor properties in terms of $\varphi_l(z)$. Mathematically, the crossing of the Fermi level by one such QWS is represented by

$$\frac{\hbar^2\pi^2\,(l+1)}{2mL_z^2} = \mu \tag{3.19}$$

where the left-hand side is the energy associated with $\varphi_l(z)$. The resonant thickness is then given by

$$L_z = \frac{\hbar\pi(l+1)}{\sqrt{2m\mu}}. \tag{3.20}$$

Thus, two consecutive resonances are separated by a thickness difference of

$$\Delta L_z = \frac{\hbar\pi}{\sqrt{2m\mu}} = \frac{\pi}{k_F} = \frac{\lambda_F}{2}. \tag{3.21}$$

3.2.2 Nanowires

The methods presented in the previous section are also applicable to nanowires. We can take as an example a cylindrical nanowire in the clean limit and in the absence of magnetic fields. The nanowire has radius R and periodic boundary conditions are imposed in the longitudinal direction, with periodicity length L. The most natural way to describe such a system is in the cylindrical coordinates ρ, φ, z. Thus, the electron-like and hole-like eigenfunctions may be written as

$$\begin{pmatrix} u_i(\mathbf{r}) \\ v_i(\mathbf{r}) \end{pmatrix} = \frac{e^{im\phi}}{\sqrt{2\pi}}\frac{e^{ikz}}{\sqrt{L}} \begin{pmatrix} u_i(\rho) \\ v_i(\rho) \end{pmatrix}, \tag{3.22}$$

where the wavefunction label i is understood to be of the form $i = (j, m, k)$, in which j stands for the quantum number in the radial direction, m the quantum number in the azimuthal direction, and k the wave vector in the logitudinal z-direction. Confinement of the electrons in the radial direction implies the boundary conditions:

$$u_i(\rho = R) = 0 = v_i(\rho = R) \tag{3.23}$$

Hence, in such a cylindrically symmetric system, normalized Bessel functions $\vartheta_n(\rho)$ provide a convenient set of basis functions for the expansion of $u_i(\mathbf{r})$ and $v_i(\mathbf{r})$:

$$\begin{pmatrix} u_i(\rho) \\ v_i(\rho) \end{pmatrix} = \sum_n \begin{pmatrix} u_n^i \\ v_n^i \end{pmatrix} \vartheta_n(\rho) \tag{3.24}$$

with

$$\vartheta_n(\rho) = \frac{\sqrt{2}}{RJ_{m+1}(\alpha_{mn})} J_m\Big(\frac{\alpha_{mn}\rho}{R}\Big). \tag{3.25}$$

where J_m is the Bessel function of the first kind of order m and α_{mn} is the n^{th} zero of J_m. The multiplicative factor in Eq.(3.25) is chosen so that the $\phi_l(\rho)$ are normalized.

The order parameter only varies in the transverse direction, so $\Delta(\mathbf{r}) = \Delta(\rho)$.

These expressions for $u(\mathbf{r})$ and $v(\mathbf{r})$ given by Eqs.(3.22) and (3.24) can now be substituted in the Bogoliubov-de Gennes equations. Those equations are then multiplied by some new $\vartheta_{n'}(\rho)$ and integrated from 0 to R, resulting in

$$\Big(T_n^i - E_i\Big)\, u_n^i + \sum_{n'} \Delta_{nn'} v_{n,}^i \tag{3.26a}$$

$$\Big(E_i - T_n^i\Big)\, v_n^i + \sum_{n'} \Delta_{nn'} u_n^i, \tag{3.26b}$$

in which

$$T_n^i = \frac{\hbar^2}{2m}\left[\frac{\alpha_{mn}^2}{R^2} + k^2\right] - \mu \tag{3.27}$$

and

$$\Delta_{nn'} = \int d\rho \vartheta_{n'}(\rho)\Delta(\rho)\vartheta_n(\rho). \tag{3.28}$$

Once again, this set of coupled equations for u_n^i and v_n^i can be interpreted as a matrix equation. The problem is solved iteratively, at each step diagonalizing the governing matrix to obtain values for u_n^i, v_n^i, E_i and $\Delta_{nn'}$. The process goes on until self-consistency is achieved.

Some results obtained with this method are presented in Figure 5. They correspond to aluminum (Al) nanowires, with $gN(0) = 0.18$ and $\hbar\omega_D/k_B = 195$ K, at $T = 0$ K and two different values of electron density n_e. The quantities Δ_R and μ_R are the averages of $\Delta(\rho)$ and μ, respectively, taken over the wire cross-section. The oscillatory pattern of the superconducting gap is again present and the amplitudes of the shape resonances of Δ_R above the bulk value are even higher then those observed in nanofilms, but less regular.

3.2.3 Binding Energy of Cooper pairs in Nanostructures

We have seen in Chapter 2 how Cooper approached the problem of the interaction of two electrons above the Fermi surface. Working with electrons of opposite momenta and spins in a three-dimensional system, one can show that their binding energy is given by (see Chapter

Figure 5 – Superconducting energy gap Δ_R and chemical potential μ_R, relative to their respective bulk values, as functions of nanowire radius R. The data corresponds to an aluminum (Al) nanowire at $T = 0\ K$. For the panels on the left, $n_e = 3.878\ nm^{-3}$ and $\mu_{bulk} = 900\ meV$. For those on the right, $n_e = 20\ nm^{-3}$ and $\mu_{bulk} = 2687\ meV$.

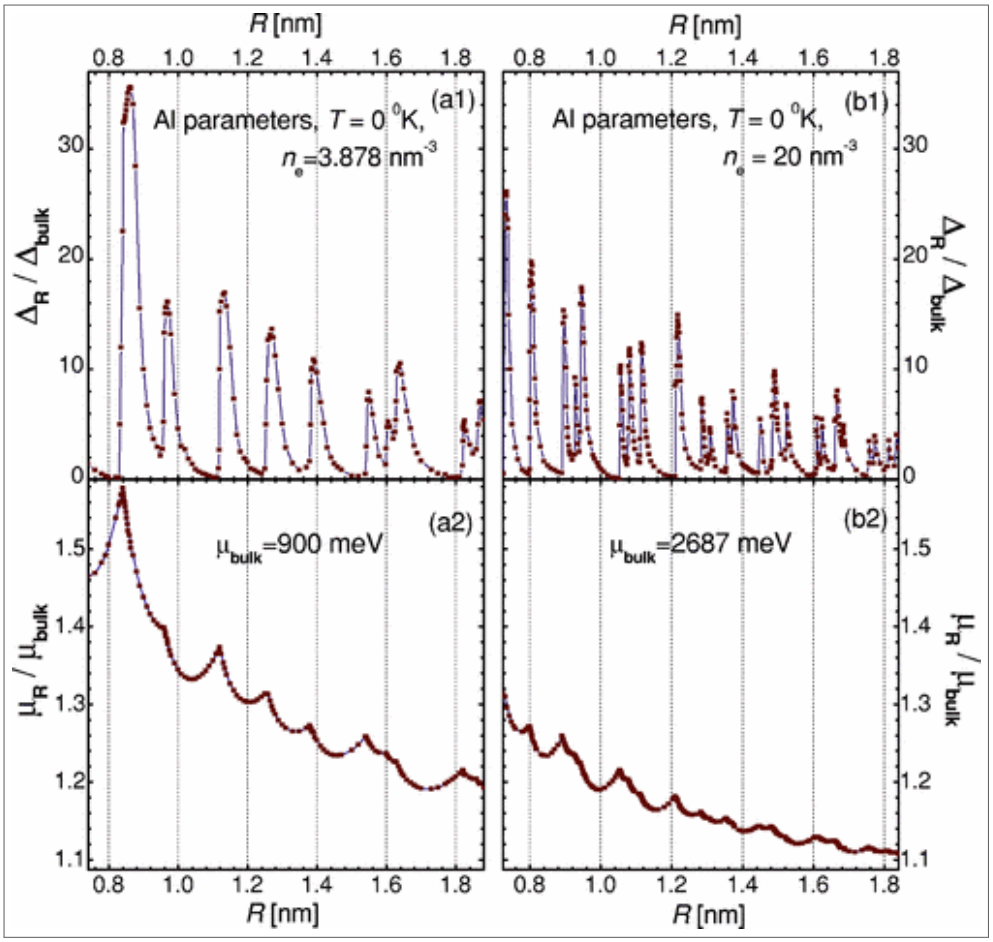

Source: Shanenko and Croitoru (2006)

2 and Tinkham (1996)):

$$E_0 = -2\hbar\omega_D \exp\left(-\frac{2}{gN(0)}\right) \tag{3.29}$$

Any attractive interaction, however weak, will lead to the formation of a bound pair. If the momenta of the two electrons is not exactly opposite, the strength of their binding energy will be somewhat weaker.

One might now inquire how the introduction of quantum confinement of the charge carriers in the problem would modify this result. Croitoru et al. (2012) set out to do just that. As already pointed, in the presence of quantum confinement the band of single-electron states is divided into a series of subbands, the energy of which changes as the thickness of the system is altered. They found that when the bottom of a subband reaches the Fermi surface, the binding energy of a Cooper pair increases considerably.

Also significant is the calculation of the size of a Cooper pair along the non-confined

direction. It is given by

$$\xi_C^2 = \frac{\hbar^2}{8mE_0} \tag{3.30}$$

From this, we see that at size resonances E_0 is significantly enhanced, and thus the corresponding Cooper pair size (along the non-confined direction) will diminish considerably.

4 PROXIMITY EFFECT

4.1 OVERVIEW

If a superconductor (S) is put in good electrical contact with a normal metal (N), Cooper pairs can diffuse into the latter, leading that material to manifest superconductor-like properties, such as the ability to maintain a supercurrent and a lower density of states near the Fermi level. Conversely, the strength of superconductivity in the S region is reduced close to the interface. This apparent dilution of superconducting order from S into N is called the proximity effect.

In the process of setting up an experiment to study the proximity effect, some precautions are necessary in order to have a SN contact that can actually be considered good:

i) materials that form intermetallic compounds should not be used, as this would lead to anomalies in the system's transition temperature (CHIOU; KLOKHOLM, 1964).

ii) The atoms from one of the materials should not be able to migrate into the other, i.e, their mutual solubility should be the lowest possible, otherwise impurity is introduced in the vicinity of the SN boundary and the mean free path is altered (ROSE-INNES; SERIN, 1961).

iii) Care must be taken to avoid moisture in the environment. If the system is exposed to moisture, the more anodic of the metals will be oxidized at the boundary (HAUSER; THEUERER; WERTHAMER, 1966).

The first indications of the proximity effect were detected as early as in the 1930s, by Holm and Meissner (1932), who studied the electrical resistance of contacts of two metals separated by an oxide layer. They observed that when the temperature is sufficiently reduced, allowing one of the metals to become superconducting, the resistance of the second metal greatly decreases, suggesting the induction of superconducting correlations in the normal metal. Later experiments corroborated the idea that superconducting correlations can be induced in normal metals (BEDARD; MEISSNER, 1956; MEISSNER, 1958; SMITH et al., 1961). Meissner (1960) observed that a supercurrent can be maintained between two superconducting samples separated by a normal metal (an SNS junction) for N with thickness up to 100 nm.

Hilsch (1962) found that the transition temperature of a superconductor is greatly reduced when it is in contact with a normal metal. This demonstrates that superconductivity is weakened in the vicinity of a normal metal (this aspect of the proximity effect is sometimes called the inverse proximity effect).

A review of early experimental investigations of the proximity effect and their relationships to theory is provided by Clarke (1968). The first theoretical studies were based on the Ginzburg-Landau theory and on the linearized Gor'kov equations, both valid close to the critical temperature. Important early contributions were made by de Gennes and partners (GENNES; GUYON, 1963; GENNES, 1964). A good review of the theory of proximity effect in SN junctions can be found in Deutscher and Gennes (1969). See also Wolf (2012) and Estève et al. (1996).

Several studies of the proximity effect focus on the spatial variation of the order parameter across the SN interface and how it decays on the normal region. For a bulk system with an interface lying at $z = 0$ perpendicularly to the z-axis, the pair potential depends only on the z coordinate: $\Delta(\mathbf{r}) = \Delta(z)$. It is related to the pair amplitude $F(z)$ by the expression $\Delta(z) = g(z)F(z)$, where $g(z)$ is the coupling parameter governing the electron-electron interaction. $F(z)$ is essentially the probability amplitude of finding a pair of electrons at the position z. The coupling function can be written as

$$g(z) = \begin{cases} V_N, \text{in the normal metal;} \\ V_S, \text{in the superconductor.} \end{cases} \tag{4.1}$$

4.1.1 Characteristic scales in non-magnetic normal metals

Extensive work has be can carried out concerning the situation in which $V_N = 0$. In this case, $g(z) = V_S\Theta(z)$ and $\Delta(z)$ vanishes identically on the N side. Hence, the appropriate quantity from which information can be obtained about the induced superconducting order in N is the pair amplitude $F(z) = \Delta(z)/g(z)$, since it maintains a finite value in the normal region.

What is the range of the superconducting pairing induced in N, in other words, what is the range of $F(z)$? The answer to this question depends on parameters like temperature and impurity concentration. First, if the normal metal is in the clean limit, that is, it has been calculated that $F(z)$ will, at finite temperatures T, decay exponentially (DEUTSCHER; GENNES, 1969):

$$F(z) \propto \exp(-K|z|) \tag{4.2}$$

over a range

$$K^{-1} = \frac{\hbar v_N}{2\pi k_B T}, \tag{4.3}$$

where v_N is the Fermi velocity in N and $|z|$ measures the distance away from the SN interface.

When temperatures tend towards zero, this decay is much slower. The pair amplitude no longer falls off exponentially, but is instead asymptotically characterized by an inverse power-law decay (FALK, 1963):

$$F(z) = \frac{\xi}{|z|}, \tag{4.4}$$

where ξ is the proximity length.

The implication is that at $T \approx 0$ the Cooper pairs diffusing from S can penetrate far deeper into N, as compared to what happens at finite temperatures.

If, on the other hand, N is a dirty metal, the leakage of superconductivity is now controlled by a diffusion process and the characteristic length for $F(z)$ in Eq. (4.2) is altered to

$$K^{-1} = \sqrt{\frac{\hbar D_N}{2\pi kT}}, \tag{4.5}$$

where D_N is the diffusion coefficient in N.

It must be pointed out, however, that some of the results mentioned above were originally derived based on theories with considerable limitations, although they have been re-obtained by other means and corroborated by experiments. The more simplistic early formulations are problematic in the sense that they are unable to explain the mechanism by which charge is transferred across the interface and do not take into account the implications on the electronic structure of the normal metals. Additionally, it turns out that the thermal decay length presented in Eq.(4.5) is not the most fundamental length in N over which the Cooper pairs coming from S will survive.

A proper description of the proximity effect must take into account the phenomenon of Andreev reflection (ANDREEV, 1964; BLONDER; TINKHAM; KLAPWIJK, 1982). An incoming electron from the N side with energy E (measured from the Fermi level) will not be able to penetrate into S if $E < \Delta$, the superconductor energy gap. The electron can still cross the interface, however, if it pairs up with another electron from N and enters the superconductor as a Cooper pair. In the process, the second electron from N leaves a hole with energy $-E$ which is reflected back into N. Conversely, the Andreev reflection can be seen as the means by which Cooper pairs can tunnel into the normal metal Cuevas et al. (2017).

Upon entering the normal metal, the pair turns into two time-reversed electron states with energy difference $2E$. They will dephase over time by a factor $\exp(-i2Et/\hbar)$, which becomes

of the order of unit for $t \approx \hbar/E$. By this time, the pair will have travelled a distance

$$L_E \approx \sqrt{D_N t} = \sqrt{\frac{\hbar D_N}{E}}. \tag{4.6}$$

This is the coherence length in the normal metal, a more fundamental scale for the diffusion of pairs in N. Clearly, sates with lower energy E are associated with a longer L_E but this cannot extend indefinitely. At some point, other dephasing mechanisms come into play, setting an upper limit for L_E, the phase breaking length L_ϕ. See the discussions in Cuevas et al. (2017) and Sohn, Kouwenhoven and Schön (1996). In summary, the proximiy effect can be understood as the interplay of two things: Andreev reflection at the interface and the maintenance of phase coherence over appreciable distances inside the normal metal. The role of Andreev reflection in the proximity effect has been elucidated relatively recently by Pannetier and Courtois (2000) and Klapwijk (2004).

Additionally, we already pointed out in Eq.(4.1) that situations in which there is some non-vanishing interaction between electrons in N are also possible. If some slightly attractive interaction is present in the normal region, it is itself of superconducting nature and possesses a critical temperate T_{cN}. In this case, the expression for the range K^{-1} will actually possess a factor of the type $(T - T_{cN})^{-1}$ instead of T^{-1}, and K^{-1} diverges as $T \to T_{cN}$ (WOLF, 2012).

Investigating the proximity effect at $T = 0$ in the case of a clean normal metal with a repulsive effective electronic interaction, Alexandrov and Kabanov (2008) found that the relation $F(z) = \tilde{\xi}/|z|$ is maintained, but with a reduced characteristic decay length $\tilde{\xi}$ in comparison with the situation in which there is no interaction in N.

Valls, Bryan and Žutić (2010) also considered the proximity effect in the presence of repulsive pairing interaction and list several other earlier works that directly investigated or suggest this problem with negative interaction in N. In particular, they concluded that a stronger repulsion in N corresponds to reduced values of F both in N and in S and to a considerable attenuation of the superconducting correlations in S near the interface.

4.1.2 Ferromagnets

Ferromagnets are materials in which individual atomic magnetic moments will attempt to align other atomic magnetic moments with themselves through the so-called exchange interaction. This characteristic alignment of spins contrasts with the picture of electrons with opposite spins making up the Coopers pairs in BCS superconductors. Ferromagnets, therefore,

might not seem the ideal hosts for superconducting correlations. Nevertheless, superconductivity can still be induced in ferromagnetic materials through the proximity effect, albeit with noticeable differences in comparison with SN junctions. The manifestation of proximity effects in ferromagnets is reviewed in Buzdin (2005) See also Bulaevskii, Buzdin and Panyukov (1982) and Buzdin, Bulaevskii and Panyukov (1982).

Again, if the superconductor is of the usual BCS type, the electrons in a Cooper pair have opposite spins. What follows is that the electron with spin aligned with the exchange field has its kinetic energy increased, while the electron with spin opposite to the exchange field acquires a higher energy. The consequence of this is that the Cooper pair acquires a net center of mass momentum δk_F. This means that the order parameter is modulated by a factor $e^{\delta k_F}$. In more physical terms, the implication is that the pair wave function in the ferromagnet does not decay monotonically, as is the case in ordinary normal metals, but instead decreases in an oscillatory manner.

For a dirty SF system, that is, with a small mean free path l_F, the Usadel equations for the Green's functions are the natural starting point (USADEL, 1970). Working with these equations and considering an SF junction in which a BCS-type superconductor is connected to a ferromagnet where the coupling constant is zero, one can derive the following expression for the Cooper pair wave function inside the ferromagnet:

$$\Psi \approx \Delta \exp\left(-\frac{z}{\xi_{1f}}\right) \cos\left(\frac{z}{\xi_{2f}}\right) \tag{4.7}$$

where $\xi_{1f} = \xi_{2f} = \sqrt{\frac{\hbar D_F}{E_{ex}}}$, $D_F = \frac{1}{3} v_F l$ is the diffusion coefficient and v_F is the Fermi velocity in F.

It is clear that the already mentioned oscillatory decay of superconductivity in F is indeed obtained. A notable result is the fact that the two characteristic lengths in this process are equal: the exponential decay range ξ_{1f} and the spatial period of the oscillations ξ_{2f}.

In the case of a ferromagnet in the clean limit, solving the quasiclassical Eilenberger equations (EILENBERGER, 1968) yields

$$\Psi \approx \frac{1}{z} \exp\left(-\frac{z}{\xi_{1f}}\right) \sin\left(\frac{z}{\xi_{2f}}\right), \tag{4.8}$$

where $\xi_{1f} = \frac{\hbar v_F}{2\pi kT}$ and $\xi_{2f} = \frac{\hbar v_F}{2E_{ex}}$. Hence, in the clean limit the characteristic decay length and oscillating length are no longer equal.

In the limit of low temperatures, $T \to 0$, we see that $\xi_{1f} \to \infty$ and from the expressions above we conclude that the wave function decays more slowly Buzdin (2005):

$$\Psi \approx \frac{1}{z} \sin\left(\frac{z}{\xi_{2f}}\right). \tag{4.9}$$

In summary, we see that the proximity effect is long ranged both in clean normal metals and in clean ferromagnets at low temperatures. The mean free path sets a limit to the diffusion of pairs inside the nonsuperconductor. If this parameter is relatively small (dirty system), the penetration length of the Cooper pairs will be greatly reduced, even at low temperatures. At finite temperatures, on the other hand, the asymptotic behavior of the pair wave function amounts to an exponential decay in both types of materials. The most striking difference between the pair amplitude in ferromagnets and in normal metals is that it exhibits oscillations in ferromagnets. Additionally, the typical length scales for this phenomenon are generally much smaller in ferromagnets then in non magnetic normal metals. A comparison of typical length scales of the proximity effect in non-magnetic normal metals and in ferromagnets is given in Table 2.

Table 2 – Typical length scales of the proximity effect

	N	F – decay	F – oscillation
Clean	$\frac{\hbar v_N}{2\pi kT}$	$\frac{\hbar v_F}{2\pi kT}$	$\frac{\hbar v_F}{2E_{ex}}$
Dirty	$\sqrt{\frac{\hbar D_N}{2\pi kT}}$	$\sqrt{\frac{\hbar D_F}{E_{ex}}}$	$\sqrt{\frac{\hbar D_F}{E_{ex}}}$

Source: The author (2022)

Intermediate impurity concentration regimes are considered by Linder, Zareyan and Sudbø (2009).

4.1.3 Lower dimensional systems

We emphasize that the results quoted so far concern three-dimensional systems, but the proximity effect has also been explored in lower dimensional systems. For clean SF junctions, it has been calculated that the pair wave function for the proximity-induced superconducting correlations in F oscillate with a characteristic length $\xi_{fb} = \frac{\hbar v_F}{E_{ex}}$ (BUZDIN; BULAEVSKII; PANYUKOV,

1982), the same as mentioned before, but decay much slower than in the three-dimensional case. In 2D systems, this decay is of the form $\sqrt{\frac{\xi_{fb}}{z}}$, where z measures the distance ton the SF interface. For 1D system, there's essentially no decay (KONSCHELLE; CAYSSOL; BUZDIN, 2008; CAYSSOL; MONTABAUX, 2004; KONSCHELLE; CAYSSOL; BUZDIN, 2010).

4.1.4 Limitations of traditional approaches

As pointed out by Halterman and Valls (2001), a huge body of research concerning the proximity effect has been created, both for SN and SF junctions. However, most of these investigations were based on non-self-consistent treatments and/or on not always reasonable approximations. For a complete and accurate treatment of the problem, the appropriate microscopic equations (BdG or Gor'kov) should be solved self-consistently and with as few approximations as possible.

We emphasize that the results presented above regarding the proximity effect in ferromagnets are obtained in the quasiclassical approximation, when the fast, less important variations in the relevant quantities are averaged out. Some of these and other results of proximity in ferromagnets were confirmed by numerical simulations carried out by Halterman and Valls (2001) and Halterman and Valls (2002). These works are based on the self-consistent solution of the full Bogoliubov-de Gennes equations with minimum assumptions or approximations.

Based on a more complete theoretical framework, these studies are also able to perceive phenomena at scales of the order of the Fermi wavelength, such as the rapid oscillations in the pair amplitude that appear near the boundaries of the system and close to the SN(F) interface, which are called Friedel oscillations.

4.2 THEORETICAL RESULTS FOR CLEAN THREE-DIMENSIONAL NS JUNCTIONS

Later on in the thesis on focus our attention on the proximity effect in clean samples of non-magnetic normal metals at zero temperature. A pioneering work on the proximity effect under this circumstances is (FALK, 1963). Here we follow the arguments presented in that paper to derive some theoretical results. The starting point are the Gor'kov equations. In a

superconductor, these equations take the form

$$\left[i\hbar\omega_n + \frac{\hbar^2}{2m}\nabla^2 + \mu\right] G_{\omega_n}(\mathbf{r},\mathbf{r}') + \Delta(z) F^{\dagger}_{\omega_n}(\mathbf{r},\mathbf{r}') = \hbar\delta(\mathbf{r}-\mathbf{r}'), \tag{4.10a}$$

$$\left[-i\hbar\omega_n + \frac{\hbar^2}{2m}\nabla^2 + \mu\right] F^{\dagger}_{\omega_n}(\mathbf{r},\mathbf{r}') - \Delta^*(z) G_{\omega_n}(\mathbf{r},\mathbf{r}') = 0, \tag{4.10b}$$

where $G_{\omega_n}(\mathbf{r},\mathbf{r}')$ and $F^{\dagger}_{\omega_n}(\mathbf{r},\mathbf{r}')$ are the coefficients in the Fourier representations of the normal and anomalous Green's functions, respectively, and ω_n are the Matsubara frequencies, which take the discrete set of values $\omega_n = (2n+1)\pi kT,\ n = 0, 1, 2, 3\ldots$ These equations must be solved together with the expression for the pair wave function $\Delta^*(z)$:

$$\Delta^*(z) = \frac{gkT}{\hbar}\sum_{n=-\infty}^{\infty} F^{\dagger}_{\omega_n}(\mathbf{r},\mathbf{r}) \tag{4.11}$$

As it stands, this problem is rather difficult to solve. We can attempt to work with a model $\Delta_m(z)$ that could simplify the calculations instead of the original $\Delta(z)$. It is not in our interest, however, to simply assume $\Delta(z)$ to be small. That would not be necessary if we could guess a simplified $\Delta_m(z)$ such that the deviation $\Delta(z) - \Delta_m(z)$ would be small. Actually, for the geometries we consider here, a reasonable approximation is to take $\Delta_m(z)$ independent of position inside the superconductor:

$$\Delta_m(z) = \Delta. \tag{4.12}$$

This is used in Eqs. (4.10). When $F^{\dagger}_{\omega_n}(\mathbf{r},\mathbf{r}')$ is obtained, $\Delta^*(z)$ can calculated from Eq. (4.11).

For the situations of interest here, spatial change happens solely in the z direction. We can make this dependence explicit from the beginning by taking Fourier transforms of the relevant Green's functions in the x and y directions:

$$\begin{aligned} G_{\omega_n}(\mathbf{r},\mathbf{r}') &= \int \frac{d\mathbf{k}_\perp}{(2\pi)^2} e^{i\mathbf{k}_\perp\cdot(\mathbf{r}_\perp - \mathbf{r}'_\perp)} G_{\omega_n,k_\perp}(z,z'), \\ F^{\dagger}_{\omega_n}(\mathbf{r},\mathbf{r}') &= \int \frac{d\mathbf{k}_\perp}{(2\pi)^2} e^{i\mathbf{k}_\perp\cdot(\mathbf{r}_\perp - \mathbf{r}'_\perp)} F^{\dagger}_{\omega_n,k_\perp}(z,z'), \end{aligned} \tag{4.13}$$

in which vectors with the subscript $\perp$ are perpendicular to the z axis, i.e, lie in the xy plane. $G_{\omega_n}(\mathbf{r},\mathbf{r}')$ and $F^{\dagger}_{\omega_n}(\mathbf{r},\mathbf{r}')$ can then be substituted in Eq.(4.10), resulting in the modified Gor'kov equations

$$\frac{1}{2m}\left(a^2 + \frac{d^2}{dz^2}\right) G_{\omega_n,k_\perp}(z,z') + \Delta F^{\dagger}_{\omega_n,k_\perp}(z,z') = \delta(z-z'), \tag{4.14a}$$

$$\frac{1}{2m}\left(a^{*2}+\frac{d^2}{dz^2}\right)F_{\omega_n}{}^{\dagger}(z,z',k_\perp)-\Delta^* G_{\omega_n,k_\perp}(z,z')=0, \tag{4.14b}$$

where the newly introduced symbols are defined by

$$\xi_\perp=\frac{\hbar^2k_\perp^2}{2m}-\mu, \tag{4.15}$$

the kinetic energy associated with motion in the xy-plane, measured from the Fermi level μ, and

$$a=[2m(-\xi_\perp+i\hbar\omega_n)]^{1/2} \text{ and } a^*=-[2m(-\xi_\perp-i\hbar\omega_n)]^{1/2}. \tag{4.16}$$

The convention adopted here for the phase of a complex number is such that it lies between 0 and 2π. If a is taken to be in upper half plane, the minus sign in a^* guarantees that it lies in the lower half plane.

4.2.1 Contact of a superconductor and a normal metal

To derive some general results in the theory of the proximity effect, we consider as a model system a superconductor in contact with a normal (non-superconducting) metal. The interface lies in the $z=0$ plane. The superconductor is taken to be in the $z>0$ region, while the normal metal lies in the $z<0$ region. In each of the two materials, the characteristic parameters, like effective mass m or chemical potential μ, have different values. To distinguish between them, quantities related to the normal metal are topped by a bar: $\bar{m}$, $\bar{\mu}$, $\bar{\xi}_\perp$ and $\bar{a}$, for example.

In the normal metal considered here, the coupling constant is zero, i.e., $g(z)=0$ for $z<0$. It then lacks a proper mechanism by which electrons could interact attractively to form Cooper pairs (superconducting correlations, however, can still be present if they are induced by the neighboring superconductor, as we shall see). Thus, from Eq.(4.11), the order parameter vanishes in this region: $\Delta(z)=0,\ z<0$. Therefore, the Gor'kov equations for the normal metal take the form

$$\frac{1}{2\bar{m}}\left(\bar{a}^2+\frac{d^2}{dz^2}\right)G_{\omega_n,k_\perp}(z,z')=\delta(z-z'), \tag{4.17a}$$

$$\frac{1}{2\bar{m}}\left(\bar{a}^{*2}+\frac{d^2}{dz^2}\right)F^{\dagger}_{\omega_n,k_\perp}(z,z')=0,\quad z<0 \tag{4.17b}$$

The whole NS system may be considered at once if we combine Eqs. (4.17) and Eqs. (4.14) using step functions. The final coupled differential equations are given by

$$\begin{aligned}\left[\theta(z)\frac{1}{2m}\left(a^2+\frac{d^2}{dz^2}\right)+\theta(-z)\frac{1}{2\bar{m}}\left(\bar{a}^2+\frac{d^2}{dz^2}\right)\right]G_{\omega_n,k_\perp}(z,z') \\ +\theta(z)\Delta F^{\dagger}_{\omega_n,k_\perp}(z,z')=\delta(z-z')\end{aligned} \tag{4.18a}$$

$$\begin{aligned}\left[\theta(z)\frac{1}{2m}\left(a^{*2}+\frac{d^2}{dz^2}\right)+\theta(-z)\frac{1}{2\bar{m}}\left(\bar{a}^{*2}+\frac{d^2}{dz^2}\right)\right]F^{\dagger}_{\omega_n,k_\perp}(z,z') \\ -\theta(z)\Delta^* G_{\omega_n,k_\perp}(z,z')=0.\end{aligned} \tag{4.18b}$$

To properly solve these equations, it is necessary to know what the boundary conditions are. Some considerations are important here, as pointed out by Harrison (1961). First, we note that a current passing through the interface must be continuous in order to avoid accumulation of charge at the boundary. In the absence of a magnetic field, a general expression for the current density is given by (FETTER; WALECKA, 2003)

$$\mathbf{j}(z)=-\frac{e\hbar}{2mi}\left[\psi^*(z)\frac{\mathrm{d}\psi}{\mathrm{d}z}(z)-\psi(z)\frac{\mathrm{d}\psi^*}{\mathrm{d}z}(z)\right]. \tag{4.19}$$

In this expression we can observe the dependence of $\mathbf{j}(z)$ on m, which changes discontinuously across the boundary, as pointed out before. Thus, to ensure continuity of the current, the wave function $\psi(z)$ and its derivative have to be discontinuous at the interface. These boundary conditions can be written as

Bloch theorem establishes that the actual wave function of a system in a periodic potential are the product of plane waves and periodic functions with the same period as the potential. It is these Bloch functions that must be continuous across the boundary. In the context of a effective mass approximation, the Bloch functions are replaced by plane waves, which can be discontinuous at the interface.

$$\psi(0^-)=\sigma\psi(0^+),\ \frac{\mathrm{d}\psi(0^-)}{\mathrm{d}z}=\rho\frac{\mathrm{d}\psi(0^+)}{\mathrm{d}z}, \tag{4.20}$$

where the $-$ and $+$ superscripts denote that these expressions are to be evaluated at points arbitrarily close to the interface, but approaching it from the negative z-axis (normal metal) or positive z-axis (superconductor), respectively. We can now impose the continuity of the current density, $\mathbf{j}(0^-)=\mathbf{j}(0^+)$, leading to

$$\frac{m}{\bar{m}}\,\mathrm{Im}\left[\psi(0^-)\frac{\mathrm{d}\psi(0^-)}{\mathrm{d}z}\right]=\mathrm{Im}\left[\psi(0^+)\frac{\mathrm{d}\psi(0^+)}{\mathrm{d}z}\right]. \tag{4.21}$$

Substituting Eqs. (4.20) in Eq. (4.21), we obtain the relation

$$\rho\sigma = \frac{\bar{m}}{m}. \tag{4.22}$$

4.2.2 Solving for Green's functions

To solve Eqs. (4.18), we employ the method of Laplace transforms, and begin by introducing new quantities defined by

$$\begin{aligned} G_{\pm}(K, z') &= \pm \int_0^{\pm\infty} dz e^{iKz} G_{\omega_n, k_\perp}(z, z') \\ F_{\pm}(K, z') &= \pm \int_0^{\pm\infty} dz e^{iKz} F^{\dagger}_{\omega_n, k_\perp}(z, z') \end{aligned} \tag{4.23}$$

Some considerations about Laplace transforms are in order here. Let us take a function $f(t)$ such that $\int_0^\infty dt e^{-ct}|f(t)| < \infty$ for some $c \in \mathbb{R}$. The Laplace transform $\tilde{f}(s)$ of $f(t)$ is defined as

$$\tilde{f}(s) = \int_0^\infty dt e^{-st} f(t),\ \mathrm{Re}(s) \geq c. \tag{4.24}$$

An important result is that $\tilde{f}(s)$ is analytic in the open half plane $\mathrm{Re}(s) \geq c$. With this in mind, we can rewrite the complex variable K as $K_{Re} + iK_{Im}$ and substitute it in the exponential in Eq.(4.23), obtaining $e^{iKz} = e^{-(K_{Im} - iK_{Re})z}$. Thus, $G_+(K, z')$ is analytic where $\mathrm{Re}(K_{Im} > 0)$, i.e., the upper half plane, and so is $F_+(K, z')$. Similarly, we can conclude that $G_-(K, z')$ and $F_-(K, z')$ are analytic in the lower half plane.

We now multiply Eq.(4.18a) by e^{iKz} and integrate in z from $-\infty$ to ∞, which results in the following expression:

$$\begin{aligned} \frac{1}{2m}\left(a^2 - K^2\right) G_+(K, z') + \frac{1}{2\bar{m}}\left(\bar{a}^2 - K^2\right) G_-(K, z') + \Delta F_+(K, z') = e^{iKz'} \\ + \frac{iK}{2m} G_{\omega_n, k_\perp}\left(0^+, z'\right) - \frac{iK}{2\bar{m}} G_{\omega_n, k_\perp}\left(0^-, z'\right) \\ - \frac{1}{2m}\frac{dG_{\omega_n, k_\perp}}{dz}\left(0^+, z'\right) + \frac{1}{2\bar{m}}\frac{dG_{\omega_n, k_\perp}}{dz}\left(0^-, z'\right) \end{aligned} \tag{4.25}$$

At this point, it is convenient to simplify the notation by introducing

$$\begin{aligned} A_{\pm}(z') &= G_{\omega_n, k_\perp}\left(0^{\pm}, z'\right), \quad B_{\pm}(z') = \frac{dG_{\omega_n, k_\perp}}{dz}\left(0^{\pm}, z'\right), \\ C_{\pm}(z') &= F^{\dagger}_{\omega_n, k_\perp}\left(0^{\pm}, z'\right), \quad D_{\pm}(z') = \frac{dF^{\dagger}_{\omega_n, k_\perp}}{dx}\left(0^{\pm}, z'\right), \end{aligned} \tag{4.26}$$

and noting that G_{ω_n} and $\frac{dG_{\omega_n}}{dz}$ are subject to the same boundary conditions as $\psi(z')$ and $\frac{d\psi}{dz}(z')$. The parts of Eq. (4.25) which are evaluated at the interface can now be written in

terms of the quantities defined in Eq.(4.26). As an example, we consider the terms involving G_{ω_n}:

$$\frac{1}{2m}G_{\omega_n,k_\perp}\left(0^+,z'\right)-\frac{1}{2\bar{m}}G_{\omega_n,k_\perp}\left(0^-,z'\right)=\begin{cases}\dfrac{1}{2m}\left(1-\dfrac{1}{\rho}\right)G_{\omega_n,k_\perp}\left(0^+,z'\right)\\ \dfrac{1}{2m\sigma}\left(1-\dfrac{1}{\rho}\right)G_{\omega_n,k_\perp}\left(0^-,z'\right)\end{cases}, \tag{4.27}$$

where we used Eq.(4.22) (the two lines represent alternative ways of writing the same thing). We further introduce two coefficients:

$$\eta=\frac{1}{2m}\left(1-\frac{1}{\rho}\right),\ \zeta=\frac{1}{2m}\left(1-\frac{1}{\sigma}\right). \tag{4.28}$$

The line of reasoning employed in the derivation of Eq.(4.27) can be followed with the remaining boundary terms, which are then more succinctly written as

$$\frac{1}{2m}G_{\omega_n,k_\perp}\left(0^+,z'\right)-\frac{1}{2\bar{m}}G_{\omega_n,k_\perp}\left(0^-,z'\right)=\eta A_+\left(z'\right)=\frac{\eta}{\sigma}A_-\left(z'\right), \tag{4.29a}$$

$$\frac{1}{2m}\frac{dG_{\omega_n,k_\perp}}{dz}\left(0^+,z'\right)-\frac{1}{2\bar{m}}\frac{dG_{\omega_n,k_\perp}}{dz}\left(0^-,z'\right)=\zeta B_+\left(z'\right)=\frac{\zeta}{\rho}B_-\left(z'\right), \tag{4.29b}$$

$$\frac{1}{2m}F_{\omega_n,k_\perp}\left(0^+,z'\right)-\frac{1}{2\bar{m}}F_{\omega_n,k_\perp}\left(0^-,z'\right)=\eta C_+\left(z'\right)=\frac{\eta}{\sigma}C_-\left(z'\right), \tag{4.29c}$$

$$\frac{1}{2m}\frac{dF_{\omega_n,k_\perp}}{dz}\left(0^+,z'\right)-\frac{1}{2\bar{m}}\frac{dF_{\omega_n,k_\perp}}{dz}\left(0^-,z'\right)=\zeta D_+\left(z'\right)=\frac{\zeta}{\rho}D_-\left(z'\right), \tag{4.29d}$$

After all these considerations, Eq.(4.25) attains the more favorable form

$$\begin{aligned}&\frac{1}{2m}\left(a^2-K^2\right)G_+\left(K,z'\right)+\Delta F_+\left(K,z'\right)-\theta\left(z'\right)e^{iKz'}=\\&-\frac{1}{2\bar{m}}\left(\bar{a}^2-K^2\right)G_-\left(K,z'\right)+\theta\left(-z'\right)e^{iKz'}+\zeta B_+\left(z'\right)-iK\eta A_+\left(z'\right)\end{aligned} \tag{4.30}$$

The same procedure discussed so far can be carried out for Eq.(4.18b), leading to

$$\begin{aligned}&\frac{1}{2m}\left(a^{*2}-K^2\right)F_+\left(K,z'\right)-\Delta^* G_+\left(K,z'\right)=\\&-\frac{1}{2\bar{m}}\left(\bar{a}^{*2}-K^2\right)F_-\left(K,z'\right)+\zeta D_+\left(z'\right)-iK\eta C_+\left(z'\right)\end{aligned} \tag{4.31}$$

The terms of Eqs.(4.30) and (4.31) are not randomly arranged. Based on the exposition presented earlier, one can see that in both of these equations the first term is the limit of an

analytic function of the variable K in the upper half plane, while the second term is the limit of a function which is analytic in the lower half plane. Thus, for each equation, we can set both sides equal to the same function, analytic both in the upper and in the lower half planes, i.e., an entire function of K. This is quite useful because it allows us to solve the problem by using the properties of analytic functions. As an example, we investigate the right hand side of Eqs.(4.30), for $z' > 0$. We can set this expression equal to an entire function $P'(K, z')$ and solve for $G_-(K, z')$:

$$G_-(K, z') = \frac{2\bar{m}}{(K - \bar{a})(K + \bar{a})} \left[P'(K, z') - \zeta B_+(z') + iK\eta A_+(z')\right] \tag{4.32}$$

We recall that $G_-(K, z')$ is analytic in the lower half plane by construction. Since $-\bar{a}$ lies in that region, the apparently problematic factor in the denominator is compensated by the numerator, assuring that no pole exists at $K = -\bar{a}$. This can be made explicit by introducing a new entire function $P(K, z')$:

$$G_-(K, z') = \frac{2\bar{m}P(K, z')}{(K - \bar{a})} \tag{4.33}$$

In a similar manner, the right hand side of Eq.(4.31) gives

$$F_-(K, z') = \frac{2\bar{m}Q(K, z')}{(K + \bar{a}^*)}, \tag{4.34}$$

where $Q(K, z')$ is another entire function of K.

We can now go back to Eqs.(4.30) and (4.31) and solve for $F_+(K, z')$ and $G_+(K, z')$ using the above expressions for $F_-(K, z')$ and $G_-(K, z')$. From the left hand side of Eqs.(4.31), we get

$$\begin{aligned} &F_+(K, z') \\ &= \frac{-2m}{(K - a^*)(K + a^*)}[\Delta^* G_+(K, z') + (K - \bar{a}^*)Q(K, z') + \zeta D_+(z') - iK\eta C_+(z')]. \end{aligned} \tag{4.35}$$

Similarly, the remaining part of Eqs.(4.30) results in

$$\begin{aligned} &G_+(K, z') \\ &= \frac{2m}{(K - a)(K + a)}\left[\Delta F_+(K, z') - e^{iKz'} - (K + \bar{a})P(K, z') - \zeta B_+(z') + iK\eta A_+(z')\right] \end{aligned} \tag{4.36}$$

We now have two different formulas for each of the transformed Green's functions, one being from the original definitions (Eq.(4.23)) and the other being an expression in terms of an yet undetermined entire function and of boundary terms (Eqs. (4.33), (4.34), (4.35) and

(4.36)). We focus, for the sake of illustration, on $G_{-}(K,z')$. Further insight about $P(K,z')$ can be gained by investigating the behaviour of the different expressions for $G_{-}(K,z')$ in the limit of large K. From the definition,

$$G_{-}(K,z') = \int_{-\infty}^{0} dz e^{iKz} G_{\omega_n,k_\perp}(z,z') \approx \frac{1}{iK} A_{-}(x') + \frac{1}{K^2} B_{-}(z') + \cdots \tag{4.37}$$

On the other hand, we note that the Laurent series expansion of $\dfrac{1}{x-x_0}$ for $x \to \infty$ is given by

$$\frac{1}{x} + \frac{x_0}{x^2} + \frac{x_0^2}{x^3} + \frac{x_0^3}{x^4} + \cdots \tag{4.38}$$

Thus, the expansion of the denominator of Eq.(4.33) gives

$$G_{-}(K,z') \approx 2\bar{m} P(K,x') \left[\frac{1}{K} + \frac{\bar{a}}{K^2} \cdots\right] \tag{4.39}$$

Now, $A_{-}(z')$ and $B_{-}(z')$ clearly do not depend on K, so the comparison of Eqs.(4.37) and (4.38) shows that $P(K,z')$, as a function of K, approaches a constant value for large K in the lower half plane. An analogous argument involving G_{+} reveals, on the other hand, that $P(K,z')$ approaches a constant also in the upper half plane. Liouville's theorem in complex analysis establishes that every bounded entire function must be constant. Therefore, $P(K,z')$ does not depend on K:

$$\begin{aligned} P(K,z') = P(z') &= \frac{1}{2\bar{m}i} A_{-}(z') = \frac{\sigma}{2\bar{m}i} A_{+}(z') \\ &= \frac{1}{2\bar{m}\bar{a}} B_{-}(z') = \frac{\rho}{2\bar{m}\bar{a}} B_{+}(z'). \end{aligned} \tag{4.40}$$

Analysis of the asymptotic behavior of F_{+} and F_{-} yields similar results for $Q(K,z')$:

$$\begin{aligned} Q(K,x') = Q(x') &= \frac{1}{2\bar{m}i} C_{-}(x') = \frac{\sigma}{2\bar{m}i} C_{+}(x') \\ &= \frac{-1}{2\bar{m}\bar{a}^*} D_{-}(x') = \frac{-\rho}{2\bar{m}\bar{a}^*} D_{+}(x'). \end{aligned} \tag{4.41}$$

The expressions obtained so far can be inserted in Eq.(4.35). Solving for F_{+} yields

$$\begin{aligned} F_{+}(K,z') = \frac{(2m)^2}{(K^2-b^2)(K^2-b^{*2})} \Big[&\Delta^* e^{iKz'} + \Delta^* (\rho K + \sigma\bar{a}) P(x') \\ &-(1/2m)\left(K^2 - a^2\right)(\rho K - \sigma\bar{a}^*) Q(x')\Big], \end{aligned} \tag{4.42}$$

where new quantities have been introduced:

$$\begin{gathered} b = [2m(-\xi_\perp + i\epsilon_n)]^{1/2},\ b^* = -[2m(-\xi_\perp - i\epsilon_n)]^{1/2} \\ \text{and } \epsilon_n = \left[\omega_n^2 + |\Delta|\right]^{1/2} \end{gathered} \tag{4.43}$$

Again, F_+ is analytic in the upper half plane, so the expression in brackets must vanish in the otherwise problematic points $K = b$ and $K = -b^*$. This leads to two equations that determine $P(z')$ and $Q(z')$:

$$\begin{aligned} Q\left(z'\right) =& \frac{2m\Delta^*}{D\left(b,b^*\right)}\left[\left(\rho b^* - \sigma\bar{a}\right)e^{ibz'} + \left(\rho b + \sigma\bar{a}\right)e^{-ib^*z'}\right], \\ P\left(z'\right) =& \frac{1}{D\left(b,b^*\right)}\left[\left(b^{*2} - a^2\right)\left(\rho b^* + \sigma\bar{a}^*\right)e^{ibz'} + \left(b^2 - a^2\right)\left(\rho b - \sigma\bar{a}^*\right)e^{-ib^*z'}\right]. \end{aligned} \tag{4.44}$$

The factor $D\left(b,b^*\right)$ has been introduced to simplify the notation. I is defined as

$$D\left(b,b^*\right) \equiv \left(b^2 - a^2\right)\left(\rho b^* - \sigma\bar{a}\right)\left(\rho b - \sigma\bar{a}^*\right) - \left(b^{*2} - a^2\right)\left(\rho b + \sigma\bar{a}\right)\left(\rho b^* + \sigma\bar{a}^*\right) \tag{4.45}$$

In this investigation of the proximity effect, we are ultimately interested in deriving an expression for $F^{\dagger}_{\omega_n}\left(z\right)$, since it is the one that appears in the self-consistency equation for the pair potential: $\Delta^*(z) = gkT\sum_n F^{\dagger}_{\omega_n}\left(z\right)$. Thus, our main interest lies in F_+ and F_-. We remark that the calculations carried out so far concern the case $z' > 0$. Let us suppose that $z > 0$ too, as an example. In this case, inverting the definition, Eq.(4.23), results in

$$F^{\dagger}_{\omega_n,k_\perp}\left(z,z'\right) = \int_{-\infty}^{\infty}\frac{dK}{2\pi}e^{-iKz}F_+\left(K,z'\right),\ z' > 0, z > 0, \tag{4.46}$$

where F_+ is the one given in Eq.(4.42). The integration can be performed with the aide of techniques in complex analysis, as described in Chapter 15 of Boas (1983).

The arguments discussed until now can again be applied in solving Eqs.(4.23) for $z' < 0$. Finally, the result for all values of z and z' is of the form

$$F^{\dagger}_{\omega_n,k_\perp}\left(z,z'\right) = \begin{cases} \mathcal{F}_{\mathcal{I}},\ z,z' > 0; \\ \mathcal{F}_{\mathcal{II}},\ z > 0,\ z' < 0 \\ \mathcal{F}_{\mathcal{III}}, z < 0,\ z' > 0; \\ \mathcal{F}_{\mathcal{IV}}, z, z' < 0. \end{cases} \tag{4.47}$$

where

$$\begin{aligned} \mathcal{F}_{\mathcal{I}} &= F^{\infty\dagger}_{\omega_n,k_\perp}\left(z,z'\right) \\ &+ \frac{4m^2i\Delta^*}{D\left(b,b^*\right)\left(b^2 - b^{*2}\right)}\left\{\rho\sigma(\bar{a} + \bar{a}^*)\left[\left(b^2 - a^2\right)e^{ibz}e^{-ib^*z'} + \left(b^{*2} - a^2\right)e^{\cdot -ib^*z}e^{ibz'}\right]\right. \\ &\left. - \frac{D\left(-b,b^*\right)}{2b}e^{ib(z+z')} - \frac{D\left(b,-b^*\right)}{2b^*}e^{-ib^*(z+z')}\right\}; \end{aligned} \tag{4.48}$$

$$\mathcal{F}_{\mathcal{II}} = \frac{4m\bar{m}i\Delta^*}{D\left(b,b^*\right)}\left[\left(\rho b^* + \sigma\bar{a}^*\right)e^{ibz}e^{-i\bar{a}z'} + \left(\rho b - \sigma\bar{a}^*\right)e^{-ib^*z}e^{-i\bar{a}z'}\right]; \tag{4.49}$$

$$\mathcal{F}_{\mathcal{III}} = \frac{4m\bar{m}i\Delta^*}{D\left(b,b^*\right)}\left[\left(\rho b^* - \sigma\bar{a}\right)e^{i\bar{a}^*z}e^{ibz'} + \left(\rho b + \sigma\bar{a}\right)e^{i\bar{\alpha}^*z}e^{-ib^*z'}\right]; \tag{4.50}$$

$$\mathcal{F}_{\mathcal{IV}} = \frac{4\bar{m}^2 i\Delta^*}{D\left(b,b^*\right)}\left(b+b^*\right)e^{i\bar{a}^*z}e^{-i\bar{a}z'}. \tag{4.51}$$

As a first evaluation of the correctness of this expression, we can examine its asymptotic limits as $z, z' \to \infty$ or $-\infty$, while $z - z'$ remains finite. For $z, z' < 0$, only the last quantity, $\mathcal{F}_{\mathcal{IV}}$, is relevant. The quantities a, $\bar{a}$ and b all have positive imaginary parts, so that both the exponentials in this term of $F^{\dagger}_{\omega_n,k_\perp}$ are of the types $e^{-\kappa z}$, $e^{-\kappa z'}$, where κ is some positive quantity. Thus, for $z, z' < 0$, $F^{\dagger}_{\omega_n,k_\perp} \to 0$, what is expected since we are in the normal metal. For $z, z' > 0$, which corresponds to the superconductor, only $\mathcal{F}_{\mathcal{I}}$ contributes. The same line of reasoning as above leads to the conclusion that in this region $F^{\dagger}_{\omega_n,k_\perp} \to F^{\infty\dagger}_{\omega_n,k_\perp}$, i.e., the system behaves as if it were an infinite superconductor, as it should.

4.2.3 Pair wave function

We can attempt to derive more precise equations for the pair wave function. Here we study the case $z > 0$. It is convenient to rewrite the relevant quantities in such a way that their bulk values are singled out. This defines the primed quantities in the following expressions:

$$F^{\dagger}_{\omega_n,k_\perp} = F^{\infty\dagger}_{\omega_n,k_\perp} + F'^{\dagger}_{\omega_n,k_\perp}, \tag{4.52}$$

$$\Delta^*(z) = \Delta^* + \Delta'^*(z). \tag{4.53}$$

Hence, from Eq. (4.11),

$$\Delta'^*(z) = \frac{gkT}{\hbar}\sum_n F'^{\dagger}_{\omega_n}(z), \quad z > 0. \tag{4.54}$$

From Eq. (4.13) we get

$$F^{\dagger}_{\omega_n}(z) = \int \frac{d\mathbf{k}_\perp}{(2\pi)^2} F^{\dagger}_{\omega_n,k_\perp}(z), \tag{4.55}$$

but the relevant quantities are given in terms of the energy $\xi_\perp = \frac{\hbar^2 k_\perp^2}{2m} - \mu$, so it is convenient to change the integration variable:

$$\int \frac{d\mathbf{k}_\perp}{(2\pi)^2} = \int \frac{k dk_\perp}{(2\pi)} \to \frac{m}{2\pi}\int_{-\mu}^{\infty} d\xi_\perp. \tag{4.56}$$

At this point, it is also fitting to rewrite the exponentials in a more suitable way for integration:

$$e^{i(b-b^*)z} = \frac{i}{mz}\frac{bb^*}{b^*-b}\frac{d}{d\xi_\perp}e^{i(b-b^*)z} \tag{4.57}$$

$$e^{2ibz} = \frac{i}{z}\frac{b}{2m}\frac{d}{d\xi_\perp}e^{2ibz} \tag{4.58}$$

This integration is, unfortunately, quite difficult. However, if we are interested in obtaining $\Delta^*(z)$ only for large z, some helpful simplifications can be made.

In the upper limit, $\xi_\perp \to \infty$, the quantities b, $-b^*$, and $b-b^*$ tend towards $i\infty$, so that the exponentials in Eq. (4.47) relevant for the case $z > 0$ all become of the form $exp[-(\textit{positive quantity}) \times z]$. These rapidly decaying terms are of course negligible in comparison with the terms resultant from the lower limit, $\xi_\perp = -\mu$. With this in mind, we simplify the calculations by setting $\xi_\perp = -\mu$ in the coefficients of the exponentials in Eq. (4.55) before evaluating the integral. With these simplifying assumptions, we finally get

$$F'^{\dagger}_{\omega_n}(z) \approx \frac{2m^2\Delta^*}{\pi z}\frac{1}{D\left(b,b^*\right)\left(b^2-b^{*2}\right)}\times$$
$$\left\{\rho\sigma\left(a^{*2}-a^2\right)\left(\bar{a}+\bar{a}^*\right)\frac{bb^*}{b^*-b}e^{i(b-b^*)z} + \frac{1}{4}\left[-D\left(-b,b^*\right)e^{2ibz} + D\left(b,-b^*\right)e^{-2ib^*z}\right]\right\}, \tag{4.59}$$

noting that we must set $\xi_\perp = -\mu$ in this expression.

4.2.4 NS contact at $T \approx T_c$

4.2.4.1 Superconductor, $z > 0$

We may now consider the situation in which the system is in the vicinity of its critical temperature. In this case, $\Delta^* \approx 0$ and $\epsilon_n \approx \omega_n$. The terms in Eq.(4.59) that depend directly on ω_n cancel out. In the end, $F'^{\dagger}_{\omega_n}(z)$ depends on ω_n solely through $\epsilon_n = \sqrt{\hbar^2\omega_n^2 + |\Delta|^2} \approx |\hbar\omega_n|$. Thus, $F'^{\dagger}_{\omega_n}(z)$ is an even function of ω_n and we can make a change in Eq. (4.54):

$$\sum_{n=-\infty}^{\infty} \to 2\sum_{n=0}^{\infty} \tag{4.60}$$

Moreover, Eq.(4.59) contains exponentials of the kind $\exp\left[izp_0\sqrt{1 \pm i\frac{\hbar\omega_n}{\mu}}\right]$, where p_0 is defined by $\frac{p_0^2}{2m} = \mu$. Therefore, for large z, the only relevant contribution comes from the lowest

value of $\hbar\omega_n$, $\hbar\omega_0 = \pi k T_c$. Higher values of ω_n lead to exponentials that decay too rapidly. In these calculations the approximation $\frac{kT_c}{\mu} \ll 1$ and $\frac{kT_c}{\bar{\mu}} \ll 1$ is employed.

We consider first the last two terms of Eq. (4.59), keeping in mind that several relations can be derived given the approximations we made:

$$\sqrt{1 \pm i\frac{\pi k T_c}{\mu}} \approx \pm 1 + i\frac{\pi k T_c}{2\mu}, \tag{4.61}$$

$$b \approx p_0\left(1 + i\frac{\epsilon_n}{2\mu}\right) \approx p_0\left(1 + i\frac{\pi k T_c}{2\mu}\right), \tag{4.62}$$

$$b^* \approx p_0\left(1 - i\frac{\epsilon_n}{2\mu}\right) \approx p_0\left(1 - i\frac{\pi k T_c}{2\mu}\right), \tag{4.63}$$

$$b^2 - b^{*2} = 4mi\epsilon_n \approx i\frac{2\pi k T_c p_0^2}{\mu} \tag{4.64}$$

$$b - b^* \approx i\frac{\pi k T_c p_0}{\mu}, \tag{4.65}$$

$$D(b, b^*) \approx -\left(b^{2*} - a^2\right)(\rho b + \sigma\bar{a})(\rho b^* + \sigma\bar{a}^*) = -\left(b^{2*} - a^2\right)\rho^2 p_0^2\left(1 + \frac{\sigma}{\rho}\frac{\bar{p_0}}{p_0}\right), \tag{4.66}$$

$$D(b, -b^*)e^{-2ib^*z} - D(-b, b^*)e^{2ibz} \approx \rho\sigma(b\bar{a} - b\bar{a})\left(e^{2ibz} + e^{2ibz}\right) + \left(\rho^2 bb - \sigma^2\bar{a}\bar{a}\right)\left(e^{2ibz} - e^{2ibz}\right), \tag{4.67}$$

The first part vanishes of Eq.(4.67), since $b\bar{a} \approx b\bar{a}$ for $T \approx T_c$. The last two will result in a term proportional to

$$e^{2ibz} - e^{-2ib^*z} \approx e^{-p_0\omega_n z/\mu}\left[e^{2ip_0 z} - e^{-2ip_0 z}\right] \approx 2i\sin(2p_0 z)e^{-p_0\omega_n z/\mu} \tag{4.68}$$

Hence, we see that the last terms of Eq. (4.59) lead to a rapidly oscillating term with frequency $2p_0$, which averages to zero over any relevant scale and can therefore be ignored.

The only relevant contribution comes from the first term of Eq. (4.59). After substituting all the factors appropriately modified to take into account the approximations associated with the regime $T \approx T_c$ we get

$$\theta(z)\Delta'^*(z) \approx -\theta(z)\frac{gm\Delta^*}{2\pi^2 z}\frac{\mu}{\pi k T_c}\left[4\frac{\sigma}{\rho}\frac{\bar{p}_0}{p_0}\Big/\left(1 + \frac{\sigma\bar{p}_0}{\rho p_0}\right)^2\right]e^{-p_0 z\pi k T_c/\hbar\mu}. \tag{4.69}$$

To simplify the notation, we introduce

$$T_\mu = 4\frac{\sigma}{\rho}\frac{\bar{p}_0}{p_0}\Bigg/\left(1+\frac{\sigma\bar{p}_0}{\rho p_0}\right)^2 \tag{4.70}$$

This quantity can be interpreted as a transmission coefficient across the boundary at an energy $E = \mu$.

By replacing $\Delta'^*(z)$ in Eq.(4.53) with Eq.(4.69), we get, for large positive z:

$$\theta(z)\Delta^*(z) = \theta(z)\Delta^*\left[1 - \frac{gmT_\mu}{2\pi^2 z}\frac{\mu}{\pi kT_c}e^{-p_0 z\pi kT_c/\hbar\mu}\right] \tag{4.71}$$

It is interesting to note that changes in the magnitude of the transmission coefficient, i.e., how easily particles can cross the interface, will alter the amplitude of the second term in Eq.(4.71), but its range remains unchanged (the argument of the exponential does not depend on T_μ).

This result clearly reproduces the previously mentioned inverse proximity effect: the pair wave function within the superconductor decreases from its bulk value over a distance $\frac{\hbar\mu}{\pi kT_c p_0}$ before the interface. This distance is approximately the coherence length, $\xi_0 = \frac{\hbar v_N}{\pi|\Delta|} = \frac{2\hbar\mu}{\pi|\Delta|p_0}$, where v_N is the Fermi velocity in the normal metal.

4.2.4.2 Normal metal, $z < 0$

Similar calculations in the normal metal $(z < 0)$ lead to an exponential decay of the pair amplitude as the dominant behavior over an analogous length scale (with the difference that now the normal metal parameters are used):

$$\theta(-z)F(z) = \theta(-z)\Delta\frac{\bar{m}T_\mu}{2\pi^2|z|}\frac{\bar{\mu}}{\pi kT_c}e^{-\bar{p}_0|z|\pi kT_c/\hbar\bar{\mu}} \tag{4.72}$$

The characteristic length scale for this decay is indeed what was already pointed out in Eq.(4.2). Since $2\bar{\mu}/\bar{p}_0 = v_N$:

$$\frac{\hbar\bar{\mu}}{\bar{p}_0|z|\pi kT_c} = \frac{\hbar v_N}{2|z|\pi kT_c} = K^{-1}. \tag{4.73}$$

4.2.5 NS contact at $T = 0$

4.2.5.1 Superconductor, $z > 0$

At zero temperature, the summation in Eq.(4.54) must be replaced by an integration (ABRIKOSOV; GOR'KOV; DZYALOSHINSKII, 1959):

$$kT \sum_{\omega_n} \rightarrow \frac{1}{2\pi} \int_{-\infty}^{\infty} d\omega_n \ldots \tag{4.74}$$

As was the case for a system at its critical temperature, the second and terms of Eq.(4.59) result in a rapidly oscillating term that averages to zero and therefore can be disregarded. The remaining exponential in Eq.(4.59) has the form

$$\exp\left[i\left(b - b^*\right)z\right] = \exp\left\{-z\left[4m\left[\left(\mu^2 + |\Delta|^2 + \hbar^2\omega_n^2\right)^{1/2} - \mu\right]\right]^{1/2}\right\} \tag{4.75}$$

Hence, the main contribution for large z comes from the vicinity of $\omega_n \approx 0$ (higher values of ω_n would yield more rapidly decaying exponentials), so this expression can be expanded in around $\omega_n = 0$, taking into account that $\Delta \ll \mu, \bar{\mu}$. Ultimately, one arrives at the result for the pair wave function in the superconductor, at $T = 0$:

$$\theta(z)\Delta^*(z) = \theta(z)\Delta^*\left[1 - \frac{gmp_0}{2\pi^2}\frac{\pi^2}{4}\frac{T_\mu}{1+R_\mu}\left(\frac{\xi_0}{z}\right)^2 \exp\left(-\frac{2}{\pi}\frac{z}{\xi_0}\right)\right] \tag{4.76}$$

Here, $R_\mu = 1 - T_\mu$ can be interpreted as a reflection coefficient.

Once again, we see a decrease in $\Delta^*(z)$ before the interface over a distance that is essentially ξ_0. The actual range appearing in the argument of the exponential is longer than the analogous quantity at $T \approx T_c$ by a factor of less than 2.

4.2.5.2 Normal metal, $z < 0$

In this case we need not begin with the approximations that led to Eq. (4.59). We can instead go back to Eq. (4.17b), the Gor'kov equation for $F^\dagger_{\omega_n k_\perp}(z, z')$ in the normal metal, and make general considerations about this region. For convenience, we reproduce this equation here:

$$\frac{1}{2\bar{m}}\left(\bar{a}^{*2} + \frac{d^2}{dz^2}\right) F^\dagger_{\omega_n, k_\perp}(z, z') = 0, \quad z < 0. \tag{4.77}$$

First, the general solution of Eq.(4.77) is easy to guess: it would be given in terms of increasing and decaying exponentials. More specifically, because we want $F^\dagger_{\omega_n} \rightarrow 0$ as $x \rightarrow$

$-\infty$, the solution has the form

$$F^{\dagger}_{\omega_n,k_\perp}(z,z') = f_{\omega_n}(z',k_\perp)\, e^{ia^* z} \tag{4.78}$$

From the definition,

$$F^{\dagger}_{\omega_n,k_\perp}(z',z) = F^{\dagger}_{-\omega_n,k_\perp}(z,z')\,. \tag{4.79}$$

If ω_n is changed to $-\omega_n$, a^* becomes $-a$. The reasoning above leads us to write

$$F^{\dagger}_{-\omega_n,k_\perp}(z,z') = f_{-\omega_n}(z',k_\perp)\, e^{-iaz'} \tag{4.80}$$

Combining Eqs.(4.81) and (4.80) yields

$$F^{\dagger}_{\omega_n,k_\perp}(z,z') = f_{\omega_n}(k_\perp)\, e^{ia^* z} e^{-iaz'} \quad z,z'<0, \tag{4.81}$$

with $f_{\omega_n}(k_\perp) = f_{-\omega_n}(k_\perp)$. In obtaining $F^{\dagger}_{\omega_n}(z)$ from $F^{\dagger}_{\omega_n,k_\perp}(z,z')$, the integration in $k_\perp$ can once again be conveniently transformed to an integration in $\xi_\perp$. As in Eq.(4.74), the summation in Eq.(4.11) becomes an integral at $T=0$:

$$\theta(-z)\Delta^*(z) = \theta(-z)\frac{gm}{4\pi^2}\int_{-\infty}^{\infty} d\omega_n \int_{-\mu}^{\infty} d\xi_\perp f_{\omega_n}(k_\perp)\, e^{i(a-a^*)|z|} \tag{4.82}$$

From the definitions of a and a^*, it follows that

$$i(a-a^*)|z| = -\left[4m\left[\left(\xi_\perp^2+\hbar^2\omega_n^2\right)^{1/3}+\xi_\perp\right]\right]^{1/2}|z|. \tag{4.83}$$

As argued in other situations before, the most relevant contribution comes from $\xi_\perp<0$ and the vicinity of $\omega_n=0$, so we replace $f_{\omega_n}(k_\perp)$ by $f_{\omega_0}(k_\perp)$ in the coefficient of the exponential:

$$\theta(-z)\Delta^*(z) \approx \theta(-z)\frac{gm}{2\pi^2}\int_{-\mu}^{0} d\xi_\perp f_0(k_\perp)\int_0^{\infty} d\omega_n \exp\left\{-|z|\left[4m\left[\left({\xi_\perp}^2+\hbar^2{\omega_n}^2\right)^{1/2}+\xi_\perp\right]\right]^{1/2}\right\} \tag{4.84}$$

If we carry out the integration in ω_n, keeping in mind that $\sqrt{\xi_\perp^2}=|\xi_\perp|=-\xi_\perp$, we obtain the general asymptotic behavior of the pair wave function in the normal metal:

$$\theta(-z)F(z) \;\approx \theta(-z)\frac{1}{2\pi^2|z|}\left(\frac{m}{2}\right)^{1/2}\int_{-\mu}^{0} d\xi_\perp f_0(k_\perp)\,(-\xi_\perp)^{1/2} \tag{4.85}$$

Now, if the approximations developed for $F^{\dagger}_{\omega_n}(z)$ (as in Eq.(4.59)) are taken into account and if we consider the case with perfect current transmission, this result becomes

$$\theta(-z)F(z) \approx \theta(-z)\Delta\frac{\xi_0}{|z|}\frac{mp_0}{2\pi^2}\frac{\pi}{6}. \tag{4.86}$$

Clearly, the pair wave function dies off in the normal metal much more slowly than the exponential decay derived for finite temperatures. We recall that this derivations assume a three dimensional NS junction in the clean limit in which the metals are separated by a plane boundary. Under this circumstances, the pair wave function becomes long-ranged in N, since there is simply no mechanism in that region that could cause the disruption of superconducting correlations. The situation would be different if there were some interaction in normal metal or if the system was not in the clean limit.

5 QUANTUM CONFINEMENT INFLUENCE ON THE PROXIMITY EFFECT IN NANOWIRES

We have given, in Chapter 3, a brief overview of the remarkable consequences of reducing some dimensions of a superconductor to sizes well smaller than its coherence length. In Chapter 4, we discussed how the placement of a normal metal in good electronic contact with a superconductor can induce superconducting correlations in the former. Thus, we have set the stage to discuss that which is the main goal of this thesis, namely the study of the interplay of these two effects. That is, how the proximity effect in a normal metal/superconductor junction is affected in the presence of quantum confinement of the charge carriers.

5.1 MODEL AND METHODS

To explore this phenomenon, we chose cylindrical nanowires as model systems. Each of these nanowires is comprised of two parts: a superconductor and a normal (non-superconducting) metal. The two metals are connected through a plane transverse boundary. The electronic interactions in the nanowires considered in this work can be described by a space dependent coupling parameter, $g(z)$: it has a constant finite value in the superconducting side and some other value on the normal metal side (generally zero, meaning that, in isolation, this region would not sustain the electron-electron attraction necessary for superconductivity).

Figure 6 – Simplified representation of a cylindrical nanowire comprised of a superconductor and a normal metal.

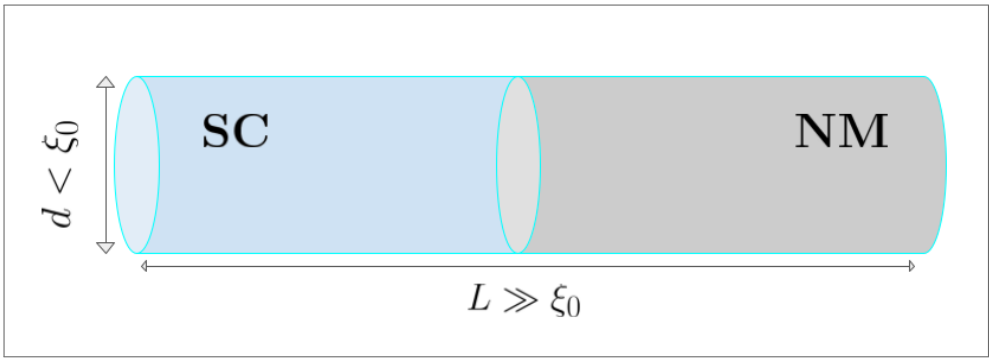

Source: The author (2022)

We take the system to be in the clean limit, i.e., the mean-free path is much larger than the coherence length, so that impurity scattering is not an issue. Additionally, we work with very low temperatures, T $\approx$ 0 K, and we consider that the nanowire is not under the influence

of any external field.

The investigation is based on the numerical self-consistent solution of the Bogoliubov-de Gennes equations in the nanowire, as described in Chapter 3. Here, however, a slight modification is introduced. Since now we work with finite nanowires of length L, instead of utilising periodic boundary conditions in the longitudinal direction and expanding the wave function in terms of $e^{ik_z z}/\sqrt{L}$, we do so in terms of $\Gamma_l(z) = \sqrt{\frac{2}{L}}\sin\left(\frac{l\pi z}{L}\right)$, with $l = 1, 2, 3\ldots$

Due to the azimuthal symmetry in the system, the electron-like and hole-like wavefunctions can be written in the form

$$\begin{pmatrix} u_i(\mathbf{r}) \\ \\ v_i(\mathbf{r}) \end{pmatrix} = \frac{e^{im\phi}}{\sqrt{2\pi}} \begin{pmatrix} u_i(\rho, z) \\ \\ v_i(\rho, z) \end{pmatrix}. \tag{5.1}$$

Similarly, the pair wave function depends only on ρ and z:

$$\Delta(\mathbf{r}) = \Delta(\rho, z) \tag{5.2}$$

Then $u_i(\rho, z)$ and $v_i(\rho, z)$ can be expanded in terms of the appropriate basis functions as follows:

$$\begin{pmatrix} u_i(\rho, z) \\ \\ v_i(\rho, z) \end{pmatrix} = \sum_{l,n} \begin{pmatrix} u^i_{nl} \\ \\ v^i_{nl} \end{pmatrix} \vartheta_n(\rho)\Gamma_l(z), \tag{5.3}$$

where the $\vartheta_n(\rho)$ are the normalized basis functions in terms of the Bessel functions J_m with zeros α_{mn}:

$$\vartheta_n(\rho) = \frac{\sqrt{2}}{RJ_{m+1}(\alpha_{mn})} J_m\left(\frac{\alpha_{mn}\rho}{R}\right). \tag{5.4}$$

As a result, the Bogoliubov-de Gennes equations attain a more convenient form for numerical treatment:

$$\left(T^i_{n,l} - E_i\right) u^i_{n,l} + \sum_{n',l'} \Delta_{nn',ll'} v^i_{n,l} \tag{5.5a}$$

$$\left(E_i - T^i_{n,l}\right) v^i_{n,l} + \sum_{n',l'} \Delta_{nn',ll'} u^i_{n,l}, i \tag{5.5b}$$

in which

$$T^i_{n,l} = \frac{\hbar^2}{2m}\left[\frac{\alpha^2_{mn}}{R^2} + \frac{\pi^2 l^2}{L^2}\right] - \mu \tag{5.6}$$

and

$$\Delta_{nn',ll'} = \iint d\rho dz \vartheta_{n'}(\rho)\Gamma_{l'}(z)\Delta(\rho,z)\Gamma_{l}(z)\vartheta_{n}(\rho). \tag{5.7}$$

This is in fact a symmetrical eigenvalue problem. To solve it, we employ the resources available at the Lapack Library of numerical routines.

5.1.1 Numerical Procedure

The numerical procedure for the self-consistent solution of the BdG equations can be roughly summarized as follows: first, the bulk value of the gap parameter Δ_{bulk} is used as an initial approximation for $\Delta(\mathbf{r})$. The BdG equations are solved, yielding a first set of eigenfuctions $u_i(\mathbf{r})$, $v_i(\mathbf{r})$ and eigenenergies E_i. These are then substituted in the self-consistency equation for $\Delta(\mathbf{r})$, resulting in a new value of the energy gap which will be substituted back in BdG equations for a new round of calculations. This iterative process continues until $\Delta(\mathbf{r})$ stops changing appreciably, that is, the maximum difference between values of $\Delta(\mathbf{r})$ from consecutive interactions is smaller than a prescribed tolerance ϵ, which is set to $\epsilon = 0.001$.

Figure 7 – Schematic representation of the numerical procedure for the self-consistent solution of the Bogoliubov-de Gennes equations.

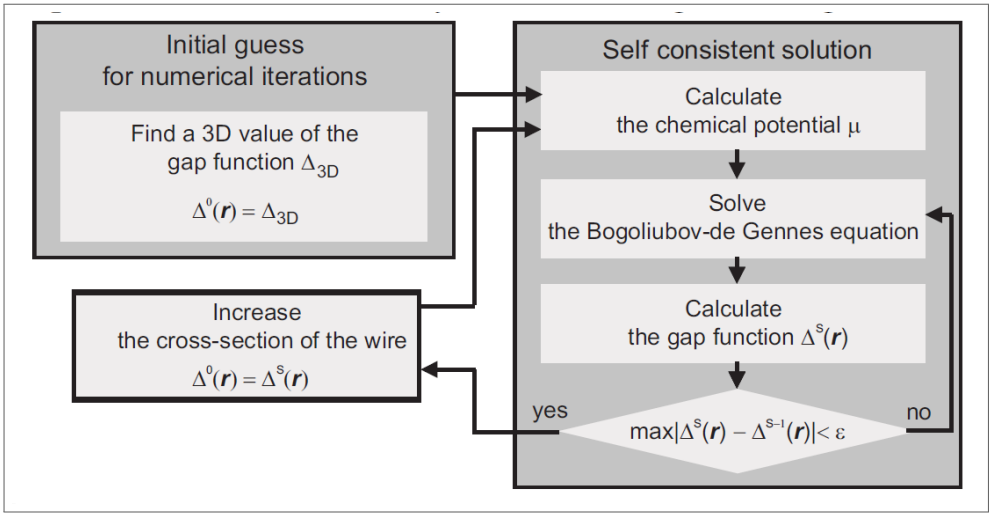

Source: Croitoru, Shanenko and Peeters (2007b)

For the simulations, we begin with $d = 1.08$ nm, where the first shape resonance in the order parameter is detected. The diameter is gradually increased, in steps of 0.02 nm, until around 4.0 nm, so that we go through multiple shape resonances. Throughout this work, the length and temperature of the nanowires were kept constant at $L = 2000$ nm and $T = 0$ K, respectively, but systems with slightly different characteristics were simulated by varying the

values of $g(z)$. For the mean electron density, the value used was $n = 4.0\ \mathrm{nm}^{-3}$. We recall that the Debye window is the interval inside which single-electron states with energy ξ_i (measured from the Fermi level) can participate in the formation of Cooper pairs and is determined by $-\hbar\omega_D < \xi_i < \hbar\omega_D$, where ω_D is the Debye frequency. The value of this governing parameter was set through $\hbar\omega_D/k_B = 0.96\ \mathrm{K}$.

Here we present the results obtained for 3 different scenarios, distinguished from each other by the values of coupling constant. In two of them, the product of the Gor'kov coupling constant and the electron density at Fermi level is set to $gN(0) = 0.39$ in the superconductor. We note that this particular combination of parameters (n, $\hbar\omega_D/k_B$, $gN(0)$) is typical of the metal lead (Pb).

In Case 1, the coupling constant was taken to be zero throughout the normal metal. In Case 2, the coupling in the normal side was set to $gN(0) = -0.195$, meaning that the electrons interact repulsively in that region, and this interaction has half the strength of that which takes place in the superconducting side. The idea behind Case 2 is to investigate how the introduction of some repulsion affects the leakage of Cooper pairs into the normal metal as compared to the situation where no repulsion is present.

For Case 3, we considered a hypothetical superconducting material with $gN(0) = 0.49$, but without any interaction in the normal metal side. This is the same situation as in Case 1, but with a higher value of $gN(0)$ in the superconducting side, to understand how varying this parameter changes the decay of superconductivity across the interface.

5.2 RESULTS

5.2.1 Qualitative discussion

The model system adopted for the simulations is comprised of a superconductor on the left side $(0\ \mathrm{nm} - 1000\ \mathrm{nm})$ and a normal metal on the right side $(1000\ \mathrm{nm} - 2000\ \mathrm{nm})$. The data generated by the numerical procedure allows us to visualize how the pair potential $\Delta(\mathbf{r})$ depends on the spatial coordinates. The 3D plot in Figure (8) shows $\Delta(\rho, z)$ for a Pb nanowire of diameter $1.30\ \mathrm{nm}$. This plot confirms visually a point discussed before about the behaviour of the pair potential. Introduction of quantum confinement in the radial direction breaks translational invariance, so that $\Delta(\mathbf{r})$ could not be considered constant throughout the wire, as is typically done in the BCS framework for bulk superconductors. Instead, $\Delta(\mathbf{r})$

is strongly dependent on the radial coordinate ρ, but does not change appreciably in the longitudinal direction, except near the boundaries.

Figure 8 – Three-dimensional representation of $\Delta(\rho, z)$ in an entirely superconducting nanowire, with $d = 1.30\ \mathrm{nm}$ and $g(z)N(0) = 0.39$.

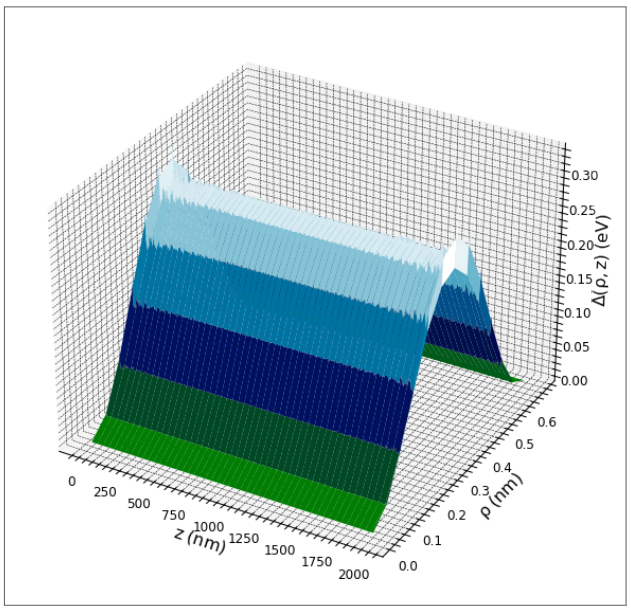

Source: The author (2022)

These calculations were repeated for several values of the wire's thickness. At each step, the diameter was increased by an amount of $0.02nm$. We have seen, in Chapter 3, that varying the thickness of nanowires such as these leads to oscillations in characteristic properties of the superconducting material, such as the order parameter. This phenomenon is exemplified here in Figure (9). As is clear from Figure (8), $\Delta(\rho, z)$ and $F(\rho, z)$ depend significantly on ρ, but not so much on z. For Figure (9), we chose, for each nanowire diameter, the value of ρ corresponding to the peak value of $F(\rho, z)$ and took an average along the z-direction. The shape resonances are evident: for certain diameters, F reaches remarkably high values, but decreases as the diameter is increased until another resonant thickness is reached. Again, the appearance of such shape resonances is related to the crossing of the Fermi surface by one of the discrete subbands that appear due to quantum confinement.

Next, we can attempt to perceive visually the consequences of connecting a normal metal to the superconductor, with a planar transverse interface between them. This is the situation in Figure 10, where we present data for the pair amplitude $F(\rho, z) = \Delta(\rho, z)/g(z)$. The plots shown here for illustrative purposes correspond to a Pb nanowire , with $gN(0) = 0.39$ in SC and 0.0 in NM. Thus, $\Delta(z) = g(z)F(\rho, z)$ simply vanishes throughout the NM region. We

Figure 9 – Some of the shape resonances in the pair amplitude F. The peak value of F is plotted for each value of wire diameter.

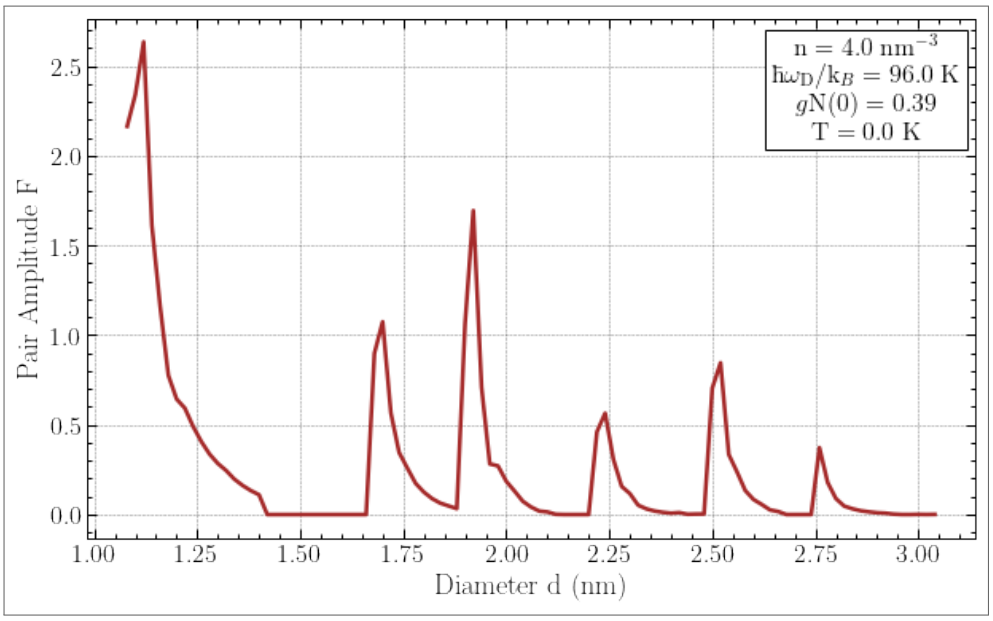

Source: The author (2022)

clearly observe the expected decay in $F(\rho, z)$ across the wire cross section which takes place close to the interface at $z = 1000$ nm.

To better understand this phenomenon and to approach the data in a more quantitative fashion, we consider separately the points lying in the plane intersecting the plot vertically through its peak. The result is shown in Figure 11. Figure 11a and Figure 11b show the profile of the pair amplitude and pair potential, respectively, corresponding to a wire of diameter 1.30nm and taken at a radial distance ρ associated with their peaks. Because we work with a fixed value of ρ, it is convenient to update our notation to $F(z)$ and $\Delta(z)$. In the figures, these quantities are normalized with respect to their average z values in the absence of the proximity effect.

The plot of $F(z)$ is quite interesting, since it displays several features of proximity phenomena. First of all, we clearly observe that the pair amplitude decays in NM, but is seen to maintain a finite value deep inside that region, away from from the interface. At this point we cannot make any precise quantitative claim about the functional form of this decay, but it already seems to be in accordance with an inverse power law decay typical for SN junctions at zero temperature. An exponential decay, which characterizes the proximity effect at finite temperatures, leads to $F(z)$ vanishing not too far away from the interface. At zero temperature, the absence of a disruptive mechanism means that the superconducting correlations can

Figure 10 – Three-dimensional plot of $F(\rho, z)$ in a nanowire which is half superconductor and half normal metal. The interface lies at 1000 nm and $g(z)N(0) = 0.39\ (\mathrm{SC}),\ 0.0\ (\mathrm{NM})$

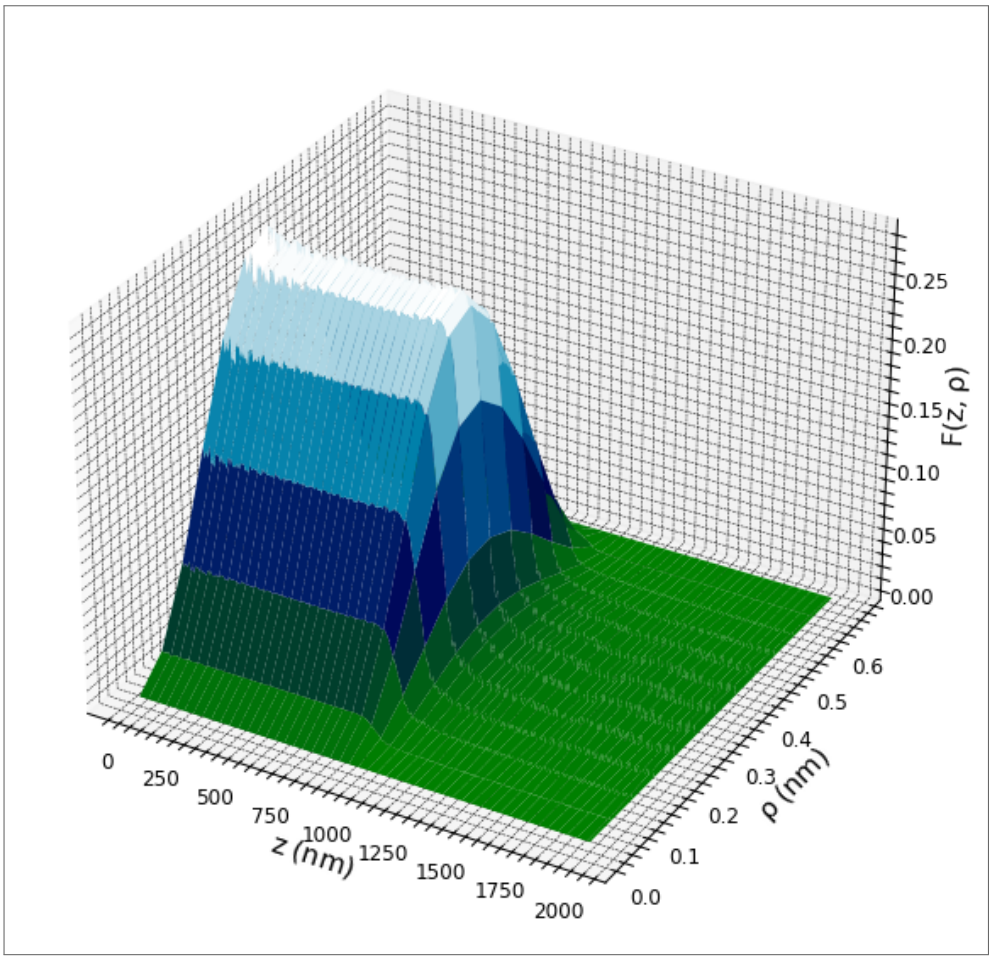

Source: The author (2022)

be seen deep inside the normal metal (FALK, 1963).

A second remarkable feature is the weakening of superconductivity in SC close to the interface, in some papers presented as the inverse proximity effect (BUZDIN, 2005). Other authors, like Zaikin and Zharkov (1983) and Falk (1963), estimate that the distance from the interface over which this weakening takes place is approximately ξ_0, the superconductor coherence length. For Pb, $\xi_0 \approx 83\ \mathrm{nm}$ (FETTER; WALECKA, 2003). In Figure 11a, the distance over which $F(z)$ decreases before the interface is of the order of $70\ \mathrm{nm}$, which seems reasonably close to the expected value, ξ_0. Thirdly, we note that Zaikin and Zharkov (1983) also conclude that at the interface the pair amplitude should be approximately half of its value inside SC, away from the boundary with NM, which we denote by F_S. From Figure 11, this is close to what we observe, as the plot crosses the line representing the interface at around $0.6 \times F_S$.

We note, however, that although the results we obtained for a nanowire with this par-

Figure 11 – Profiles of the normalized pair amplitude $F(z)$, (a), and pair potential $\Delta(z)$, (b). $\Delta(z)$ is identically zero in NM, whilst $F(z)$ remains finite over a significant distance from the interface. The parameters used for the superconductor correspond to lead (Pb).

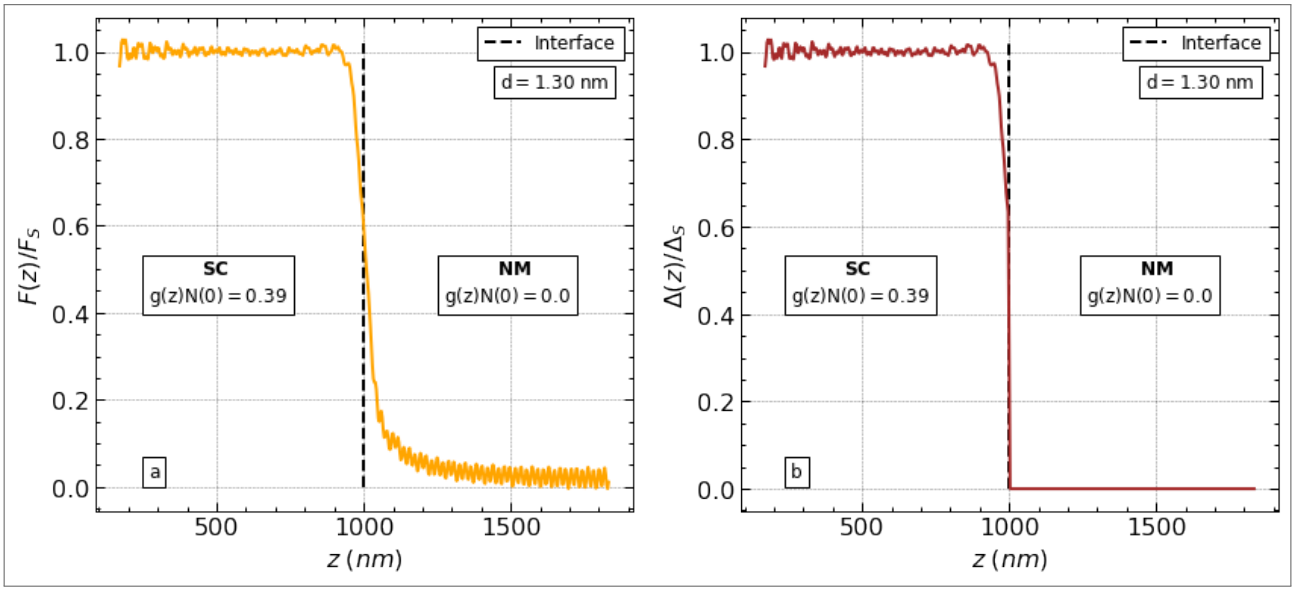

Source: The author (2022)

ticular radius are in line with the literature concerning the traditional 3D proximity effect, complications may arise due to finite-size effects. As a matter of fact, Figure 12 is precisely an example of that. The data shown in this figure corresponds to a diameter value associated with a shape resonance. The reduction in $F(z)$ in S near the interface, typical of the inverse proximity effect, is not seen in this case. On the contrary, the pair amplitude actually develops a bump/peak right before the interface. This phenomenon seems to arise from the interplay of two effects: the actual inverse proximity effect and Friedel oscillations.

When a metal is subject to a local disturbance, like a localized impurity, its electron density can acquire a spatial modulation that resembles a standing wave. This perturbations are called Friedel oscillations (HARRISON, 1979), (WOLF, 2012). Friedel-like oscillations are observed in superconductor-normal-metal interfaces, arising due to the sharpness of the interface (VALLS; BRYAN; ŽUTIĆ, 2010).

The range for the reduction of superconductivity in S away from the interface is set by the coherence length, as pointed out by Shanenko, Croitoru and Peeters (2010), the coherence length drops radically at resonant points. On the other hand, the barrier is much enhanced at a resonance and, as a consequence, Friedel oscillations become very pronounced near the interface. This interplay of strong Friedel oscillations and a weak inverse proximity effect leads to the particular configuration seen in Figure 12.

Figure 12 – Profiles of the normalized pair amplitude $F(z)$, (a), and pair potential $\Delta(z)$, (b). The diameter chosen here corresponds to a resonance in $F(z)$ and $\Delta(z)$. The pronounced Friedel oscillations near the interface are shown. The parameters used for the superconductor correspond to lead (Pb).

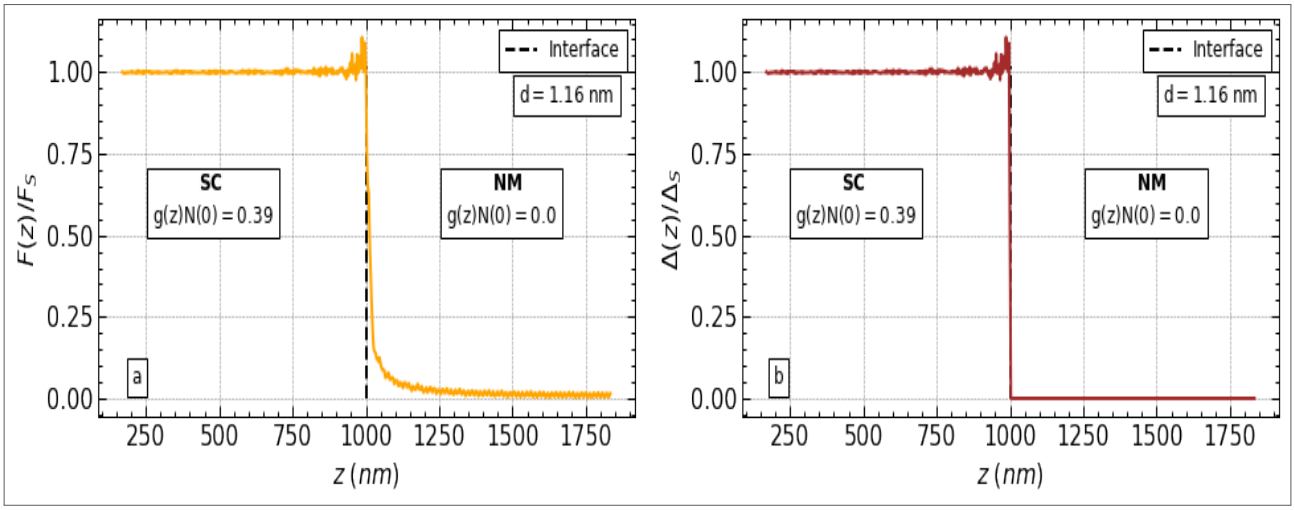

Source: The author (2022)

5.2.2 Power law decay of the pair amplitude

Having made this preliminary exposition of results, we can now move on to a more systematic treatment of the data. As before, we work with data points in NM corresponding to a radial distance ρ associated with the peak of $F(\rho, z)$. The idea is to fit a model function to the discretized values of $F(z)$ in the normal metal obtained through the numerical procedure. Motivated by what is already known for the proximity effect, as presented in Chapter 4, we take as fitting model

$$F(z) = A + \frac{B}{(z - z_0)^{\alpha}}, \tag{5.8}$$

where the parameters A, B and α are to be determined numerically through the curve fitting procedure, and z_0 marks the location of the SN interface. In our case, $z_0 = 1000\ \mathrm{nm}$. From the literature, we expect A to be essentially zero. In this thesis, we are primarily interested in understanding how the power-law decay parameter α changes as the thickness of the nanowires varies, under three different configurations of coupling constant, as stated previously.

The so-called Levenberg-Marquardt method is a standard numerical routine used in curve fitting problems when the model depends nonlinearly on the unknown parameters, as is the case in Eq.(5.8) (PRESS et al., 2007). In our work, we made use of the Levenberg-Marquardt method as implemented in the *curve_fit* function of Python's Scipy library. This function receives as arguments the model function, two data arrays containing the values of the dependent and

independent variables, an array with data uncertainties and a tuple containing a user provided first approximation of the parameters. It yields, if no error occurs, an array containing the optimized values of the fitting parameters and the covariance matrix. This matrix contains, at each of its entries, the covariance of two of the parameters. Roughly speaking, the covariance measures how much two variables change together. The covariance of a variable with itself is its variance. Thus, in our case the covariance matrix has the form

$$\begin{pmatrix} var(A) & cov(A,B) & cov(A,\alpha) \\ cov(B,A) & var(B) & cov(B,\alpha) \\ cov(\alpha,A) & cov(\alpha,B) & var(\alpha) \end{pmatrix} \tag{5.9}$$

If alternative ways of writing the same model function are available, one should choose the one that results in the minimum correlation between any two different adjustable parameters. The result of this optimization procedure is exemplified in Figure 13, where the red curve is

Figure 13 – Example of a curve fitting procedure. $F(z)$ is normalized with respect to its average value inside the superconductor, away from the interface. The data corresponds to a wire of diameter d = 1.30 nm and $g(z)N(0) = 0.39\ (\mathrm{SC}),\ 0.0\ (\mathrm{NM})$.

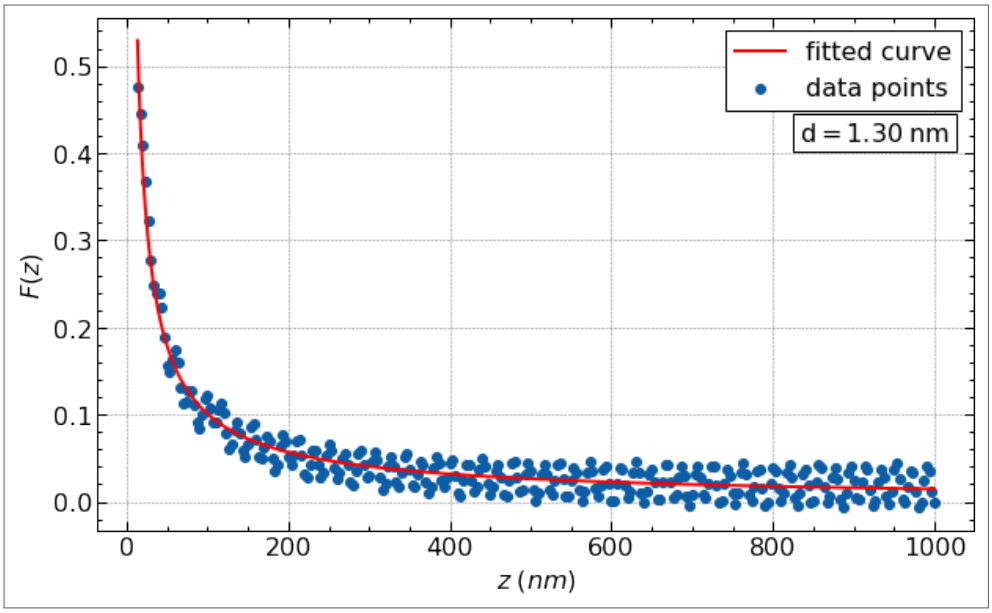

Source: The author (2022)

the optimal fitting and the blue dots are the original data. Once again, the exemplifying figure corresponds to a wire of diameter 1.30 nm and $g(z)N(0) = 0.39\ (\mathrm{SC}),\ 0.0\ (\mathrm{NM})$.

The fitting procedure described above is carried out for multiple wire thicknesses. Our main interest, as stated before, is to understand how the parameter α depends on the diameter in

order to see how the proximity effect is influenced by quantum confinement. In Figure 14 several values of α (green dots) plotted against wire diameter. We see that a pattern of peaks in the value of α develops as the diameter is increased. The red line is simply a reproduction of Figure 9. Indeed, this figure shows a remarkable correlation between the peaks of the pair amplitude $F(z)$ and those of α.

Figure 14 – Comparison of the oscillations in the parameter α with the oscillations in F. The peaks and troughs occur at the same diameters for the two quantities. The data corresponds to $g(z)N(0) = 0.39$ (SC), 0.0 (NM)

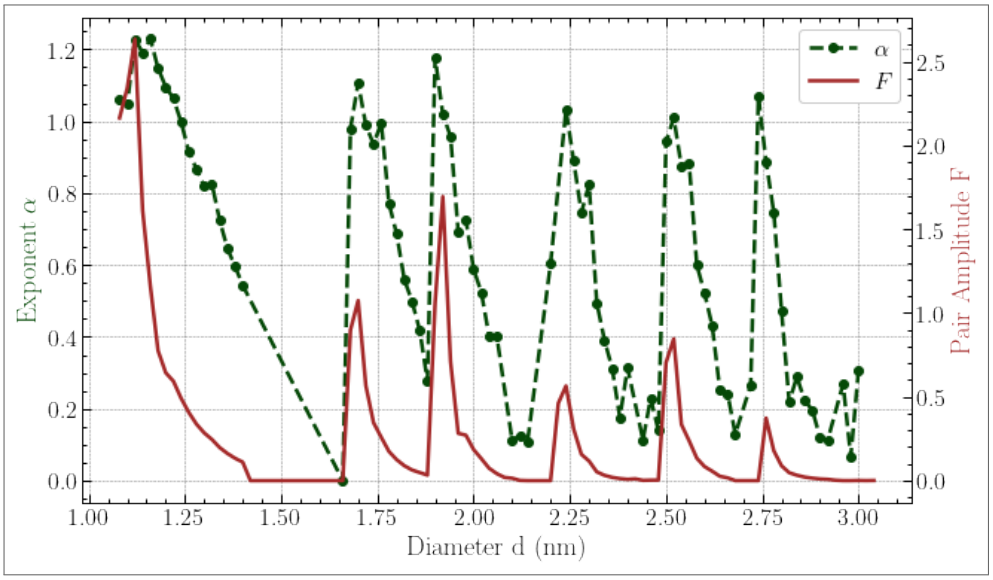

Source: The author (2022)

More data is presented in the following plots. Figure 15 is concerned with Case 1 ($g(z)N(0) = 0.39$ in SC but no interaction in NM). Figure 16. corresponds to Case 2 ($g(z)N(0) = 0.39$ in SC with some repulsion in NM), and Figure 17 presents the data of Case 3 ($g(z)N(0) = 0.49$ in SC, no interaction in NM). In the plots, the purple horizontal line marks the $\alpha = 1.0$ value, which is expected for 3D systems at $T = 0$ K, as discussed and derived in 4.

The results for the 3 cases are generally very similar. The trend uncovered in Figure 14 is present throughout all the plots: α, as a function of wire thickness, develops a distinct oscillatory pattern and the peaks of the oscillations occur at the resonant thicknesses, i.e, the diameters where the pair amplitude reaches its maxima as well. In all cases, the peak value of α are very close to 1.0. That, as we recall, is the characteristic power-law decay of $F(z)$ for 3D SN junctions. As the thickness is increased past a resonant point, α gradually decreases and can reach values well below 1.0 right before the next shape resonance comes into play. Now, we have pointed out before (Chapter 4) that investigations of the proximity effect in 2D

Figure 15 – Oscillatory behavior of α as a function of wire diameter. Case 1.

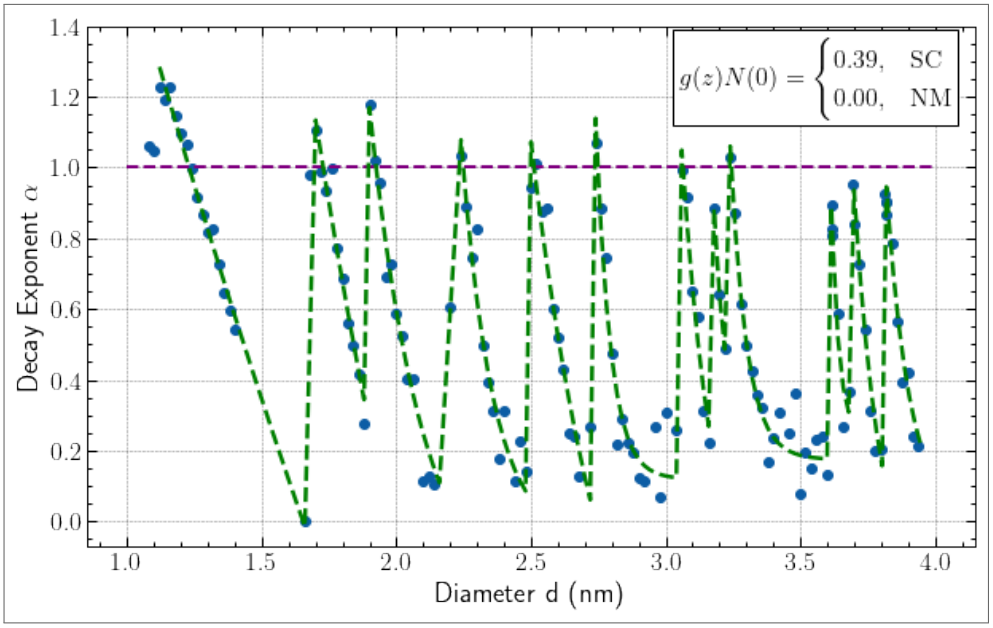

Source: The author (2022)

Figure 16 – Oscillatory behavior of α as a function of wire diameter. Case 2.

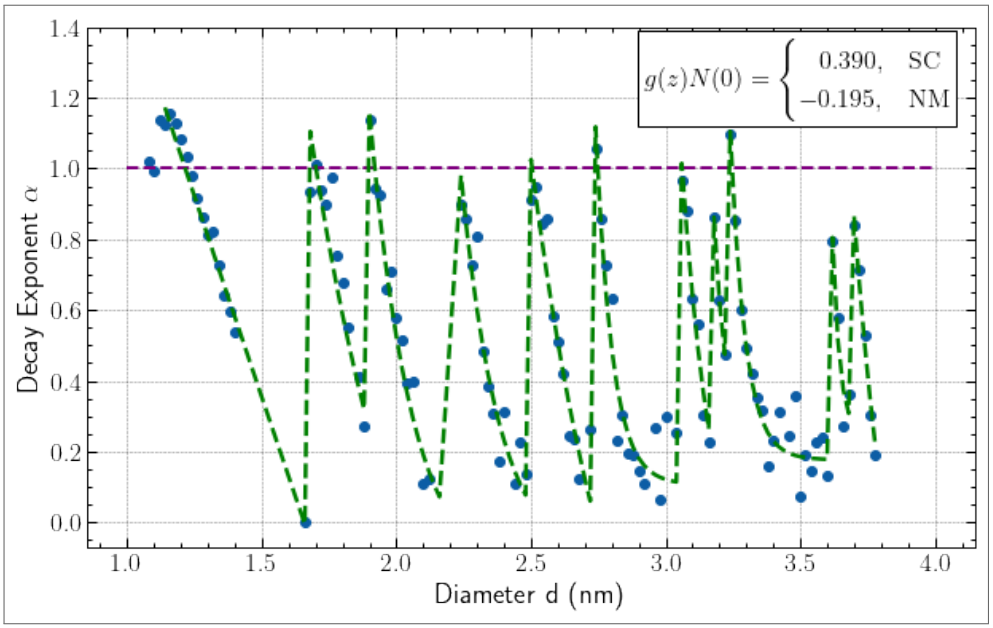

Source: The author (2022)

and 1D superconductor/ferromagnet junctions found reduced values for the power-law decay parameter compared to the 3D situation, namely $\alpha_{2D} = \frac{1}{2}$ (KONSCHELLE; CAYSSOL; BUZDIN, 2008) and $\alpha_{1D} \approx 0$ (CAYSSOL; MONTABAUX, 2004). One might wonder if this reduction in α due to reduced dimensionality has any connection to the confinement induced oscillations we observed in this parameter. One can try to make sense of this similarity by recalling how

Figure 17 – Oscillatory behavior of α as a function of wire diameter. Case 3.

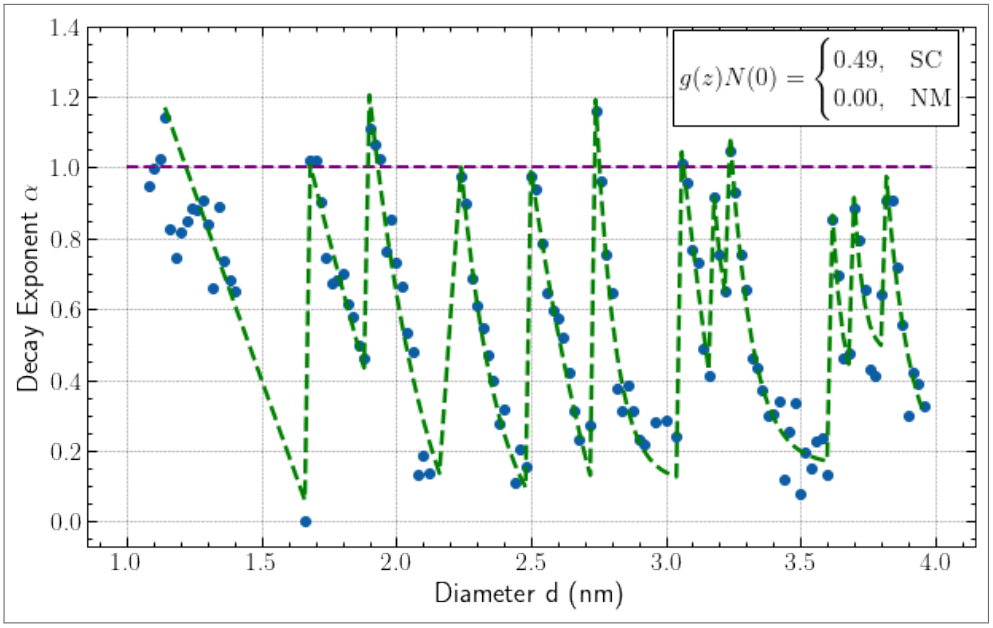

Source: The author (2022)

quantum confinement influences the binding energy of electrons in a Cooper pair and its length along a non-confined direction. Although the results alluded to in Chapter 3 are for only 2 electrons above the Fermi surface, they still provide useful insight for this discussion. At a resonant point, the binding energy E_g dramatically increases and ξ_c, the size of a cooper pair along the non-confined direction, reaches its smallest value. When the thickness is increased to off-resonant values, E_g decreases and ξ_c increases. So we may say that the Cooper pairs are least deformed from a spatially symmetric form when resonances are at play. If the wire diameter is taken to off-resonant values, ξ_c increases considerably and the Cooper pair can be thought to be greatly elongated in the longitudinal direction. Thus, resonance points are expected to be the ones with the least pronounced deviation from the spherically symmetric Cooper pair in 3D and that would lead to values of α close to 1.0 (the typical 3D value) for nanowires with resonant thickness. As the diameter is increased, the cooper pairs become elongated and can resemble the situation found in 2D and 1D system. Hence, one could expect α to approach 2D and 1D values as well when wire thickness is increased before next shape resonance.

6 CONCLUSION

In this thesis, we investigated the clean limit proximity effect in nanowires at low temperatures and under the influence of quantum size effects. More precisely, the nanowires are half superconductor, half normal metal, and are connected through a transverse plane boundary.

For sufficiently thin nanowires, size-resonance effects become relevant and several properties of a superconductor are modified with respect to the bulk values. In order to have systems in this regime, we considered nanowires with diameters varying from approximately 1.0 nm to 4.0 nm.

For clean samples at T=0, the literature indicates that the decay of the pair wave function in the non-superconducting region follows an inverse power law relation:

$$F(z) \propto \frac{1}{|z - z_0|^{\alpha}}, \begin{cases} \alpha = 1.0, \ \mathrm{3D}, \\ \alpha = 0.5, \ \mathrm{2D}, \\ \alpha = 0.0, \ \mathrm{1D}, \end{cases} \tag{6.1}$$

where again z_0 is the position of the interface.

Based on this, the main objective of this thesis was to try and determine how the parameter α varies for nanowires in the regime in which quantum confinement of the electrons affects the properties of the system and causes the pair amplitude, among others, to gain an oscillatory behavior as a function of thickness. We considered 3 slightly different situations, by varying the value of the coupling constant in the superconductor and in the normal metal.

By extracting the value of α for SN wires of several diameters, we obtained that this parameter also oscillates as a function of sample thickness, and its peaks and troughs match those of the pair amplitude, i.e., the size resonances in α match those in F(z). For a given resonant wire diameter, α peaks at about 1.0 (the 3D typical value) and diminishes subsequently to values much smaller than 1.0 (reminiscent of the 1D situation) until the next resonance comes into play. We speculate that this variation of α between values close to 3D, 2D, and 1D systems is related to the fact the Cooper pair form and size also go over those typical of 3D, 2D, and 1D systems. Overall, α seems to approximate 1.0 as diameter increases, as is expected, since for sufficiently large diameters the 3D value $\alpha = 1.0$ should be observed. Not much difference is noticed in the behavior of the parameter α in the situations considered here.

REFERENCES

ABRIKOSOV, A. A.; GOR'KOV, L. P.; DZYALOSHINSKII, I. E. On the application of quantum-field-theory methods to problems of quantum statistics at finite temperatures. *Soviet Phys. JETP*, v. 9, n. 3, p. 636, Sep 1959. Available at: <http://jetp.ras.ru/cgi-bin/e/index/e/9/3/p636?a=list>.

ALEXANDROV, A. S.; KABANOV, V. V. Low-temperature proximity effect in clean metals with repulsive electron-electron interaction. *Phys. Rev. B*, American Physical Society, v. 78, p. 132510, Oct 2008. Available at: <https://doi.org/10.1103/PhysRevB.78.132510>.

ALTOMARE, F.; CHANG, A. M. *One-Dimensional Superconductivity in Nanowires*. [S.l.]: WILEY-VCH, 2013.

ANDERSON, P. W. Theory of dirty superconductors. *J. Phys. Chem. Solids*, Elsevier, v. 11, p. 26, Sept 1959. Available at: <https://doi.org/10.1016/0022-3697(59)90036-8>.

ANDREEV, A. F. The thermal conductivity of the intermediate state in superconductors. *Soviet Phys. JETP*, v. 19, n. 5, p. 1823, May 1964. Available at: <http://www.jetp.ras.ru/cgi-bin/dn/e_019_05_1228.pdf>.

BARDEEN, J.; COOPER, L. N.; SCHRIEFFER, J. R. Microscopic theory of superconductivity. *Phys. Rev.*, v. 106, n. 1, p. 162, Apr 1957. Available at: <https://journals.aps.org/pr/abstract/10.1103/PhysRev.106.162>.

BARDEEN, J.; COOPER, L. N.; SCHRIEFFER, J. R. Theory of superconductivity. *Phys. Rev*, American Physical Society, v. 108, n. 5, p. 1175, Dec 1957. Available at: <https://journals.aps.org/pr/abstract/10.1103/PhysRev.108.1175>.

BEDARD, F.; MEISSNER, H. Measurements of contact resistance between normal and superconducting metals. *Phys. Rev.*, American Physical Society, v. 101, n. 1, p. 26, Jan 1956. Available at: <https://journals.aps.org/pr/abstract/10.1103/PhysRev.101.26>.

BERGERET, F. S.; VOLKOV, A. F.; EFETOV, K. B. Odd triplet superconductivity and related phenomena in superconductor-ferromagnet structures. *Rev. Mod. Phys*, American Physical Society, v. 77, n. 4, p. 1321, Nov 2005. Available at: <https://doi.org/10.1103/RevModPhys.77.1321>.

BLATT, J. M.; THOMPSON, C. J. Shape resonances in superconducting thin films. *Phys. Rev. Lett.*, American Physical Society, USA, v. 10, n. 8, p. 332, Apr. 1963. Available at: <https://journals.aps.org/prl/abstract/10.1103/PhysRevLett.10.332>.

BLONDER, G. E.; TINKHAM, M.; KLAPWIJK, T. M. Transition from metallic to tunneling regimes in superconducting microconstrictions: Excess current, charge imbalance, and supercurrent conversion. *Phys. Rev. B*, v. 25, n. 7, p. 4515, Apr 1982. Available at: <https://journals.aps.org/prb/abstract/10.1103/PhysRevB.25.4515>.

BOAS, M. L. *Mathematical methods in the physical sciences; 2nd ed.* [S.l.]: Wiley, 1983.

BULAEVSKII, L. N.; BUZDIN, A. I.; PANYUKOV, S. V. The oscillation dependence of the critical current on the exchange field of ferromagnetic metals (f) in josephson junction s-f-s. *Solid State Commum.*, v. 44, n. 4, p. 539, Oct 1982. Available at: <https://doi.org/10.1016/0038-1098(82)90141-7>.

BUZDIN, A. I. Proximity effects in superconductor-ferromagnet heterostructures. *Rev. Mod. Phys.*, American Physical Society, v. 77, n. 3, p. 935, sep 2005. Available at: <https://journals.aps.org/rmp/abstract/10.1103/RevModPhys.77.935>.

BUZDIN, A. I.; BULAEVSKII, L. N.; PANYUKOV, S. V. Critical-current oscillations as a function of the exchange field and thickness of the ferromagnetic metal (f) in an s-f-s josephson junction. *JETP Lett.*, v. 35, n. 4, p. 178, Feb 1982. Available at: <http://jetpletters.ru/ps/1314/article_19853.shtml>.

CAYSSOL, J.; MONTABAUX, G. Exchange-induced ordinary reflection in a single-channel superconductor-ferromagnet-superconductor junction. *Phys. Rev. B*, American Physical Society, v. 70, n. 22, p. 224520, Dec. 2004. Available at: <https://journals.aps.org/prb/abstract/10.1103/PhysRevB.70.224520>.

CHANDRAN A.; IADECOLA, T. et al. Quantum many-body scars: A quasiparticle perspective. v. 14, p. 443, 2023. Available at: <https://www.annualreviews.org/doi/abs/10.1146/annurev-conmatphys-031620-101617>.

CHEN, Y.; CROITORU, M. D.; SHANENKO, A. A.; PEETERS, F. M. Superconducting nanowires: quantum confinement and spatially dependent hartree–fock potential. *J. Phys.: Condens. Matter*, v. 21, n. 43, p. 435701, Oct 2009. Available at: <https://doi.org/10.1088/0953-8984/21/43/435701>.

CHIOU, C.; KLOKHOLM, E. A study of superimposed tin and silver films etude de films d'etain et d'argent superposes eine untersuchung übereinandergeschichteter zinn- und silberfilme. *Acta Metallurgica*, Elsevier, v. 12, n. 8, p. 883, Aug 1964. Available at: <https://doi.org/10.1016/0001-6160(64)90147-6>.

CLARKE, J. The proximity effect between superconducting and normal thin films in zero field. *J. Phys. Colloques*, v. 29, n. C2, Feb 1968. Available at: <https://doi.org/10.1051/jphyscol:1968201>.

CROITORU, M. D.; SHANENKO, A. A. et al. Superconducting nanowires: Interplay of discrete transverse modes with supercurrent. *Phys. Rev. B*, American Physical Society, v. 80, p. 024513, jul 2009. Available at: <https://doi.org/10.1103/PhysRevB.80.024513>.

CROITORU, M. D.; SHANENKO, A. A.; PEETERS, F. M. Dependence of superconducting properties on the size and shape of a nanoscale superconductor: From nanowire to film. *Phys. Rev. B*, American Physical Society, v. 76, p. 024511, Jul 2007. Available at: <https://doi.org/10.1103/PhysRevB.76.024511>.

CROITORU, M. D.; SHANENKO, A. A.; PEETERS, F. M. Size-resonance effect in cylindrical superconducting nanowire. *Moldavian Journal of the Physical Sciences*, v. 6, n. 1, p. 39, jan 2007. Available at: <https://mjps.nanotech.md/archive/2007/article/3680>.

CROITORU, M. D.; VAGOV, A.; SHANENKO, A. A.; AXT, V. M. The cooper problem in nanoscale: enhancement of the coupling due to confinement. *Superconductor Science and Technology*, IOP Publishing, v. 25, n. 12, p. 124001, Nov 2012. Available at: <https://doi.org/10.1088/0953-2048/25/12/124001>.

CUEVAS, J.; RODITCHEV, D.; CREN, T.; BRUN, C. Proximity effect: A new insight from in situ fabricated hybrid nanostructures. In: NARLIKAR, A. V. (Ed.). *The Oxford Handbook of Small Superconductors*. Oxford: Oxford University Press, 2017. p. 108.

DEUTSCHER, G.; GENNES, P. G. de. Proximity effects. In: PARKS, R. D. (Ed.). *Superconductivity*. New York: CRC Press, 1969. v. 2, p. 1005.

EILENBERGER, G. Transformation of gorkov's equation for type ii superconductors into transport-like equations. *Z. Physik*, Springer, v. 214, p. 195, Apr 1968. Available at: <https://doi.org/10.1007/BF01379803>.

ESTèVE, D.; POTHIER, H.; GUéRON, S.; BIRGE, N. The proximity effect in mesoscopic diffusive conductors. In: SOHN, L. L.; KOUWENHOVEN, L. P.; SCHöN, G. (Ed.). *Mesoscopic Electron Transport*. [S.l.: s.n.], 1996. p. 375.

FALK, D. S. Superconductors with plane boundaries. *Phys. Rev*, American Physical Society, v. 132, n. 4, p. 1576, nov 1963. Available at: <https://journals.aps.org/pr/abstract/10.1103/PhysRev.132.1576>.

FETTER, A. L.; WALECKA, J. D. *Quantum Theory of Many-Particle Systems*. [S.l.]: Dover Publications, 2003.

FRöHLICH, H. Theory of the superconducting state. i. the ground state at the absolute zero of temperature. *Phys. Rev.*, v. 79, p. 845, Sep 1950. Available at: <https://doi.org/10.1103/PhysRev.79.845>.

GENNES, P. G. de. Boundary effects in superconductors. *Rev. Mod. Phys.*, American Physical Society, v. 36, n. 1, p. 225, jan 1964. Available at: <https://journals.aps.org/rmp/abstract/10.1103/RevModPhys.36.225>.

GENNES, P. G. de. *Superconductivity of Metals and Alloys*. [S.l.]: W. A. Benjamin, 1966.

GENNES, P. G. de; GUYON, E. Superconductivity in "normal" metals. *Phys. Lett.*, Elsevier, v. 3, n. 4, p. 168, Jan 1963. Available at: <https://doi.org/10.1016/0031-9163(63)90401-3>.

HALTERMAN, K.; VALLS, O. T. Proximity effects at ferromagnet-superconductor interfaces. *Phys. Rev. B*, American Physical Society, v. 65, n. 1, p. 014509, nov 2001. Available at: <https://journals.aps.org/prb/abstract/10.1103/PhysRevB.65.014509>.

HALTERMAN, K.; VALLS, O. T. Proximity effects and characteristic lengths in ferromagnet-superconductor structures. *Phys. Rev. B*, American Physical Society, v. 66, n. 22, p. 332, dec 2002. Available at: <https://journals.aps.org/prb/abstract/10.1103/PhysRevB.66.224516>.

HARRISON, W. A. Tunneling from an independent-particle point of view. *Phys. Rev.*, American Physical Society, v. 123, n. 1, p. 85, Jul 1961. Available at: <https://journals.aps.org/pr/abstract/10.1103/PhysRev.123.85>.

HARRISON, W. A. *Solid State Theory*. [S.l.]: Dover Publications, 1979.

HAUSER, J. J.; THEUERER, H. C.; WERTHAMER, N. R. Proximity effects between superconducting and magnetic films. *Phys. Rev.*, American Physical Society, v. 142, n. 1, p. 118, Feb 1966. Available at: <https://journals.aps.org/pr/abstract/10.1103/PhysRev.142.118>.

HILSCH, P. Zum verhalten von supraleitern im kontakt mit normalleitern. *Z. Phys.*, Springer, v. 167, p. 511, Oct 1962. Available at: <https://link.springer.com/article/10.1007%2FBF01378178>.

HOLM, R.; MEISSNER, W. Messungen mit hilfe von flüssigem helium. xiii. *Z. Phys.*, Springer, v. 74, p. 715, November 1932. Available at: <https://link.springer.com/article/10.1007%2FBF01340420>.

KIVELSON, S. A.; ROKHSAR, D. S. Bogoliubov quasiparticles, spinons, and spin-charge decoupling in superconductors. *Phys. Rev. B*, American Physical Society, v. 41, n. 16, p. 11693, Jun 1990. Available at: <https://journals.aps.org/prb/abstract/10.1103/PhysRevB.41.11693>.

KLAPWIJK, T. M. Proximity effect from an andreev perspective. *J. Supercond.*, Springer, v. 17, p. 593, Oct 2004. Available at: <https://doi.org/10.1007/s10948-004-0773-0>.

KONSCHELLE, F.; CAYSSOL, J.; BUZDIN, A. Long-range singlet proximity effect in ferromagnetic nanowires. *Phys. Rev. B*, American Physical Society, v. 82, p. 180509, Nov 2010. Available at: <https://doi.org/10.1103/PhysRevB.82.180509>.

KONSCHELLE, F.; CAYSSOL, J.; BUZDIN, A. I. Nonsinusoidal current-phase relation in strongly ferromagnetic and moderately disordered sfs junctions. *Phys. Rev. B*, American Physical Society, v. 78, n. 13, p. 134505, Oct. 2008. Available at: <https://journals.aps.org/prb/abstract/10.1103/PhysRevB.78.134505>.

LINDER, J.; ZAREYAN, M.; SUDBØ. Proximity effect in ferromagnet/superconductor hybrids: From diffusive to ballistic motion. *Phys. Rev. B*, American Physical Society, v. 79, n. 6, p. 064514, feb 2009. Available at: <https://journals.aps.org/prb/abstract/10.1103/PhysRevB.79.064514>.

LONDON, F.; LONDON, H. The electromagnetic equations of the supraconductor. *Proc. Roy. Soc. A*, v. 149, n. 866, p. 71, March 1935. Available at: <https://doi.org/10.1098/rspa.1935.0048>.

LONDON, F.; LONDON, H. Supraleitung und diamagnetismus. *Physica*, v. 2, p. 341, 1935. Available at: <https://www.sciencedirect.com/science/article/abs/pii/S0031891435900970>.

MEISSNER, H. Measurements on superconducting contacts. *Phys. Rev.*, American Physical Society, v. 109, n. 3, p. 686, Feb 1958. Available at: <https://journals.aps.org/pr/abstract/10.1103/PhysRev.109.686>.

MEISSNER, H. Superconductivity of contacts with interposed barriers. *Phys. Rev.*, American Physical Society, v. 117, p. 672, Feb 1960. ISSN 3. Available at: <https://journals.aps.org/pr/abstract/10.1103/PhysRev.117.672>.

MEISSNER, W.; OCHSENFELD, R. Ein neuer effekt bei eintritt der supraleitfähigkeit. *Naturwiss.*, Springer, v. 21, p. 787, Nov 1933. Available at: <https://link.springer.com/article/10.1007%2FBF01504252>.

ONNES, H. K. The superconductivity of mercury. *Comm. Phys. Lab. Univ. Leiden*, 1911.

PANNETIER, B.; COURTOIS, H. Andreev reflection and proximity effect. *J. Low Temp. Phys.*, Springer, v. 118, p. 599, March 2000. Available at: <https://doi.org/10.1023/A:1004635226825>.

PEETERS, F. M.; SHANENKO, A. A.; CROITORU, M. D. Nanoscale superconductivity. In: SATTLER, K. D. (Ed.). *Handbook of Nanophysics: Principles and Methods*. [S.l.]: CRC Press, 2009.

PRESS, W. H.; TEUKOLSKY, S. A.; VETTERLING, W. T.; FLANNERY, B. P. *Numerical Recipes: The Art of Scientific Computing*. 3. ed. [S.l.]: Cambridge University Press, 2007.

REEG, C.; LOSS, D.; KLINOVAJA, J. Finite-size effects in a nanowire strongly coupled to a thin superconducting shell. *Phys. Rev. B*, American Physical Society, v. 96, n. 12, p. 125426, Sep 2017. Available at: <https://journals.aps.org/prb/abstract/10.1103/PhysRevB.96.125426>.

REEG, C.; LOSS, D.; KLINOVAJA, J. Proximity effect in a two-dimensional electron gas coupled to a thin superconducting layer. *Beilstein J. Nanotechnol.*, v. 9, p. 1263, 2018. Available at: <https://doi.org/10.3762/bjnano.9.118>.

ROSE-INNES, A. C.; SERIN, t. Superconductivity of superimposed metals. *Phys. Rev. Lett.*, American Physical Society, v. 7, n. 7, p. 278, Oct 1961. Available at: <https://journals.aps.org/prl/abstract/10.1103/PhysRevLett.7.278>.

SHANENKO, A. A.; CROITORU, M. D. Shape resonances in the superconducting order parameter of ultrathin nanowires. *Phys. Rev. B*, American Physical Society, v. 73, n. 1, p. 012510, jan 2006. Available at: <https://journals.aps.org/prb/abstract/10.1103/PhysRevB.73.012510>.

SHANENKO, A. A.; CROITORU, M. D.; PEETERS, F. M. Oscillations of the superconducting temperature induced by quantum well states in thin metallic films: Numerical solution of the bogoliubov–de gennes equations. *Phys. Rev. B*, American Physical Society, v. 75, n. 1, p. 014519, jan 2007. Available at: <https://journals.aps.org/prb/abstract/10.1103/PhysRevB.75.014519>.

SHANENKO, A. A.; CROITORU, M. D.; PEETERS, F. M. Giant drop in the bardeen-cooper-schrieffer coherence length induced by quantum size effects in superconducting nanowires. *Phys. Rev. B*, American Physical Society, v. 82, n. 10, p. 104524, Sept. 2010. Available at: <https://journals.aps.org/prb/abstract/10.1103/PhysRevB.82.104524>.

SMITH, P. H.; SHAPIRO, S.; MILES, J. L.; NICOL, J. Superconducting characteristics of superimposed metal films. *Phys. Rev. Lett.*, American Physical Society, v. 6, n. 12, p. 686, June 1961. Available at: <https://doi.org/10.1103/PhysRevLett.6.686>.

SOHN, L. L.; KOUWENHOVEN, L. P.; SCHöN, G. (Ed.). *Mesoscopic Electron Transport*. [S.l.: s.n.], 1996.

THOMPSON, C.; BLATT, J. Shape resonances in superconductors - ii simplified theory. *Phys. Lett.*, Elsevier, v. 5, n. 1, p. 6, june 1963. Available at: <https://www.sciencedirect.com/science/article/abs/pii/S0375960163800031>.

TINKHAM, M. *Introduction to superconductivity; 2nd ed.* [S.l.]: McGraw Hill, 1996.

USADEL, K. D. Generalized diffusion equation for superconducting alloys. *Phys. Rev. Lett.*, American Physical Society, v. 25, p. 507, Aug 1970. Available at: <https://doi.org/10.1103/PhysRevLett.25.507>.

VALLS, O. T.; BRYAN, M. B.; ŽUTIć, I. Superconducting proximity effects in metals with a repulsive pairing interaction. *Phys. Rev. B*, American Physical Society, v. 82, n. 13, p. 134534, Oct 2010. Available at: <https://journals.aps.org/prb/abstract/10.1103/PhysRevB.82.134534>.

VENEMA L.; VERBERCK, B. et al. The quasiparticle zoo. *Nature Physics*, Nature, v. 12, p. 1085, December 2016. Available at: <https://www.nature.com/articles/nphys3977>.

WEI, C. M.; Y., C. M. Theory of quantum size effects in thin pb(111) films. *Phys. Rev. B*, v. 66, p. 233408, Dec 2002. Available at: <https://doi.org/10.1103/PhysRevB.66.233408>.

WOLF, E. L. *Principles of Electron Tunneling Spectroscopy; 2nd ed.* [S.l.]: Oxford University Press, 2012.

ZAGOSKIN, A. *Quantum Theory of Many-Body Systems Techniques and Applications*. [S.l.]: Springer, 2014.

ZAIKIN, A.; ZHARKOV, G. On the microscopic theory of the proximity effect in normal metal-superconductor sandwiches. *Phys. Lett.*, Elsevier, v. 95, n. 6, p. 331, may 1983. Available at: <https://www.sciencedirect.com/science/article/abs/pii/0375960183900336>.

ZHU, J. X. *Bogoliubov-de Gennes Methods and Its Applications*. [S.l.]: Springer, 2016.

ÖZER, M. M.; JIA, Y.; ZHANG, Z.; THOMPSON, J. R.; WEITERING, H. H. Tuning the quantum stability and superconductivity of ultrathin metal alloys. *Science*, v. 316, n. 5831, p. 1594, Jun 2007. Available at: <https://doi.org/10.1126/science.1142159>.